



**NAVAL
POSTGRADUATE
SCHOOL**

MONTEREY, CALIFORNIA

THESIS

**ORBIT SELECTION AND EKV GUIDANCE FOR SPACE-
BASED ICBM INTERCEPT**

by

Ahmet Tarik Aydin

September 2005

Thesis Advisor:

Co-Advisor:

Phillip E. Pace

Murali Tummala

Approved for public release; distribution is unlimited.

THIS PAGE INTENTIONALLY LEFT BLANK

REPORT DOCUMENTATION PAGE			Form Approved OMB No. 0704-0188
Public reporting burden for this collection of information is estimated to average 1 hour per response, including the time for reviewing instruction, searching existing data sources, gathering and maintaining the data needed, and completing and reviewing the collection of information. Send comments regarding this burden estimate or any other aspect of this collection of information, including suggestions for reducing this burden, to Washington headquarters Services, Directorate for Information Operations and Reports, 1215 Jefferson Davis Highway, Suite 1204, Arlington, VA 22202-4302, and to the Office of Management and Budget, Paperwork Reduction Project (0704-0188) Washington DC 20503.			
1. AGENCY USE ONLY (Leave blank)	2. REPORT DATE September 2005	3. REPORT TYPE AND DATES COVERED Master's Thesis	
4. TITLE AND SUBTITLE: Orbit Selection and EKV Guidance for Space-based ICBM Intercept		5. FUNDING NUMBERS	
6. AUTHOR(S) Ahmet Tarik Aydin		8. PERFORMING ORGANIZATION REPORT NUMBER	
7. PERFORMING ORGANIZATION NAME(S) AND ADDRESS(ES) Center for Joint Services Electronic Warfare Naval Postgraduate School Monterey, CA 93943-5000		10. SPONSORING/MONITORING AGENCY REPORT NUMBER	
9. SPONSORING /MONITORING AGENCY NAME(S) AND ADDRESS(ES) Missile Defense Agency		11. SUPPLEMENTARY NOTES The views expressed in this thesis are those of the author and do not reflect the official policy or position of the Department of Defense or the U.S. Government.	
12a. DISTRIBUTION / AVAILABILITY STATEMENT Approved for public release; distribution is unlimited.		12b. DISTRIBUTION CODE A	
13. ABSTRACT (maximum 200 words) Boost-phase intercept of a threat intercontinental ballistic missile (ICBM) is the first layer of a multi-layer defense. This thesis investigates the requirements and limitations of the U.S. space-based ICBM defense against North Korea, Iran and China by introducing an ICBM trajectory prediction, selecting an orbit for exo-atmospheric kill vehicles (EKV) and developing a hybrid guidance algorithm. The prediction of the ICBM trajectory takes the rotation of the earth and the atmospheric drag into account along with the gravitational forces and thrust. The threat ICBM locations, specifications and capabilities of the EKV and EKV carrier, and the capabilities of the space launch vehicle are analyzed to determine an appropriate orbit for the space-based intercept. The pursuit guidance, proportional navigation guidance and bang-bang guidance rules and their performances are investigated and simulated for three example ICBM threats in three-dimensional environment. The simulation results performances are compared and analyzed for minimum miss distance, intercept time and total command effort. The guidance rules are combined to meet the mission requirements, resulting in a hybrid guidance algorithm, which uses different guidance rules for different stages of a boost-phase intercept scenario.			
14. SUBJECT TERMS Spaced-based Missile Defense, Boost-phase Missile Defense, Trajectory Prediction, Space Launch Vehicle, Orbit Selection, Kill Vehicle, Intercept Geometry, Proportional Navigation, Pursuit Guidance, Beam Rider, Bang-bang Guidance			15. NUMBER OF PAGES 136
			16. PRICE CODE
17. SECURITY CLASSIFICATION OF REPORT Unclassified	18. SECURITY CLASSIFICATION OF THIS PAGE Unclassified	19. SECURITY CLASSIFICATION OF ABSTRACT Unclassified	20. LIMITATION OF ABSTRACT UL

THIS PAGE INTENTIONALLY LEFT BLANK

Approved for public release; distribution is unlimited.

**ORBIT SELECTION AND EKV GUIDANCE FOR SPACE-BASED ICBM
INTERCEPT**

Ahmet Tarik Aydin
First Lieutenant, Turkish Air Force
B.S., Turkish Air Force Academy, 1997

Submitted in partial fulfillment of the
requirements for the degree of

MASTER OF SCIENCE IN SYSTEMS ENGINEERING

from the

**NAVAL POSTGRADUATE SCHOOL
September 2005**

Author: Ahmet Tarik Aydin

Approved by: Phillip E. Pace
Thesis Advisor

Murali Tummala
Co-Advisor

Dan C. Boger
Chairman, Department of Information Sciences

THIS PAGE INTENTIONALLY LEFT BLANK

ABSTRACT

Boost-phase intercept of a threat intercontinental ballistic missile (ICBM) is the first layer of a multi-layer defense. This thesis investigates the requirements and limitations of the U.S. space-based ICBM defense against North Korea, Iran and China by introducing an ICBM trajectory prediction, selecting an orbit for exo-atmospheric kill vehicles (EKV) and developing a hybrid guidance algorithm. The prediction of the ICBM trajectory takes the rotation of the earth and the atmospheric drag into account along with the gravitational forces and thrust. The threat ICBM locations, specifications and capabilities of the EKV and EKV carrier, and the capabilities of the space launch vehicle are analyzed to determine an appropriate orbit for the space-based intercept. The pursuit guidance, proportional navigation guidance and bang-bang guidance rules and their performances are investigated and simulated for three example ICBM threats in three-dimensional environment. The simulation results performances are compared and analyzed for minimum miss distance, intercept time and total command effort. The guidance rules are combined to meet the mission requirements, resulting in a hybrid guidance algorithm, which uses different guidance rules for different stages of a boost-phase intercept scenario.

THIS PAGE INTENTIONALLY LEFT BLANK

TABLE OF CONTENTS

I.	INTRODUCTION	1
	A. THESIS OBJECTIVE	3
	B. THESIS OUTLINE.....	3
II.	ICBM DYNAMICS WITH A ROTATING EARTH	5
	A. BOOSTING TARGET MODELING.....	5
	1. Standard Atmosphere Model.....	5
	2. Boosting ICBM Description and Requirements.....	6
	3. Boosting ICBM Mathematical Modeling.....	8
	4. Initial Values of ICBM Launch Angles.....	16
	B. SIMULATION RESULTS FOR THE ICBM MODEL	20
	C. SUMMARY	27
III.	ORBIT SELECTION FOR EKV CARRIERS	29
	A. INTERCEPTOR MISSILE MODELING	29
	B. ORBITAL ELEMENTS.....	31
	1. Keplerian Orbit.....	31
	2. Orbit Perturbations	33
	C. ASSUMPTIONS AND REQUIREMENTS	34
	D. ORBIT DERIVATION.....	37
	1. Analytical Solution for Orbit Determination	37
	a) <i>Inclination Angle</i>	<i>38</i>
	b) <i>Right-ascension of the Ascending Node</i>	<i>40</i>
	c) <i>Altitude of the Orbit</i>	<i>41</i>
	2. Numerical Implementation of the Selected Orbit.....	47
	E. SUMMARY	50
IV.	EKV GUIDANCE METHODS.....	51
	A. DESCRIPTION OF THE SCENARIO.....	51
	B. COORDINATE SYSTEMS AND COORDINATE CONVERSIONS.....	51
	C. PURSUIT GUIDANCE	54
	1. Principals of Pursuit Guidance.....	55
	2. Three-Dimensional Implementation of the Pursuit Guidance	55
	D. PROPORTIONAL NAVIGATION GUIDANCE.....	60
	1. Closing Velocity Approach.....	62
	2. Missile Velocity Approach	64
	E. BANG-BANG GUIDANCE	65
	F. SUMMARY	66
V.	COMPARISON OF GUIDANCE LAWS.....	67
	A. SIMULINK[®] SIMULATION MODEL DESCRIPTION	67
	1. Simulation Initialization.....	67
	2. SIMULINK[®] Model Description	68

3.	ICBM Dynamics Subsystem.....	69
4.	Seeker Subsystem.....	70
5.	Guidance Subsystem.....	71
6.	EKV Dynamics Subsystem.....	71
B.	SIMULATION RESULTS FOR PURSUIT GUIDANCE	72
C.	SIMULATION RESULTS FOR PROPORTIONAL NAVIGATION GUIDANCE.....	77
1.	Simulation Results for the Closing Velocity Approach.....	77
2.	Simulation Results for Missile Velocity Approach	81
D.	SIMULATION RESULTS FOR THE HYBRID GUIDANCE	84
a)	<i>North Korea Case</i>	85
b)	<i>China Case</i>	90
c)	<i>Iran Case</i>	95
E.	SUMMARY	99
VI.	CONCLUDING REMARKS AND FUTURE RECOMMENDATIONS	101
A.	SUMMARY OF THE WORK	101
B.	SIGNIFICANT RESULTS.....	101
C.	RECOMMENDATIONS FOR FUTURE WORK.....	103
	APPENDIX A. CODE FLOW CHART.....	105
	LIST OF REFERENCES	113
	INITIAL DISTRIBUTION LIST	117

LIST OF FIGURES

Figure 1.	Overall space-based ICBM defense scenario.	2
Figure 2.	Exponential approximation for air density.	6
Figure 3.	Required speed for a given distance.	8
Figure 4.	ECEF and other coordinate systems.	9
Figure 5.	Forces acting on missile.	12
Figure 6.	Launch parameter geometry (After [15]).	16
Figure 7.	Trajectories of the ICBMs launched from North Korea, China and Iran.	22
Figure 8.	Magnitudes of the velocity vectors of the ICBMs throughout the entire flight. The earth's rotation and the atmospheric drag are included	23
Figure 9.	Magnitudes of the velocity vectors of the ICBMs during boost-phase.	24
Figure 10.	Altitudes of the ICBMs during the entire flight.	25
Figure 11.	Total mass of the ICBMs as a function of the time from launch.	26
Figure 12.	Propellant mass of the ICBMs during the boost-phase.	26
Figure 13.	Raytheon's exo-atmospheric kill vehicle (From [17]).	30
Figure 14.	Orbital elements (Adapted from [20]).	32
Figure 15.	The semi-major axis and the semi-minor axis of an ellipse.	33
Figure 16.	The geographical location of Kilju-kun Missile Base, North Korea (After [23]).	35
Figure 17.	The geographical location of Xining, China (After [23]).	35
Figure 18.	The geographical location of Bushehr, Iran (After [23]).	36
Figure 19.	Orbital plane and the launch sites.	37
Figure 20.	The spherical angles of the given location.	38
Figure 21.	Titan IV at liftoff (From [27]).	42
Figure 22.	Space launcher (Titan IV) payload capacity (After [20]).	43
Figure 23.	Maximum range of the EKV during a maximum allowable period of 2 minutes and 45 seconds	44
Figure 24.	The altitudes of the ICBMs at the end of boost-phase.	45
Figure 25.	Orbital plane and the intercept geometry.	45
Figure 26.	The down-look launch angle as a function of the orbit altitude.	46
Figure 27.	Maximum coverage angle as a function of orbit altitude.	47
Figure 28.	The orbit parameters in the ECEF and spherical coordinate systems.	48
Figure 29.	The orbit of the EKV and the target ICBM locations.	50
Figure 30.	Guidance coordinates geometry: ECEF coordinate system, LOS plane, ABC system.	52
Figure 31.	Pursuit guidance flow chart.	55
Figure 32.	Coordinated turn schematic (After [34]).	57
Figure 33.	Time domain response of the EKV guidance system.	60
Figure 34.	PNG collision geometry.	61
Figure 35.	Block diagram of the PNG.	64

Figure 36.	Overall space-based intercept SIMULINK [®] model for PG, PNG, BBG and HG against North Korean, Chinese and Iranian ICBMs.....	69
Figure 37.	SIMULINK [®] model for ICBM Dynamics.....	70
Figure 38.	SIMULINK [®] model for Seeker design of the EKV.....	70
Figure 39.	SIMULINK [®] model for Guidance Unit of the EKV.	71
Figure 40.	SIMULINK [®] model for EKV Dynamics.....	72
Figure 41.	The intercept geometry for PG with $K = 3$	74
Figure 42.	Miss distance for pursuit guidance with $K = 3$	75
Figure 43.	Altitude of the EKV and the ICBM for pursuit guidance with $K = 3$	75
Figure 44.	Instantaneous acceleration applied on the EKV for pursuit guidance with $K = 3$	76
Figure 45.	Cumulative acceleration applied on the EKV for pursuit guidance with $K = 3$	76
Figure 46.	Speeds of the EKV under PG with $K = 3$ and the speed of the ICBM.	77
Figure 47.	Closing velocity of the EKV to the ICBM for PG with $K = 3$	77
Figure 48.	Intercept geometry for PNG with $N = 5$	78
Figure 49.	Miss distance for PNG with $N = 5$	79
Figure 50.	Altitude of the EKV and the ICBM for PNG with $N = 5$	79
Figure 51.	Instantaneous acceleration applied on the EKV for PNG with $N = 5$	80
Figure 52.	Cumulative acceleration applied on the EKV for PNG with $N = 5$	80
Figure 53.	Speeds of the EKV and the ICBM for PNG with $N = 5$	81
Figure 54.	Closing velocity of the EKV to the ICBM for PNG with $N = 5$	81
Figure 55.	Intercept geometry for PNG with $N' = 6$	82
Figure 56.	Miss distance for PNG with $N' = 6$	82
Figure 57.	Altitudes for PNG with $N' = 6$	82
Figure 58.	Instantaneous acceleration for PNG with $N' = 6$	83
Figure 59.	Total acceleration command for PNG with $N' = 6$	83
Figure 60.	Velocities for PNG with $N' = 6$	84
Figure 61.	Closing velocity for PNG with $N' = 6$	84
Figure 62.	Intercept geometries against North Korean ICBM.	86
Figure 63.	Miss distances with HG for North Korean ICBM defense.	87
Figure 64.	Altitudes of EKV's and North Korean ICBM with HG.....	87
Figure 65.	Lateral acceleration exerted by HG on the EKV's launched from points A, B, C and D against North Korean ICBM.....	88
Figure 66.	Cumulative acceleration exerted by HG on the EKV's launched from points A, B, C and D against North Korean ICBM.	88
Figure 67.	Velocity magnitudes of the EKV's launched from points A, B, C, D and the ICBM with HG.	89
Figure 68.	Closing velocity of the EKV's to the ICBM for launch points A, B, C and D with HG.....	89
Figure 69.	LOS angular velocity magnitudes for points A, B, C and D with HG.	90
Figure 70.	Intercept geometries against Chinese ICBM.	91
Figure 71.	Miss distances with HG for Chinese ICBM defense.	92
Figure 72.	Altitudes of EKV's and Chinese ICBM with HG.....	92

Figure 73.	Lateral acceleration exerted by HG on the EKV's launched from points A, B, C and D against Chinese ICBM.	92
Figure 74.	Cumulative acceleration exerted by HG on the EKV's launched from points A, B, C and D against Chinese ICBM.	92
Figure 75.	Velocity magnitudes of the EKV's launched from points A, B, C, D and the ICBM with HG.	93
Figure 76.	Closing velocity of the EKV's to the ICBM for launch points A, B, C and D with HG.	93
Figure 77.	LOS angular velocity magnitudes for points A, B, C and D with HG.	94
Figure 78.	Intercept geometries against Iranian ICBM.	96
Figure 79.	Miss distances with HG for Iran ICBM defense.	96
Figure 80.	Altitudes of EKV's and Iran ICBM with HG.	96
Figure 81.	Lateral acceleration exerted by HG on the EKV's launched from points A, B, C and D against Iran ICBM.	97
Figure 82.	Total cumulative acceleration exerted by HG on the EKV's launched from points A, B, C and D against Iran ICBM.	97
Figure 83.	Speeds of the EKV's launched from points A, B, C, D and the ICBM with HG.	98
Figure 84.	Closing velocities of the EKV's to the ICBM for launch points A, B, C and D with HG.	98
Figure 85.	LOS angular velocity magnitudes for points A, B, C and D with HG.	99

THIS PAGE INTENTIONALLY LEFT BLANK

LIST OF TABLES

Table 1.	ICBM data matrix.	7
Table 2.	Azimuth launch angles for launch attitude	18
Table 3.	Initial launch parameters for ICBMs.	21
Table 4.	Required velocities.....	24
Table 5.	Simulation results for ICBMs from North Korea, China and Iran.	27
Table 6.	Spherical coordinates calculation for EKV at a given time.....	49
Table 7.	Code listing for the SIMULINK [®] model.....	68
Table 8.	Orbital launch points for the North Korea case.	86
Table 9.	Simulation results for North Korean ICBM intercept with HG.....	89
Table 10.	Orbital launch points for the China case.....	90
Table 11.	Simulation results for Chinese ICBM intercept with HG.....	94
Table 12.	Orbital launch points for the Iran case.....	95
Table 13.	Simulation results for Iranian ICBM intercept with HG.	98

THIS PAGE INTENTIONALLY LEFT BLANK

ACKNOWLEDGMENTS

This thesis is definitely the result of team work. First of all I would like to thank my wife Serife for her endless understanding, help and patience. I would also like to thank my advisors, Professor Phillip E. Pace and Professor Murali Tummala, for their priceless support. I would like to thank my parents Husamettin and Keziban for dedicating their entire lives to my education. I am grateful to the Turkish Air Force, for giving me the opportunity to attend NPS and receive this excellent education. I would like to thank all who contributed to this study, in particular the professors and students of NPS in the Missile Defense Team. Much thanks goes to Dr. Butch Caffall and the Missile Defense Agency (MDA) for their support and encouragement.

I dedicate this thesis to my wife Serife, the pride and joy of my life.

THIS PAGE INTENTIONALLY LEFT BLANK

I. INTRODUCTION

The National Missile Defense program was launched to protect the U.S. from ballistic missile attacks. It is well known that the former Soviet Union has provided some countries with ballistic missiles and that some of these countries are upgrading or developing their own missile systems [1]. The report of the “Commission to Assess the Ballistic Missile Threat to the United States” in 1998 showed the perimeter of the threat to Congress [2]. The report states that some of these countries have or are about to gain the ability to attack the U.S. with their missile systems.

This study will investigate the requirements, limitations and the performance of the space-based, boost-phase intercontinental ballistic missile (ICBM) defense. Boost-phase defense is investigated because previous studies showed that boost-phase defense has significant advantages when the electronic countermeasures are considered [3]. Space-based ICBM defense has been considered by the U.S. government since the beginning of the Strategic Defense Initiative [4]. It is desirable to have a space-based defense system to kill an ICBM in early stages of its trajectory [5]. The overall space-based ICBM defense scenario is illustrated in Figure 1. In the scenario, several EKV carriers are placed on a low-earth orbit to cover all possible ICBM threats. The ICBM launch is detected by the IR sensors in the geosynchronous orbit and tracked by RF sensors as shown in Figure 1. The track information is fused, and the command and control of the system is facilitated via the communication links between the assets as shown. After a launch decision is made, the EKV is launched from the appropriate EKV carrier onto the orbit.

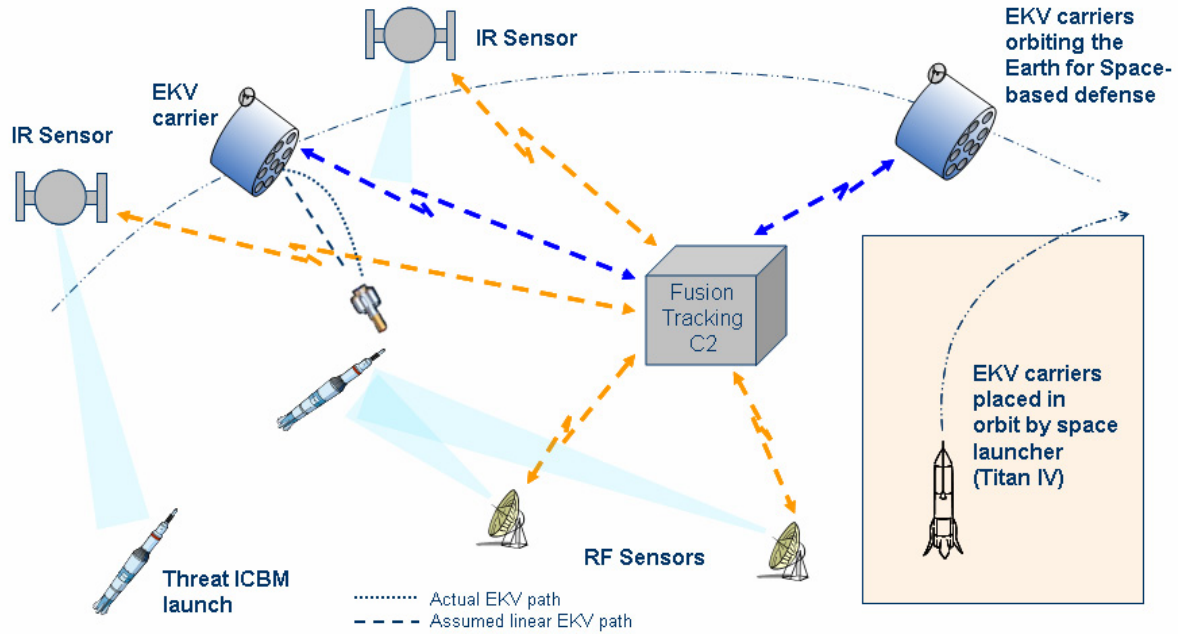


Figure 1. Overall space-based ICBM defense scenario.

Ground-based defense requires that the exact location of the threat missile be known and that the interceptor be placed in a small pre-designated area [6]. The space-based defense can be designed to provide a continuous coverage over the globe with the selection of an appropriate orbit and by launching enough number of interceptors [7]. Deblois, et al. claim that the space-based interceptors have the same performance as the ground-based interceptors, and considering the cost-benefit ratio, they suggest that space-based ICBM defense is not desirable [8]. However, they make this comparison for fixed ICBM launch sites. In contemporary world, the ICBM threat may come from anywhere on the earth, and in order to cover the most possible threats we need a space-based defense system [4].

In this study, the exo-atmospheric kill vehicle (EKV) is considered to perform a hit-to-kill intercept. With the hit-to-kill intercept, the interceptor will smash into the target at a high speed (approximately 7 km/s), which will create more destructive force than that created by the conventional explosives with the same mass [8]. In order to achieve this goal, an advanced and successful guidance algorithm is required. In this study, different types of guidance rules are examined and a hybrid algorithm is developed for the EKV.

A. THESIS OBJECTIVE

The main objective of this thesis is to investigate the space-based, boost-phase ICBM interception. This includes the modeling of the ICBM motion, selecting an orbit to place the EKV carriers on and investigating the guidance laws to achieve the intercept.

We developed a mathematical model to define the motion of an ICBM by taking the earth's rotation and the atmospheric drag into account. Three different ICBM models having different mass fractions are generated for three different example launch points in North Korea, China and Iran. The initial launch parameters (the elevation launch angle and the azimuth angle) are estimated by using the Lambert guidance for impulsive missiles.

The threat ICBM locations, specifications and capabilities of the EKV and EKV carrier, and the capabilities of the space launch vehicle are analyzed to determine an appropriate orbit for the space-based intercept. The inclination angle and the right-ascension angle of the orbit are determined to provide a uniform and continuous coverage over the three example countries. The altitude of the orbit is determined using the maximum range of the EKV and the capacity of the space launch vehicle.

The pursuit guidance, proportional navigation guidance and bang-bang guidance methods are investigated for the EKV. These methods are implemented in the guidance unit of the EKV in a three-dimensional environment. The three guidance methods are simulated in SIMULINK[®], and the results are presented.

B. THESIS OUTLINE

Chapter II of this study models the ICBM mathematically in the gravity field with the earth's rotation and atmospheric drag. The mathematical model is implemented in MATLAB[®] and the launch parameters for a San Francisco attack from North Korea, China and Iran are delineated. In Chapter III, the required orbit for a successful space-based intercept against the ICBM launched from North Korea, China and Iran is derived. The orbital elements and the orbit requirements are introduced. Chapter IV introduces the principles of the pursuit guidance, proportional navigation guidance and the bang-bang guidance. The methodology of implementing these guidance rules in a three-dimensional model is explained. Chapter V presents the simulation results and compares the different

guidance rules for the given scenarios. An analysis is based on simulation results conducted to identify the minimum intercept time with minimum guidance effort and minimum miss distance. Through trial end error the minimum miss distance is determined to achieve the hit-to-kill intercept. Chapter VI provides concluding remarks. Appendix A shows the flowchart of the simulation.

II. ICBM DYNAMICS WITH A ROTATING EARTH

The threat intercontinental ballistic missile (ICBM) launched from a hostile location is described in this chapter. The target ICBM in this study is a solid propellant, three stage, boosting missile reaching speeds above 6 km/s at the end of its boost-phase. The trajectory of the ICBM is derived as a function of the thrust that is generated by the solid propellant, the gravitational effects, the atmospheric drag and the rotation of the earth. The ICBMs are assumed to be launched from North Korea, China or Iran targeting San Francisco, California.

A. BOOSTING TARGET MODELING

In this chapter, the drag forces acting on the missile and the angular velocity resulting from the earth's rotation are considered, and a close form solution is generated as a function of these forces, along with the thrust and the weight.

1. Standard Atmosphere Model

The atmospheric drag has a significant effect on the ICBM when moving in the atmosphere. The drag force is directly proportional to the air density, along with the cross-sectional area, drag coefficient and the square of the velocity. The air density decreases proportional to the altitude and is measured in kg/m^3 in this study. The air density of the atmosphere is modeled by using an exponential approximation [9]. This approximation divides the atmosphere into two layers. The air density in the lower atmosphere (below 9144 m) and upper atmosphere (above 9144 m), respectively, are given by [9]

$$\begin{aligned}\rho_L &= 1.22557e^{-A/9144} & A < 9144 \\ \rho_U &= 1.75228763e^{-A/6705.6} & A \geq 9144\end{aligned}\tag{2.1}$$

where A is the altitude in meters and ρ is the air density in kg/m^3 . The U.S. Standard Atmosphere and the exponential approximation results are shown together in Figure 2. As shown in Figure 2, the exponential approximation for air density provides close match to the U.S. Standard Atmosphere.

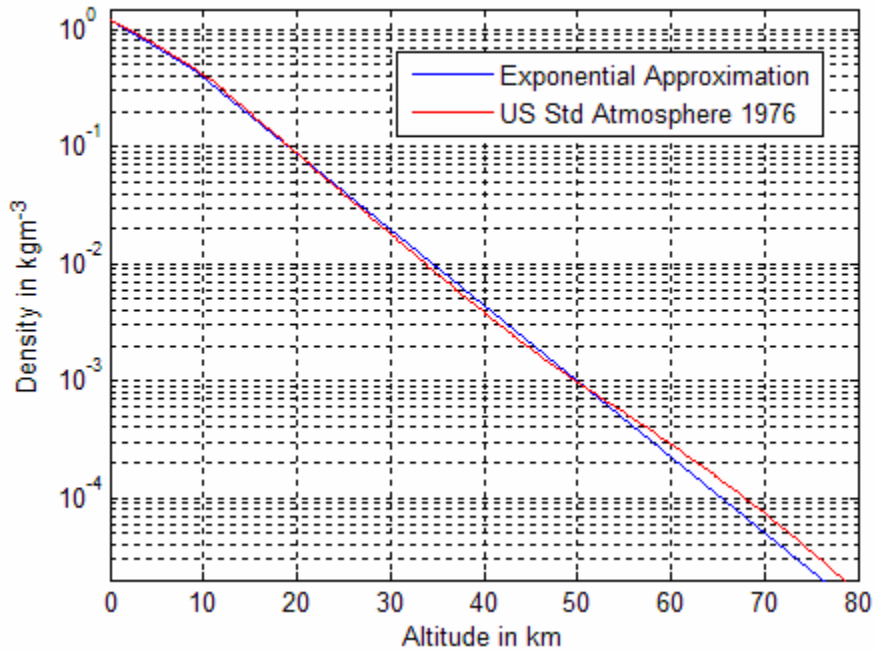


Figure 2. Exponential approximation for air density.

2. Boosting ICBM Description and Requirements

For modeling the ICBM, the U.S. Peacekeeper missile is used as an example in this study because it is well published in open literature. The missile is a three-stage solid-propellant boosting ICBM capable of carrying up to 2270 kg of payload. The mass fraction, which is the ratio of the propellant weight to the total weight of the vehicle, dictates the velocity that the missile can attain by using its fuel [9]. The mass fraction of the ICBMs modeled in this study are 83%, 84% and 85%, respectively, to represent the North Korean, Chinese and Iranian ICBMs. Increasing the amount of propellant fuel does not necessarily increase the speed and range of the missile. The efficiency of the fuel can be understood from the mass fraction. The higher the mass fraction, the greater the speed and the range of the missile [6]. Since the ranges of the missiles from three countries mentioned above are different, the mass fractions and fuel amounts necessary are also different. The stage total masses, the propellant masses and mass fractions of the ICBMs are given in Table 1.

Table 1. ICBM data matrix.

		Stage 1	Stage 2	Stage 3	Payload	Mass Fraction
North Korea	Total mass (kg)	49000	27670	7711	2268	83%
	Propellant mass (kg)	41640	23520	6554	0	
China	Total mass (kg)	53000	29670	8711	2268	84%
	Propellant mass (kg)	45640	25520	7554	0	
Iran	Total mass (kg)	54000	30670	9711	2268	85%
	Propellant mass (kg)	46640	26520	8554	0	

The ICBM has to travel intercontinental distances to achieve its strategic mission. Hence, it needs to reach near orbital speeds to ensure these distances. The required velocity to reach a given distance with a given launch angle can be calculated by using the rocket equation [9]

$$V_{req} = \sqrt{\frac{gm(1 - \cos \phi)}{r_0 \cos(\gamma)(r_0 \cos \gamma/a - \cos(\phi + \gamma))}} \quad (2.2)$$

where gm is the gravitational constant ($3.986 \times 10^{14} \text{ m}^3/\text{s}^2$), ϕ is angular distance to be traveled, r_0 is the initial distance of the ICBM from the center of the earth, γ is the elevation launch angle, and a is the radius of the earth (6371 km). Using (2.2), the required speeds needed to reach the continental U.S. from Iran, China, and North Korea are shown in Figure 3. The launch angle is taken as 45 degrees, which ensures the maximum range for the required speed [9].

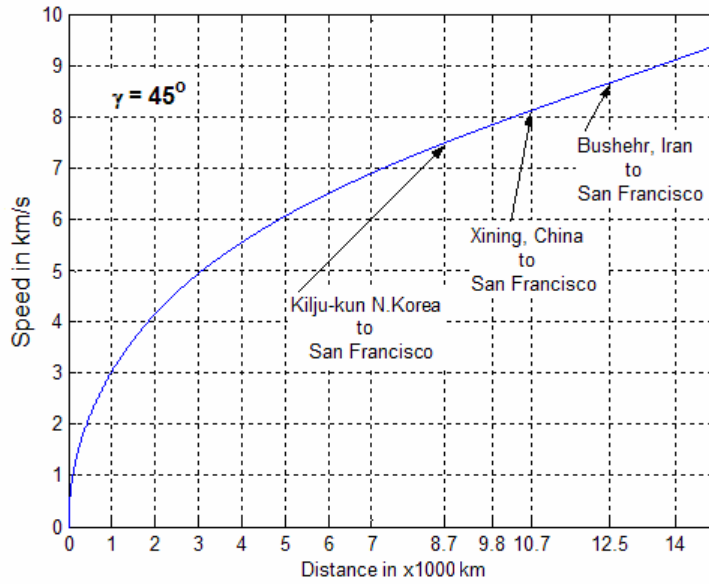


Figure 3. Required speed for a given distance.

As shown in Figure 3, the required speed increases as the distance between the target and the launch site increases. The speed required to reach San Francisco, California from Kilju-kun, North Korea is 7.49 km/s, which is in the region of a low earth orbiting vehicle speed. The required speeds for Xining, China and Busher, Iran launch sites are 8.12 km/s and 8.65 km/s, respectively. Equation (2.2) assumes an impulsive missile, which is not true for a boosting missile. The speed requirements for a boosting missile will be less than for an impulsive missile because there will be thrust acting on the missile for several minutes. In addition, the rotation of the earth and the drag forces are not considered in this rocket equation.

3. Boosting ICBM Mathematical Modeling

In this section, we derive the mathematical model for a boosting ICBM that takes the earth's rotation and the atmospheric drag into account. Kashiwagi derives a full mathematical model for re-entry vehicles, where the non-accelerating vehicle is released from space [10]. We adopt his derivation for ground-based boosting ICBMs by adding the thrust force generated by the solid propellant fuel.

Before starting to develop a closed form solution for predicting the trajectory of the ICBM, we briefly define the coordinate systems. The common coordinate system

In the derivation of the differential equation for the motion, the ICBM is considered a point mass. The force on the point mass, based on using Newton's second law, is given by

$$\vec{F} = m\vec{a} \quad (2.3)$$

where \vec{a} is the acceleration in m/s^2 and m is the point mass in kg. The unit of F is specified in N (Newtons).

The angular velocity vector of the earth, denoted by $\vec{\omega}$, is given by [10]

$$\vec{\omega} = \omega\hat{n} \quad (2.4)$$

where \hat{n} is the unit vector in the z direction, and $|\vec{\omega}| = \omega = 2\pi \text{ rad/day}$. In Figure 4, E is a point on the earth, and the vector \vec{S} representing the ICBM missile body from point E to point P is given by

$$\vec{S} = x\hat{i} + y\hat{j} + z\hat{k} \quad (2.5)$$

where x , y and z are the distance measures in ECEF coordinates, and \hat{i} , \hat{j} and \hat{k} are the unit vectors in the direction of x , y and z , respectively. The velocity of the ICBM with respect to point E can be defined as the time derivative of \vec{S} :

$$\vec{V} = \frac{d\vec{S}}{dt} = \dot{x}\hat{i} + \dot{y}\hat{j} + \dot{z}\hat{k} \quad (2.6)$$

The acceleration of the point mass with respect to point E can also be written as time derivative of the velocity:

$$\vec{a} = \frac{d\vec{V}}{dt} = \ddot{x}\hat{i} + \ddot{y}\hat{j} + \ddot{z}\hat{k} \quad (2.7)$$

The acceleration acting on the point mass is called the apparent acceleration and is denoted by

$$\vec{a}_p = \vec{a} + \dot{a}_p + a_c \quad (2.8)$$

where \vec{a} is the relative acceleration, \dot{a}_p is coincident point velocity, and a_c is the coriolis acceleration [10]:

$$\dot{a}_p = \bar{\omega} \times (\bar{\omega} \times \bar{r}) \quad (2.9)$$

$$a_c = 2\bar{\omega} \times \bar{V} \quad (2.10)$$

By substituting (2.7), (2.9) and (2.10) into (2.8), we obtain the resultant apparent acceleration that is acting on the point mass [10]:

$$a_p = \ddot{x}\hat{i} + \ddot{y}\hat{j} + \ddot{z}\hat{k} + \bar{\omega} \times (\bar{\omega} \times \bar{r}) + 2\bar{\omega} \times \bar{V} \quad (2.11)$$

The rotation of the earth $\bar{\omega}$ can be defined as a function of ECEF coordinates, which will make it easier to solve for a closed form equation, and in doing so, we will keep a common coordinate system for calculations [10]:

$$\bar{\omega} = \omega \sin(\mu)\hat{k} + \omega \cos(\mu)\hat{j} \quad (2.12)$$

The vector \bar{r} , which defines the position of the ICBM, can also be written in the ECEF coordinate system as follows [10]

$$\bar{r} = x\hat{i} + y\hat{j} + z\hat{k} \quad (2.13)$$

The cross products appearing in (2.11) are solved as shown below [10]:

$$\begin{aligned} \bar{\omega} \times (\bar{\omega} \times \bar{r}) &= -\omega^2 x\hat{i} + \omega^2 \left[(y \cos(\mu) + z \sin(\mu)) \cos(\mu) - y \right] \hat{j} \\ &\quad + \omega^2 \left[(y \cos(\mu) + z \sin(\mu)) \sin(\mu) - z \right] \hat{k} \\ \bar{\omega} \times \bar{V} &= \omega (\dot{z} \cos(\mu) - \dot{y} \sin(\mu)) \hat{i} + \dot{x} \omega \sin(\mu) \hat{j} - \dot{x} \omega \cos(\mu) \hat{k} \end{aligned} \quad (2.14)$$

where μ is the geodetic latitude of the ICBM. Substituting (2.14) into (2.11) yields the closed form of the acceleration acting on the ICBM [10]:

$$\begin{aligned} a_p &= \left[\ddot{x} + 2\omega (\dot{z} \cos(\mu) - \dot{y} \sin(\mu)) \right] \hat{i} \\ &\quad + \left[\ddot{y} + 2\dot{x}\omega \sin(\mu) + \omega^2 (y \cos(\mu) + z \sin(\mu)) \cos(\mu) \right] \hat{j} \\ &\quad + \left[\ddot{z} - 2\dot{x}\omega \cos(\mu) + \omega^2 (y \cos(\mu) + z \sin(\mu)) \sin(\mu) \right] \hat{k} \end{aligned} \quad (2.15)$$

Equation (2.15) concludes the derivation of the acceleration acting on the ICBM due to Newton's second law (2.3).

Now the left-hand side of (2.3), which contains the forces acting on the ICBM, is derived. The four major forces acting on the ICBM are the weight (W), the drag force (F_d), the lift and the thrust (T). The ICBM examined here is a cruciform missile, hence the lift on this missile is very small and can be neglected. The total force on the ICBM is the sum of all remaining force vectors as given by

$$\vec{F} = \vec{F}_d + \vec{T} + \vec{W} \quad (2.16)$$

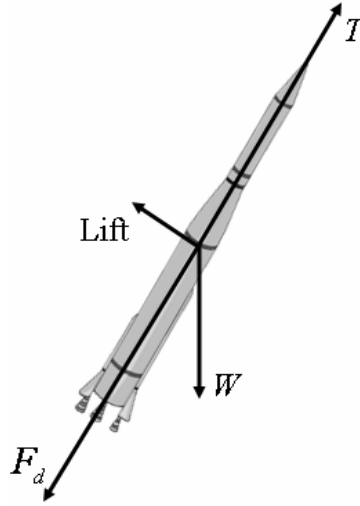


Figure 5. Forces acting on missile.

The thrust vector \vec{T} is along the velocity vector of the missile as shown in Figure 5. The magnitude of the thrust vector is proportional to the propellant used and the specific impulse of the missile I_{sp} , given by

$$I_{sp} = \frac{-T}{\dot{W}} \quad (2.17)$$

where \dot{W} represents change in mass of the propellant. In other words, it is the fuel spent in a second. The specific impulse is a measure of effectiveness of the fuel in units of seconds. The more capable missiles have a higher value of I_{sp} [9]. The ICBM examined in this study is assumed to have a specific impulse of 300 s. The derivative can also be defined as the product of the gravitational acceleration and the change in mass [6] as follows:

$$\dot{W} = \dot{m}g \quad (2.18)$$

where g is the gravitational acceleration of the earth in m/s^2 . The gravitational acceleration of the earth varies inversely proportional to the square of the altitude of the missile

$$g = \frac{GM}{r^2} \quad (2.19)$$

where G is the gravitational constant of the earth, which is approximately equal to $6.7154 \times 10^{-11} \text{ Nm/kg}^2$ [11], M is the mass of the earth, which is approximately equal to $5.98 \times 10^{24} \text{ kg}$ [12], and r is the magnitude of the vector \bar{r} as shown in Figure 4.

When we substitute (2.18) and (2.19) into (2.17) and solve for the thrust, we have a closed form solution of the thrust vector in the direction of the velocity vector \bar{V} as given by

$$\bar{T} = \dot{m} \frac{GM}{r^2} I_{sp} \left(\frac{\dot{x}\hat{i} + \dot{y}\hat{j} + \dot{z}\hat{k}}{\|\bar{V}\|} \right) = \frac{\dot{m}g I_{sp}}{\|\bar{V}\|} (\dot{x}\hat{i} + \dot{y}\hat{j} + \dot{z}\hat{k}) \quad (2.20)$$

The drag force acting on the ICBM is a function of atmospheric density (ρ), gravitational acceleration of the earth g , the ballistic coefficient β , and the velocity of the ICBM. The drag force is defined in the opposite direction of the velocity vector [9]:

$$\bar{F}_d = -\frac{m\rho\|\bar{V}\|}{2\beta} (\dot{x}\hat{i} + \dot{y}\hat{j} + \dot{z}\hat{k}) \quad (2.21)$$

The weight vector of the ICBM is towards the center of the earth and is defined as the product of the mass and the gravitational acceleration g as given by

$$\bar{W} = -\frac{mGM}{r^2} \left(\frac{x\hat{i} + y\hat{j} + z\hat{k}}{r} \right) = -\frac{mGM}{r^3} (x\hat{i} + y\hat{j} + z\hat{k}) \quad (2.22)$$

Now we can write the left-hand side of the equation, which defines the forces acting on the missile. Substituting (2.20), (2.21) and (2.22) into (2.16) gives the total forces acting on the ICBM as follows:

$$\begin{aligned}
\bar{F} = & \left(\dot{m} \frac{GM}{r^2} I_{sp} \frac{\dot{x}}{\|\bar{V}\|} - \frac{m\rho\|\bar{V}\|}{2\beta} \dot{x} - m \frac{GM}{r^3} x \right) \hat{i} \\
& + \left(\dot{m} \frac{GM}{r^2} I_{sp} \frac{\dot{y}}{\|\bar{V}\|} - \frac{m\rho\|\bar{V}\|}{2\beta} \dot{y} - m \frac{GM}{r^3} y \right) \hat{j} \\
& + \left(\dot{m} \frac{GM}{r^2} I_{sp} \frac{\dot{z}}{\|\bar{V}\|} - \frac{m\rho\|\bar{V}\|}{2\beta} \dot{z} - m \frac{GM}{r^3} z \right) \hat{k}
\end{aligned} \tag{2.23}$$

Substituting (2.23) and (2.15) into (2.3), and the rearranging the equation for the ECEF components, yields the differential equations of the acceleration as given by

$$\begin{aligned}
\ddot{x} = & -2\omega(\dot{z} \cos \mu - \dot{y} \sin \mu) + \omega^2 x - \frac{\rho|\bar{V}|}{2\beta} \dot{x} - \frac{GM}{r^3} x + \frac{\dot{m}GM}{m|\bar{V}|} I_{sp} \dot{x} \\
\ddot{y} = & -2\omega\dot{x} \sin \mu + \omega^2 y \sin^2 \mu + \omega^2 z \sin \mu \cos \mu - \frac{\rho|\bar{V}|}{2\beta} \dot{y} - \frac{GM}{r^3} y + \frac{\dot{m}GM}{m|\bar{V}|} I_{sp} \dot{y} \\
\ddot{z} = & 2\omega\dot{x} \cos \mu + \omega^2 z \cos^2 \mu - \omega^2 y \sin \mu \cos \mu - \frac{\rho|\bar{V}|}{2\beta} \dot{z} - \frac{GM}{r^3} z + \frac{\dot{m}GM}{m|\bar{V}|} I_{sp} \dot{z}
\end{aligned} \tag{2.24}$$

The state vector of the ICBM is defined as a function of its position and velocity and denoted by

$$X = [x \quad y \quad z \quad V_x \quad V_y \quad V_z]^T = [x \quad y \quad z \quad \dot{x} \quad \dot{y} \quad \dot{z}]^T \tag{2.25}$$

The evaluation of the change in the state of the missile in discrete time is given by (2.24). Representing these equations in $\dot{X} = FX(t-t_0)$ format will require defining the state transition matrix F . The transition matrix is formed by using (2.24). The parameter t is the time of interest and t_0 is the initial time [13]:

$$F = \begin{bmatrix} 0 & 0 & 0 & 1 & 0 & 0 \\ 0 & 0 & 0 & 0 & 1 & 0 \\ 0 & 0 & 0 & 0 & 0 & 1 \\ \omega^2 - \frac{GM}{r^3} & 0 & 0 & \frac{\dot{m}gI_{sp}}{m|V|} - \frac{\rho g}{2\beta} & 2\omega \sin \mu & -2\omega \cos \mu \\ 0 & \omega^2 \sin \mu - \frac{GM}{r^3} & -\omega^2 \sin \mu \cos \mu & -2\omega \sin \mu & \frac{\dot{m}gI_{sp}}{m|V|} - \frac{\rho g}{2\beta} & 0 \\ 0 & -\omega^2 \sin \mu \cos \mu & \omega^2 \cos(\mu) - \frac{GM}{r^3} & 2\omega \cos \mu & 0 & \frac{\dot{m}gI_{sp}}{m|V|} - \frac{\rho g}{2\beta} \end{bmatrix} \quad (2.26)$$

where

- ω : earth rotation rate ($2\pi/\text{day}$)
- G : gravitational constant of earth (6.67×10^{-11})
- M : mass of earth (5.98×10^{24} kg)
- r : distance of the target from earth's center
- \dot{m} : fuel consumption of the target ICBM (kg/s)
- I_{sp} : specific impulse of the target ICBM
- m : total mass of the target ICBM
- $|V|$: magnitude of the velocity of the ICBM
- ρ : atmospheric density (kg/m^3)
- β : ballistic coefficient, and
- μ : geodetic latitude of the target ICBM

The first order Markov model for the target's state transition uses the state transition matrix F . The differential equation derived in the preceding discussion is the mathematical model for the motion of the boosting ICBM in the gravity field. It is very cumbersome to derive a closed form solution for this equation. Instead of deriving a closed form solution, we apply numerical integration using MATLAB[®]. The numerical integration method guarantees accurate results but demands high computational power. The motion of the ICBM is simulated using the discrete-time implementation of the transition matrix and the state space vectors as follows

$$X(k + \Delta t) = X(k) + FX(k)\Delta t \quad (2.27)$$

where Δt is the time step.

4. Initial Values of ICBM Launch Angles

The azimuth launch angle C is measured in the topo-centric coordinate system from the North Pole to the tip of the missile. The measurement is taken from north to east. Consider the triangle ABC shown in Figure 6 as the launch geometry, where C is the launch point and B is the target location. The North Pole is denoted by A in this geometry. The initial azimuth launch angle of the ICBM is denoted by C .

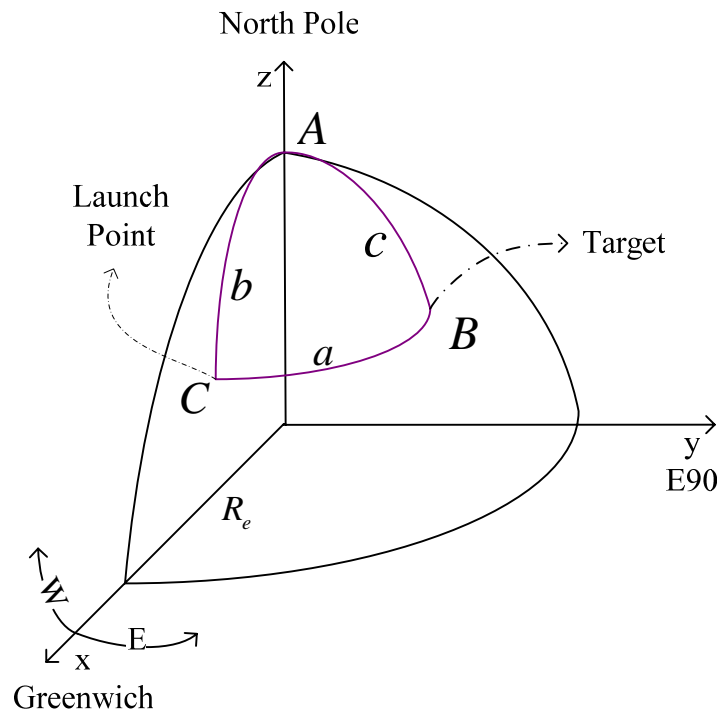


Figure 6. Launch parameter geometry (After [15]).

The lowercase letters in Figure 6 correspond to the angles subtended by the arcs measured from the center of the earth. The capital letters in Figure 6 correspond to the angles formed by the intersecting arcs. Note that angle C is the azimuth launch angle. Using the law of sines, we can obtain the relationship among the angles as

$$\frac{\sin a}{\sin A} = \frac{\sin c}{\sin C} \quad (2.28)$$

By rearranging (2.28), the azimuth launch angle can be written as

$$\tan C = \frac{\sin c \sin A}{\sin a \cos C} \quad (2.29)$$

The denominator of (2.29) can be shown to be a function of angles a , b and c as given by

$$\sin a \cos C = \frac{\cos c - \cos a \cos b}{\sin b} \quad (2.30)$$

from the law of cosines: $\cos c = \cos a \cos b + \sin a \sin b \cos C$. By substituting (2.30) into (2.29), the azimuth launch angle is obtained as

$$\tan C = \frac{\sin c \sin b \sin A}{\cos c - \cos a \cos b} \quad (2.31)$$

The angles A , b and c are defined by the target location and the launch site location. The only unknown in (2.31) is the $\cos a$ term, which in turn can be written as a function of the known parameters by using the following law of cosines:

$$\cos a = \cos b \cos c + \sin b \sin c \cos A \quad (2.32)$$

The known angles mentioned above are defined using the geodetic locations of the target and the launch site as given by [15]

$$\begin{aligned} A &= \lambda - \lambda_o \\ b &= \frac{\pi}{2} - \mu_o \\ c &= \frac{\pi}{2} - \mu \end{aligned} \quad (2.33)$$

where λ is target geodetic longitude, μ is target geodetic latitude, λ_o is launch site geodetic longitude, and μ_o is launch site geodetic latitude.

Using (2.33), we can show the azimuth launch angle to be a function of geodetic locations and the $\cos a$ term as given by

$$\tan C = \frac{\cos \mu \cos \mu_o \sin(\lambda - \lambda_o)}{\sin \mu - \cos a \sin \mu_o} \quad (2.34)$$

The azimuth launch angles from Kilju-kun, North Korea, Xining, China and Bushehr, Iran to San Francisco (N37.76 W122) are calculated by using (2.34). The results are tabulated in Table 2 in which the azimuth launch angles are defined from the North Pole eastward.

Table 2. Azimuth launch angles for launch attitude

Launch Site	North Korea	China	Iran
Location (geodetic)	N41-E129	N36-E101	N29-E51
Azimuth launch angle (degrees)	40.37	31.52	353.24

The elevation angle for the ICBM is calculated using the Lambert guidance. Lambert guidance will put the ICBM on a collision triangle that is moving in a gravity field. We will solve the Lambert's problem using a numerical method. In this solution, we assume a flat earth and use topo-centric coordinates. The elevation angle of the ICBM is denoted by γ and measured from the earth's surface to the tip of the missile. The central angular distance to be traveled is denoted by ϕ and measured from the earth's center between the target location and the launch location [9]. The radius of the earth is denoted by R_e . Note that (2.2) gives the required velocity of the ICBM for a given distance. Since the launch point and target location are both on the ground,

$$r_o = a = R_e \quad (2.35)$$

is a valid statement. Using (2.35) we can rewrite the required velocity equation in closed form [9] as

$$V_{req} = \sqrt{\frac{gm(1 - \cos \phi)}{R_e \cos(\gamma)(\cos \gamma - \cos(\phi + \gamma))}} \quad (2.36)$$

The time of flight for the ICBM can be calculated by using the formula for the elliptical travel as given by [9]

$$t_F = \frac{R_e}{V_{req} \cos(\gamma)} \left\{ \frac{\tan \gamma (1 - \cos \phi) + (1 - \lambda) \sin \phi}{(2 - \lambda) \left[\frac{1 - \cos \phi}{\lambda \cos^2 \gamma} + \frac{\cos(\gamma + \phi)}{\cos \gamma} \right]} + \frac{2 \cos \gamma}{\lambda [(2/\lambda) - 1]^{1.5}} \tan^{-1} \left(\frac{\sqrt{(2/\lambda) - 1}}{\cos \gamma \cot(\phi/2) - \sin \gamma} \right) \right\} \quad (2.37)$$

where λ is a constant and is given by [9]

$$\lambda = \frac{V_{req}^2 R_e}{gm} \quad (2.38)$$

The central angular distance ϕ can be calculated using the position vectors of the launch point and the target location:

$$\phi = \cos^{-1} \frac{\vec{r}_i \cdot \vec{r}_t}{\|\vec{r}_i\| \|\vec{r}_t\|} \quad (2.39)$$

where \vec{r}_i and \vec{r}_t are the launch point position vector and target location position vectors, respectively, in the ECEF coordinate system.

By substituting (2.38) into (2.36) and solving for the elevation angle, we obtain the minimum and maximum possible elevation angles as follows [9]:

$$\gamma_{\min} = \tan^{-1} \left(\frac{\sin \phi - \sqrt{2(1 - \cos \phi)}}{(1 - \cos \phi)} \right) \quad (2.40)$$

$$\gamma_{\max} = \tan^{-1} \left(\frac{\sin \phi + \sqrt{2(1 - \cos \phi)}}{(1 - \cos \phi)} \right)$$

We will use the method described in [9] to find the elevation angle corresponding to the desired flight time $t_{F_{des}}$, which is calculated by using (2.37). The flight time is calculated iteratively by using elevation angles between the γ_{\min} and γ_{\max} (see (2.40)) in order to reach a value that is satisfactorily close to the desired flight time as follows [9]

$$\gamma_{n+1} = \gamma_n + \frac{(\gamma_n - \gamma_{n-1})(t_{F_{des}} - t_{F_n})}{t_{F_n} - t_{F_{n-1}}} \quad (2.41)$$

where n is the index of iteration. The elevation angle γ is computed for North Korea, China and Iran are 54.22° , 55.98° and 58.92° , respectively.

Note that the Lambert Solution assumes an impulsive missile moving in free space. However, the ICBM model created is a three-stage solid-propellant missile, hence the actual elevation angles for a boosting ICBM moving on a rotating earth and in the atmosphere are different from the above values. The elevation angle for a boosting missile should be above 80° to overcome the gravity force and avoid hitting the ground [9]. To find the accurate elevation angles, the three-dimensional motion simulation is run and the results are reported in the following section.

B. SIMULATION RESULTS FOR THE ICBM MODEL

The preceding analysis is implemented numerically and simulated by using MATLAB[®]. The booster fuel consumption is simulated by decreasing the amount for every time step. The time step is selected as 0.05 s as a trade-off between the accuracy of integration and the available computational power. The initial state vector of the ICBM is denoted by its launch location and launch attitude. The launch attitude is defined by the azimuth launch angle and elevation launch angle, which are given in topo-centric coordinates and transferred to the ECEF coordinate system. The initial attitude of the missile is represented in the initial velocity vector of the ICBM. The location of the missile is given in the geodetic coordinate system and it is also transferred to the ECEF coordinate system. The location of the missile is represented in the position portion of the state vector. Having the initial state vector and the transition matrix meets the requirements to run the simulation. The launch angles for the ICBMs launched from North Korea, China and Iran to reach San Francisco are given in Table 3.

Table 3. Initial launch parameters for ICBMs.

	North Korea	China	Iran
Elevation launch angle in degrees	85.81	85.15	84.1
Azimuth launch angle in degrees from North to East	39.6	19.8	342.1
Location in geodetic coordinates	N41 E129	N36 E101	N29 E51

The initial state vectors in the ECEF coordinate system for a San Francisco attack for running simulations are as follows

$$X_{N.Korea}(0) = \begin{bmatrix} -3025933.19 \text{ m} \\ 3736716.22 \text{ m} \\ 4179752.70 \text{ m} \\ -9.10 \text{ m/s} \\ 9.82 \text{ m/s} \\ 13.04 \text{ m/s} \end{bmatrix}; X_{China}(0) = \begin{bmatrix} -983476.74 \text{ m} \\ 5059549.23 \text{ m} \\ 3744779.84 \text{ m} \\ -3.11 \text{ m/s} \\ 13.32 \text{ m/s} \\ 11.70 \text{ m/s} \end{bmatrix}; X_{Iran}(0) = \begin{bmatrix} 3506700.44 \text{ m} \\ 4330414.40 \text{ m} \\ 3088722.09 \text{ m} \\ 9.76 \text{ m/s} \\ 11.15 \text{ m/s} \\ 10.22 \text{ m/s} \end{bmatrix} \quad (2.42)$$

Given the initial state vectors, the state vectors at a future time instant $t + \Delta t$ can be computed using the iterative relationship [10]

$$X(t + \Delta t) = X(t) + FX(t)\Delta t \quad (2.43)$$

where Δt is the iteration time step and F is the state transition matrix. Equation (2.43) is iterated in time along with the decreasing amount of propellant fuel. The rotation of the earth, the drag force and the thrust are also integrated in the simulation as outlined in (2.26).

The geometry of the trajectories of the ICBMs launched from North Korea, China and Iran are illustrated in Figure 7. The trajectory of the Iranian ICBM passes through the North Pole, which explains the reason why the azimuth launch angle is towards the north.

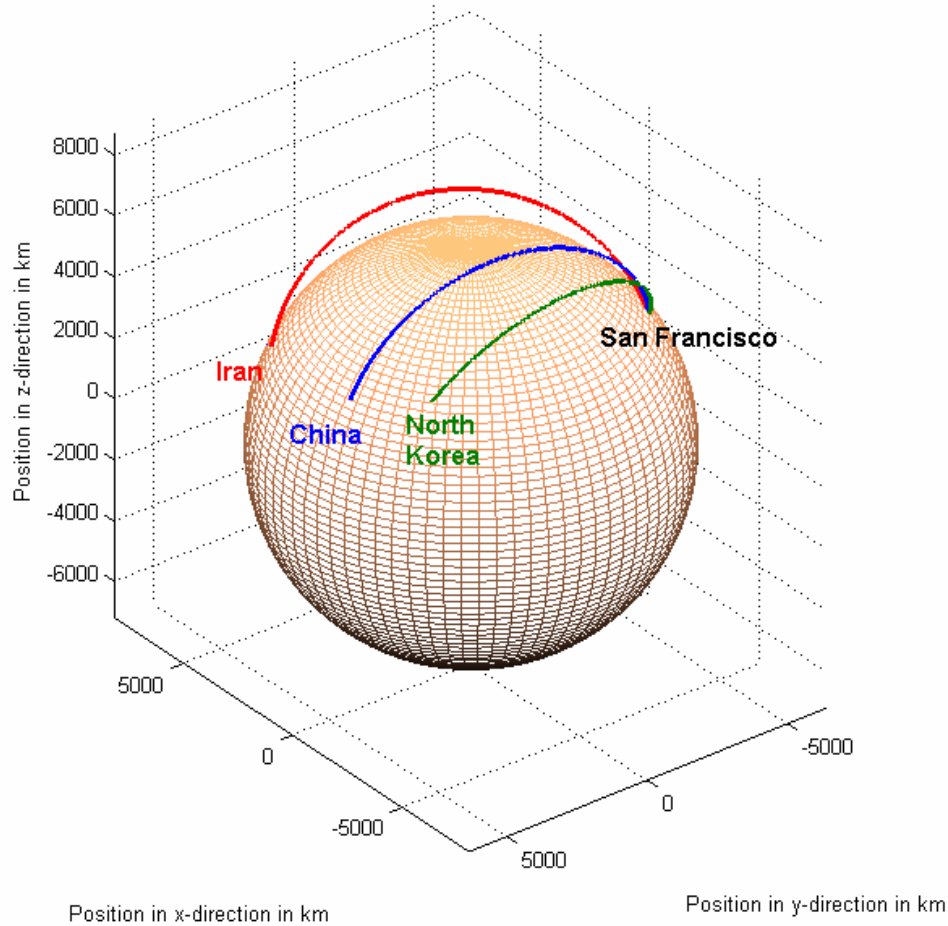


Figure 7. Trajectories of the ICBMs launched from North Korea, China and Iran.

The magnitudes of the velocities of the three ICBMs obtained from the simulation are shown in Figure 8. The velocity increases during the boost-phase, which lasts for about three minutes. After the boost-phase, the velocity starts to decrease because of the gravitational effect while the ICBM continues ascending. After the ICBM starts to turn downwards, the gravitational force acts in favor of the ICBM velocity and increases the velocity. This increase in the velocity persists until the ICBM enters the atmosphere. Once the ICBM enters the atmosphere, the drag forces become significant and decrease the ICBM velocity.

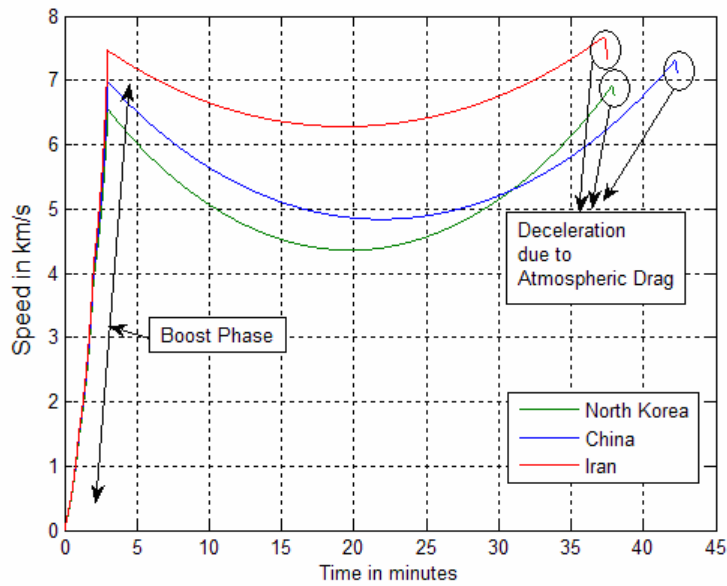


Figure 8. Magnitudes of the velocity vectors of the ICBMs throughout the entire flight. The earth's rotation and the atmospheric drag are included

The boost-phase, where the velocity increases very rapidly, is the most dynamic region for the ICBM. In taking a close look at the velocity graph during the boost-phase, Figure 9 illustrates the stage transitions of the ICBM. Remember that the required velocity of the ICBM is proportional to the distance between the target and the launch point. Note that the maximum velocity at the end of the boost-phase has the increasing order in sequence of North Korea, China and Iran. This sequence is also true for the distance between these launch points and San Francisco.

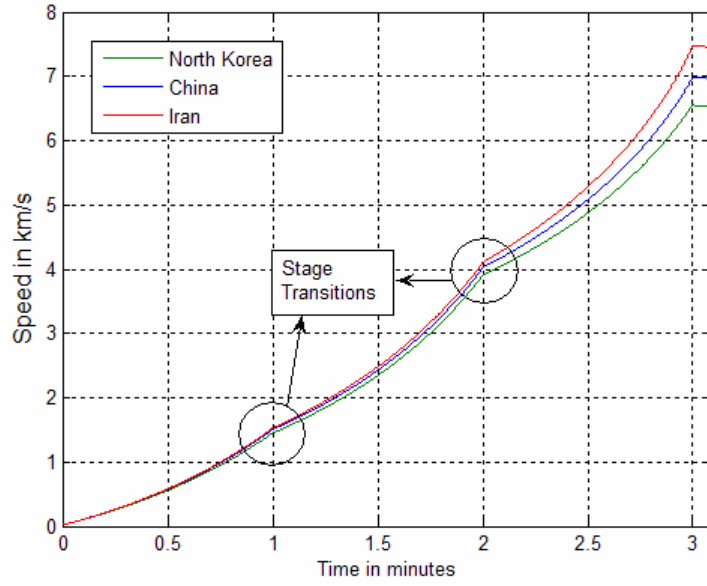


Figure 9. Magnitudes of the velocity vectors of the ICBMs during boost-phase.

In addition, the required velocity is approximately 1 km/s less than that estimated using closed form rocket equation (2.2). The required velocities computed by both the rocket equation and the simulation are shown in Table 4. The simulation results are more reliable than the rocket equation results because they include the boosting ICBM conditions whereas the rocket equation results assumes an impulsive missile (initial velocities model).

Table 4. Required velocities.

Launch Site	Required Velocity (km/s)		Distance (km)
	Rocket Equation Results	Simulation Results	
North Korea	7.49	6.55	8700
China	8.12	6.98	10700
Iran	8.65	7.47	12500

The altitudes of the ICBMs are calculated by using the state vectors. Since the earth is modeled as a sphere, the altitude of the ICBM can be written as a function of the ICBM position:

$$A = \sqrt{x^2 + y^2 + z^2} - R_e \quad (2.44)$$

where x , y and z are the position components of the ICBM in the ECEF coordinate system, and R_e is the radius of the earth. The altitudes of the ICBMs are shown in Figure 10. An exponential increase in the altitude is observed during the boost-phase, which increase is a result of the increasing velocity.

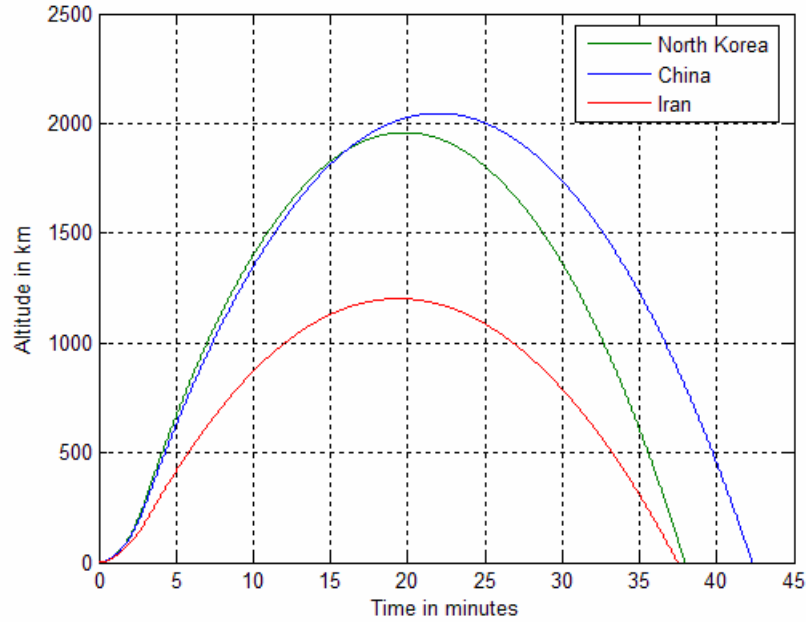


Figure 10. Altitudes of the ICBMs during the entire flight.

The total mass of the ICBM is shown in Figure 11. The total mass is the sum of the payload, the remaining propellant mass and the remaining canister mass. The total mass decreases as the ICBM burns the propellant fuel and releases the canister after the depletion of the propellant fuel. At the end of the boost-phase, only the payload is left having a mass of 2268 kg.

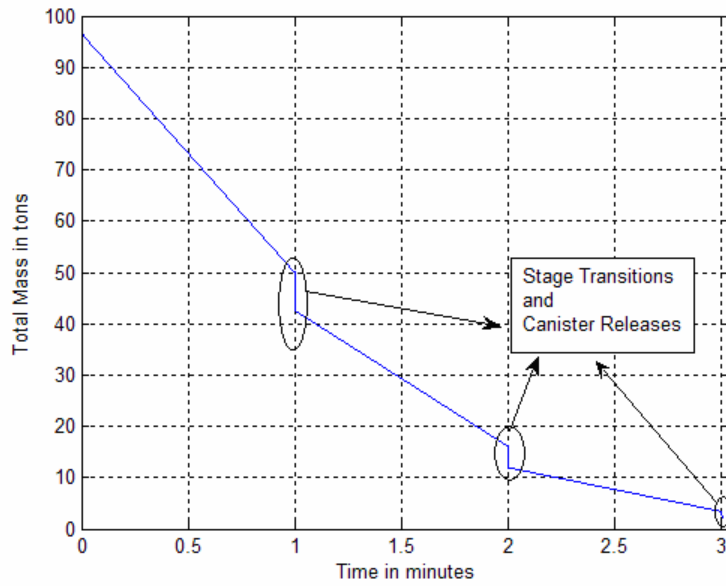


Figure 11. Total mass of the ICBMs as a function of the time from launch.

After the depletion of the propellant mass in a stage, the empty canister is released and use of the propellant fuel in the next stage begins. The decrease of the propellant mass is shown in Figure 12. The propellant mass is used up in three minutes, which is the end of the boost-phase.

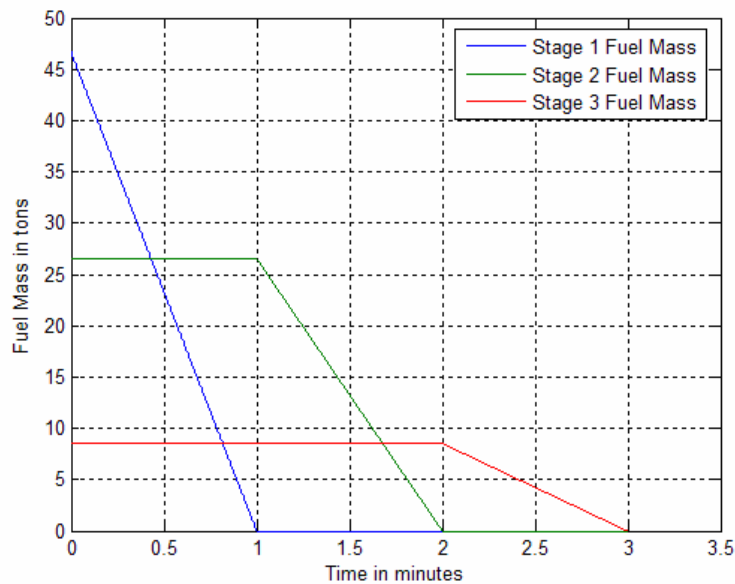


Figure 12. Propellant mass of the ICBMs during the boost-phase.

The overall simulation results are tabulated in Table 5. The burn out time, the altitude of the ICBM and the burn out velocities are tabulated for each stage transition. The maximum altitude is the utmost altitude of the ICBM during the entire flight. The total flight time denotes the time when the ICBM hits the target.

Table 5. Simulation results for ICBMs from North Korea, China and Iran.

Launch Site	Stage 1		Stage 2		Stage 3		Maximum Altitude (km)	Total Flight Time (minute)
	Altitude (km)	Velocity (km/s)	Altitude (km)	Velocity (km/s)	Altitude (km)	Velocity (km/s)		
North Korea	28.73	1.44	119.34	3.9	281.66	6.55	1959	37.96
China	28.24	1.50	112.94	4.02	262.2	6.98	2047	42.32
Iran	24.31	1.52	85.56	4.1	182.02	7.47	1202	37.47

C. SUMMARY

In this chapter, a mathematical model for the ICBM motion is derived taking the earth's rotation and the atmospheric drag into account. The three example ICBMs launched from North Korea, China and Iran have different mass fractions in order to reach San Francisco from different ranges. The entire flight of these example ICBMs are simulated by using the developed mathematical model.

THIS PAGE INTENTIONALLY LEFT BLANK

III. ORBIT SELECTION FOR EKV CARRIERS

In this chapter, we will describe the configuration and specifications of the space-based exo-atmospheric kill vehicle (EKV) carriers and the EKV itself, and determine an orbit in which to place these EKV carriers in order to intercept ICBMs launched from three example launch sites in North Korea, China and Iran prior to the release of the reentry vehicles (RVs). The trajectories of the ICBMs were derived and simulated in the previous chapter and the resulting trajectories are used to determine the orbit that is required for a successful intercept. We will show that for the given launch locations, we need a circular orbit with an altitude of 1000 km, an inclination angle of 43.5° and a right-ascension angle of 15.3° .

A. INTERCEPTOR MISSILE MODELING

In this study, we will model an EKV that conducts a hit-to-kill intercept. Hit-to-kill interception is selected because the damage applied in space is significantly more than the damage applied by conventional explosive interceptors. The EKV must hit the payload section of the ICBM in order to assure the desired hard kill [16].

Raytheon has developed a ground-based EKV and tested it successfully. The model of the EKV considered in this study will be based on the specifications of the Raytheon EKV. We will use this model as a space-based EKV instead of a ground-based EKV [17]. The Raytheon's EKV is shown in Figure 13.

The IR detectors of the EKV are capable of determining the spatial location of the target and discriminating the target from the decoys [17]. The scope of this study is focused on the boost-phase intercept in which it is assumed that the ICBM cannot deploy its decoys. However, this discrimination capability gives the EKV the flexibility to be used in mid-course as well. The EKV kills its target through the force created by the impact.

The EKV has four thrusters for applying the guidance command generated by the guidance unit, as shown in Figure 13. In addition, the EKV has two attitude controllers which will cooperate with the divert thrusters and control the attitude of the EKV. Note that the EKV would tumble in outer space without these attitude controllers. The EKV

has onboard sensor optics to track the target and a guidance unit which improves the target data refresh rate and decreases the delay between the tracking and guidance application. The optic sensors are protected by a sunshade cover, as shown in Figure 13.

An ICBM has two different IR sources, including the plume and the body friction. The plume has a mid-wave ($3-5 \mu\text{m}$) infrared signature generated by high temperature emissions from the nozzle. The body friction produces a long-wave infrared signature ($8-12 \mu\text{m}$) [18]. The EKV has to have two different infrared sensor sets to track both of these sources.

The EKV weighs 64 kg with a length of 139.7 cm and a diameter of 61 cm [17]. We added a 136 kg of booster to the EKV to give it the initial velocity when launched from the EKV carrier. The solid propellant in the booster is 100 kg, which makes the EKV's total mass 200 kg.

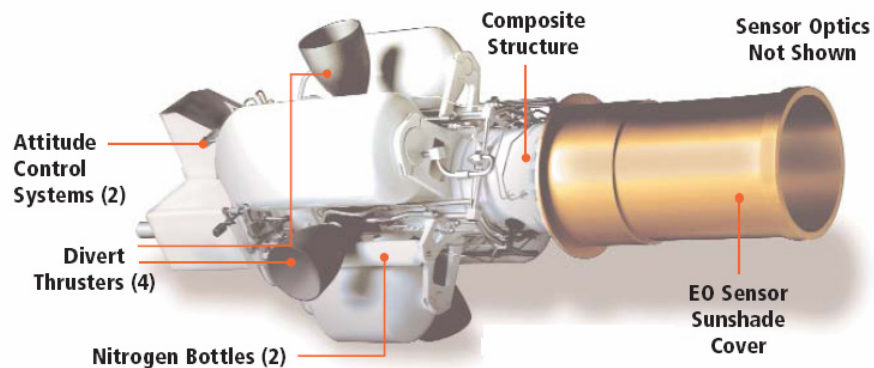


Figure 13. Raytheon's exo-atmospheric kill vehicle (From [17]).

The EKVs are stored in a space-based EKV carrier, which is assumed to hold 10 EKVs. The EKV carriers travel on an orbit that provides enough kinetic energy to allow the EKVs to succeed in destroying the ICBM before it delivers the reentry vehicles (RVs). Accomplishing a boost-phase intercept will decrease the amount of targets that need to be dealt with.

The EKV is modeled using the same methodology that was introduced in Chapter II. The EKV boosts for 10 s and then moves into the gravity field with the guidance com-

mand. The guidance command is applied by the onboard divert thrusters in pitch and yaw axis. The guidance method and application will be discussed thoroughly in Chapter IV.

B. ORBITAL ELEMENTS

The laws that describe the motion of the planets in the solar system also describe the motion of a spacecraft orbiting around a planet. Johannes Kepler (1571-1630) derived three empirical laws to describe the motion of planets by using his observations. The motion of any two bodies in space can be characterized by his laws [12].

1. Keplerian Orbit

We introduce the Keplerian orbit and orbit perturbations in the following discussion. The shape, size and orientation of the orbit is defined by its orbital elements, which are illustrated in Figure 14 [19] and are described below briefly.

Perigee is a point on the orbit that is closest to the earth's center. Apogee is a point on the orbit that is farthest from the earth's center. Ascending node is defined as the point of intersection of the orbit and the equatorial plane. The orbit passes from south to north on the ascending node. Descending node is also defined as the point of intersection of the orbit and the equatorial plane. However, the orbit passes from north to south on the descending node. Inclination angle is defined as the angle between the orbital plane and the equatorial plane. It is denoted by i and measured from the normal of the orbital plane to the normal of the equatorial plane. It is the greatest latitude of the orbit, either on the southern hemisphere or on the northern hemisphere [12].

The argument of perigee is the angle between the ascending node and the perigee. It is denoted by γ and is measured in the orbital plane at the center of the earth, in the direction of the satellite motion [12].

Right-ascension of the ascending node is measured starting from the line of Aires eastward to the ascending node. The longitude of the ascending node is frequently used as the right-ascension of the ascending node [12]. The right-ascension is denoted by Ω . In this study, we assume that the right-ascension is the angle on equatorial plane measured eastward from the E0 longitude (Greenwich) to the ascending node.

The mean anomaly is the angular position of the satellite relative to the ascending node. The angle is measured from the center of the orbit. This is the angle that a vehicle

would travel starting from the ascending node for a given time at a given angular velocity. The mean anomaly is denoted by ω [21].

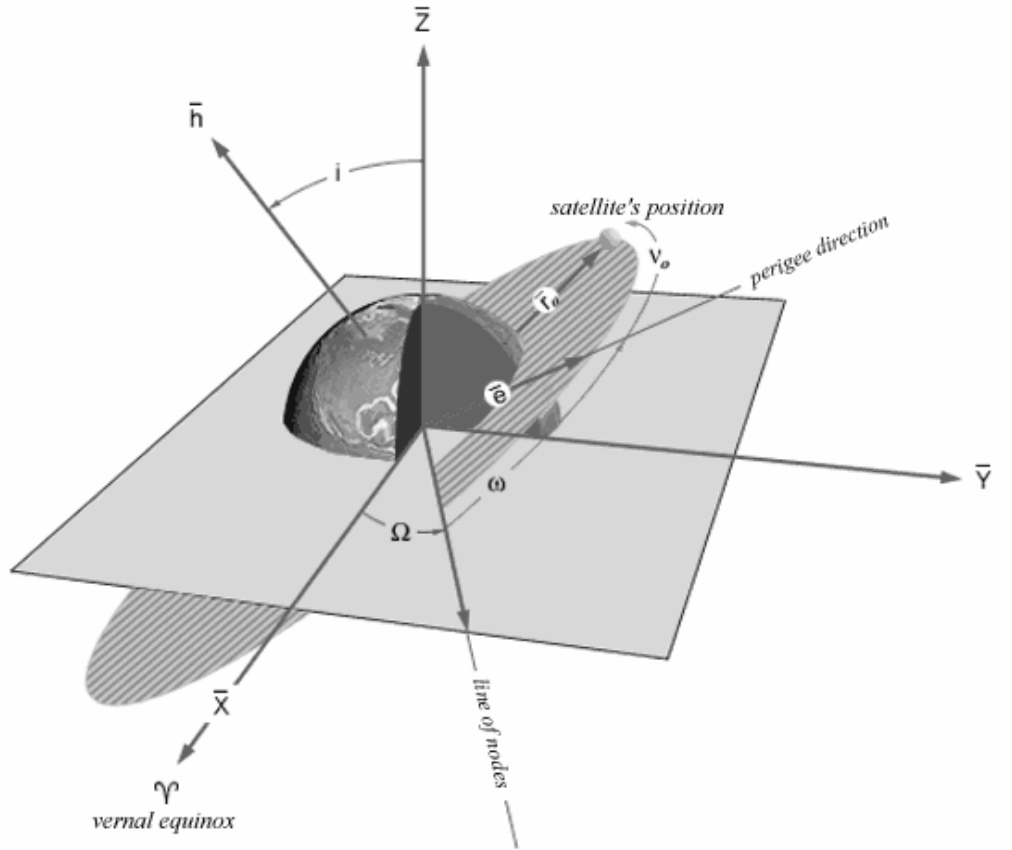


Figure 14. Orbital elements (Adapted from [20]).

Kepler's first law defines the path of the orbit that is followed by a spacecraft as an ellipse. The earth sits at the center of the ellipse. The shape and parameters of an elliptical orbit are shown in Figure 15.

The semi-major axis is denoted by a and the semi-minor axis is denoted by b [12]. The eccentricity is denoted by e and given by Kepler's first law as [21]

$$e = \frac{\sqrt{a^2 - b^2}}{a} \quad (3.1)$$

The orbit can be a circle ($e = 0$), ellipse ($0 < e < 1$), parabola ($e = 1$) or hyperbola ($e > 1$) [12].

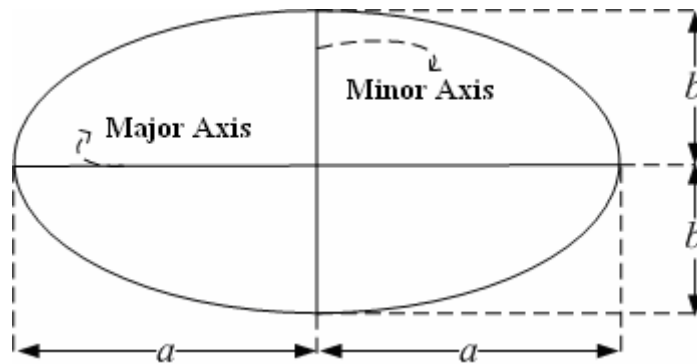


Figure 15. The semi-major axis and the semi-minor axis of an ellipse.

Kepler’s second law assumes that the area on the orbital plane subtended by each vehicle’s travel at equal time intervals will be equal to each other [21]. Kepler’s third law defines the relationship between the semi-major axis of the orbit a and the angular mean motion of the vehicle n_o (rad/s) as given by [22]

$$a^3 = \frac{\mu_e}{n_o^2} \quad (3.2)$$

where μ_e is earth’s geocentric gravitational constant ($3.986005 \times 10^{14} \text{ m}^3/\text{s}^2$).

The preceding equation assumes a perfect orbit without any perturbation effects. This law shows that there is a fixed relationship between period and the size of the orbit: the square of the angular mean motion of the spacecraft is inversely proportional to the cube of the semi-major axis [12].

2. Orbit Perturbations

The Keplerian orbit assumes that the earth is a perfect sphere with a uniform mass, and the gravitational force and the centrifugal force caused by the spacecrafts’ motion are the only forces acting on the spacecraft [12]. However, the orbit will suffer some disturbance due to several effects. Earth’s oblate shape is the major perturbation that affects the orbit. There are several other causes of perturbation, such as gravitational forces of the sun and the moon, atmospheric drag and solar radiation pressure [22]. The gravitation forces of the sun and the moon are negligible for the spacecrafts moving on a low

orbit. The oblate shape of the earth effects the mean motion of the orbit leading to a new definition for the mean motion [12]:

$$n = n_0 \left(1 + \frac{K_1 (1 - 1.5 \sin^2 i)}{a^2 (1 - e^2)^{1.5}} \right) \quad (3.3)$$

In (3.3), K_1 is a constant (66,063.1704 km²). The equation for the nominal mean motion is derived by re-arranging (3.2) as [12]

$$n_o = \sqrt{\frac{\mu_e}{a^3}} \quad (3.4)$$

The perturbation effects other than earth's oblate shape are neglected in this study. It is assumed that earth's oblate shape only affects the mean motion of the vehicle in orbit.

C. ASSUMPTIONS AND REQUIREMENTS

The hostile ICBMs are assumed to be located in Kilju-kun, North Korea (N 41° E 129°), Xining, China (N 36° E 101°) and Bushehr, Iran (N 29° E 51°). The ICBMs of these rogue states are assumed to have the same characteristics. The mathematical model for these ICBMs were introduced in Chapter II. The geographical locations of these bases are shown in Figure 16 – 18 [23]. The images of the figures were generated using Google Earth® on 5 June 2005. Recently, Iran has been seeking opportunities to improve the nuclear reactor in Bushehr. There are some clues to prove that Iran has some missile activities in Bushehr [24].



Figure 16. The geographical location of Kilju-kun Missile Base, North Korea (After [23]).



Figure 17. The geographical location of Xining, China (After [23]).



Figure 18. The geographical location of Bushehr, Iran (After [23]).

The ICBMs that are launched from the above sites are assumed to target San Francisco, California. The orbit of the EKV carriers should cover all three sites, i.e., the inclination angle and the right-ascension angle should meet this requirement. The EKVs that are in the orbit will have the same specifications and will be used against any of the three launch sites. Consequently, we should select a circular orbit to guarantee uniform coverage ($e \cong 0$).

The intercept should take place after the boost-phase of the ICBM and prior to the release of the RVs and decoys. In addition, the EKV is required to kill the ICBM with the damage caused by physical impact. In other words, the EKV should achieve a hit-to-kill intercept. The time interval (window) for the intercept is assumed to be 15 s, and the intercept should occur at the end of the boost-phase (three minutes after launch) and before the release of the RVs (three minutes and 15 s after launch). In this study, we ensure that the intercept occurs before the delivery of the RVs.

The altitude of the orbit depends on several requirements and limitations. The maximum range of the EKV within the intercept window is the major limitation for the orbit altitude. The orbit altitude should give enough time and distance to allow the EKV to accomplish its mission. That is, if you put the orbit at a very high altitude, the EKV will not be able to intercept the ICBM before it delivers the RVs. The capability of the

space launcher that will deliver the EKV carriers to the orbit is another important factor for determining the altitude of the orbit. The altitude of the orbit is also a measure of the lifetime of the system.

D. ORBIT DERIVATION

We determine the parameters of a circular orbit according to the assumptions and requirements described above. The parameters to be calculated include the inclination angle i , altitude of the orbit r_a , and the right-ascension of the ascending node Ω .

1. Analytical Solution for Orbit Determination

Since we selected the circular orbit, the semi-major axis and the semi-minor axis are both equal to the sum of the altitude of the orbit and the radius of the earth. The argument of perigee, the mean anomaly and the eccentricity are also defined inherently in the circular orbit ($e \cong 0$). After calculating these parameters and knowing the maximum range of the EKV, the required number of EKV carriers may be estimated. The parameters of interest are shown in Figure 19.

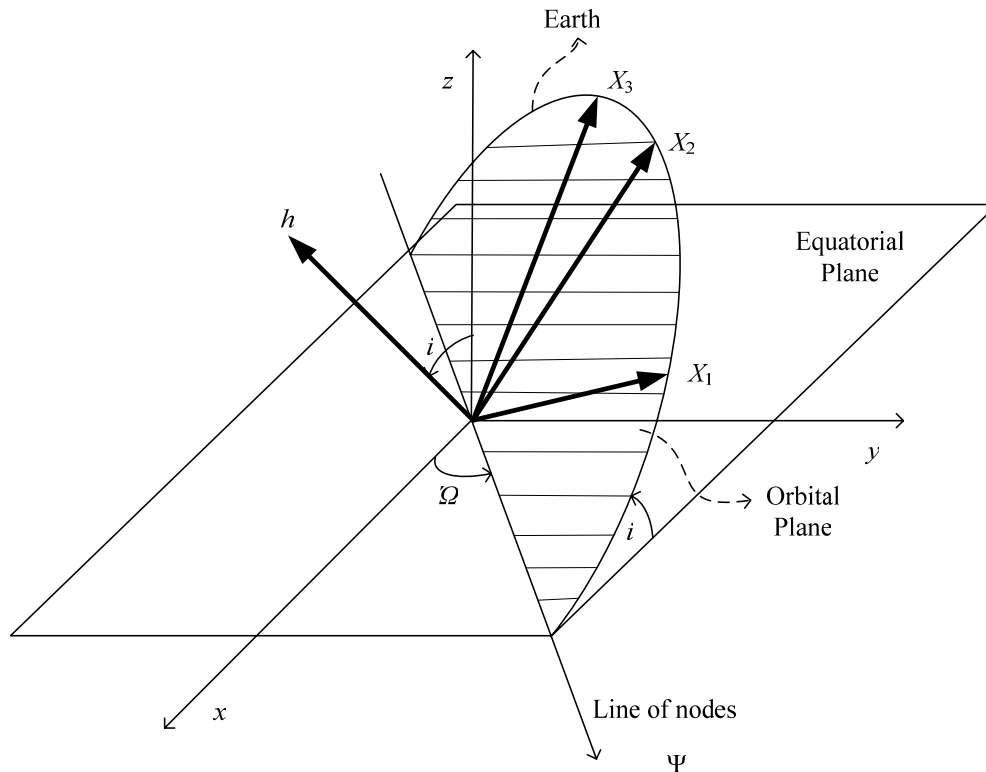


Figure 19. Orbital plane and the launch sites.

a) ***Inclination Angle***

The inclination angle is determined such that the EKV carrier passes over all the launch sites. The orbit of the EKV carriers defines an orbital plane that has the earth's center as the origin and is shown in Figure 19. The equatorial plane includes the equator as a circle and has the same origin with the earth. The angle between these two planes at the center of the earth is the inclination angle. The ICBM launch sites are denoted by vectors X_1 (North Korea), X_2 (China) and X_3 (Iran) in Figure 19. Ideally, these sites would lie on the same global circle to let us use one orbit for all. These vectors should be members of the orbital plane by definition. The launch locations are given in geodetic coordinates, so we need to convert to the ECEF coordinate system before doing further calculations. The locations are first transformed to spherical coordinates and then to the ECEF coordinates for convenience. The conversion from spherical coordinates to the ECEF is given by [25]

$$X = \begin{bmatrix} x \\ y \\ z \end{bmatrix} = \begin{bmatrix} R_e \sin \theta \cos \phi \\ R_e \sin \theta \sin \phi \\ R_e \cos \theta \end{bmatrix} \quad (3.5)$$

The spherical angles θ and ϕ are illustrated in Figure 20.

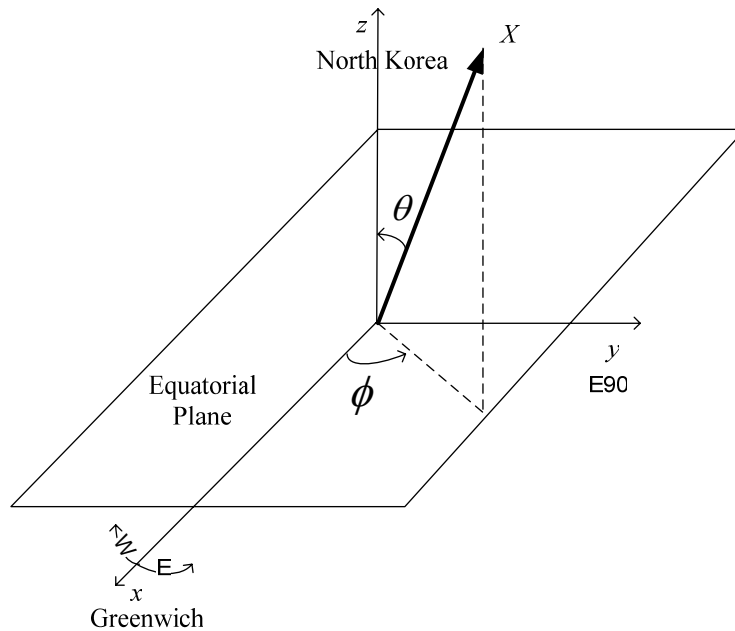


Figure 20. The spherical angles of the given location.

The spherical angle θ for the locations in the northern hemisphere is calculated using the latitude as

$$\theta = \frac{\pi}{2} - \mu \quad (3.6)$$

where μ is the geodetic latitude. The spherical angle ϕ is the longitude. The range R_e is the radius of the earth.

Kilju-kun, North Korea:

The spherical coordinate parameters for Kilju-kun are $R_e = 6371$ km, $\theta = 90^\circ - 41^\circ = 49^\circ$ and $\phi = 129^\circ$. The vector X_1 can now be calculated in the ECEF coordinate system using (3.5) as

$$X_1 = \begin{bmatrix} -3025.93 \text{ km} \\ 3736.72 \text{ km} \\ 4179.75 \text{ km} \end{bmatrix}$$

Xining, China:

The spherical coordinate parameters for Xining, China are $R_e = 6371$ km, $\theta = 90^\circ - 36^\circ = 54^\circ$, $\phi = 101^\circ$. The vector X_2 can now be calculated in the ECEF coordinate system using (3.5) as

$$X_2 = \begin{bmatrix} -983.48 \text{ km} \\ 5059.55 \text{ km} \\ 3744.78 \text{ km} \end{bmatrix}$$

Bushehr, Iran:

The spherical coordinate parameters for Bushehr, Iran are $R_e = 6371$ km, $\theta = 90^\circ - 29^\circ = 61^\circ$ and $\phi = 51^\circ$. The vector X_3 can be calculated in the ECEF coordinate system using (3.5) as

$$X_3 = \begin{bmatrix} 3506.70 \text{ km} \\ 4330.41 \text{ km} \\ 3088.72 \text{ km} \end{bmatrix}$$

The X_1 , X_2 and X_3 vectors now define the orbital plane and the inclination angle. The inclination angle can also be described as the angle between the *normal* of the orbital plane and the *normal* of the equatorial plane. The normal vector of the orbital plane h is calculated by taking the cross product of X_1 and X_3 vectors and is given by

$$h = \begin{bmatrix} 6558382.10 \\ -24003403.75 \\ 26207085.48 \end{bmatrix} \quad (3.7)$$

The normal of the equatorial plane can be any vector along the z-axis, so we can select an arbitrary vector on z-axis as

$$Z = \begin{bmatrix} 0 \\ 0 \\ 6371 \text{ km} \end{bmatrix} \quad (3.8)$$

The dot product of the *normal* of the orbital plane and the *normal* of the equatorial plane divided by the product of the magnitudes of these vectors gives us the cosine of the inclination angle. Hence the inclination is calculated as

$$i = \arccos\left(\frac{h \cdot Z}{\|h\| \cdot \|Z\|}\right) = 0.76 \text{ radians or } 43.52^\circ \quad (3.9)$$

Now we know the inclination angle of the circular orbit. We will target this orbit around the earth by calculating the right-ascension angle.

b) Right-ascension of the Ascending Node

Right-ascension angle is measured eastward from the longitude 0 (Greenwich) to the ascending node of the orbit. In other words, it is the longitude of the ascending node. As shown in Figure 19, the line of nodes is the intersection of the equatorial plane and the orbital plane. The line of nodes will pass from the ascending node and the descending node. The cross product of the normal vectors of these two planes will define the line of nodes. The line of nodes Ψ is given by

$$\Psi = Z \times h \quad (3.10)$$

which is defined from the center of the earth in the ECEF coordinate system as

$$\Psi = \begin{bmatrix} x_{\psi} \\ y_{\psi} \\ z_{\psi} \end{bmatrix} = \begin{bmatrix} 152925685295.96 \\ 41783452372.92 \\ 0 \end{bmatrix} \quad (3.11)$$

The line of nodes lies along the equatorial plane, which is ensured by the z value of the vector being zero. The tangent of the right-ascension angle (Ω) is defined by the x and y elements of the line of nodes vector. The right-ascension angle is computed as given by

$$\Omega = \arctan\left(\frac{y_{\psi}}{x_{\psi}}\right) = 0.27 \text{ radians or } 15.28^{\circ} \quad (3.12)$$

Since the right-ascension angle is the longitude of the ascending node, the orbit crosses the equator from south to north at longitude 15.28° .

c) *Altitude of the Orbit*

The EKV carriers will encounter atmospheric drag in low orbits. This drag will increase exponentially as the altitude of the orbit decreases. For example a 100-km decrease from 700-km of altitude will increase the drag to be overcome by five times [20].

The EKV carriers use their onboard thrusters to make the orbital corrections caused by the atmospheric drag, along with other altitude-dependent effects. After the depletion of the thruster fuel, the EKV carriers will start to lose altitude and reenter the atmosphere, which will be the end of their lifetime. Since the EKV carriers can carry a limited amount of thruster fuel, the altitude of the orbit will determine the lifetime of the system [20].

The launch vehicle that places the spacecraft into the orbit also has a limitation for the altitude with a given mass of payload [20]. Since we have a fixed mass of EKV, the mass of the EKV carrier is dependent on the booster fuel embedded into the EKV. Neglecting the thruster fuel that is needed to keep the EKV carrier in constant orbit, the altitude is a trade off between the mass of the booster fuel on each EKV and the capability of the space launch vehicle. As the booster fuel of the EKV increases, its maxi-

mum range will increase, which will let us choose a higher orbit. However, the increase in the booster fuel will increase the total mass of the EKV carrier, which will decrease the orbit altitude due to space launch vehicle payload mass limitations.

We have selected Titan IV as the representative launch vehicle because it is one of the most powerful expendable launch vehicles of the U.S. The total mass of Titan IV at launch is 1038 tons [26]. The payload capability of the TitanIV is up to 10,000 pounds for geosynchronous orbits and is up to 39,100 pounds for low earth orbits [28].



Figure 21. Titan IV at liftoff (From [27]).

The payload system mass as a function of the circular orbit altitude is shown in Figure 22. For example, the Titan IV can deliver a 2000 kg of payload into a circular orbit with an altitude of 1000 km.

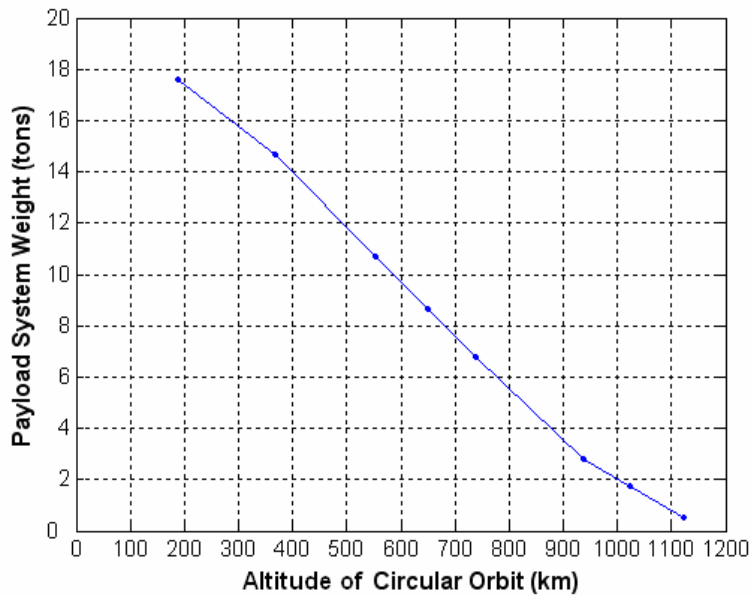


Figure 22. Space launcher (Titan IV) payload capacity (After [20]).

The resulting altitude of the EKV orbit then influences the maximum flight range of the EKV in a given time and the altitude of the desired intercept point. We assume a 30-s delay for the EKV firing after the ICBM launch, which includes the launch detection time, firing decision time and the human interface and communication latencies. We want to intercept the ICBM before the release of the RVs, which leaves the EKV two minutes and 45 s to intercept the ICBM. The maximum range of the EKV as a function of the orbit altitude for two minutes and 45 s is shown in Figure 23.

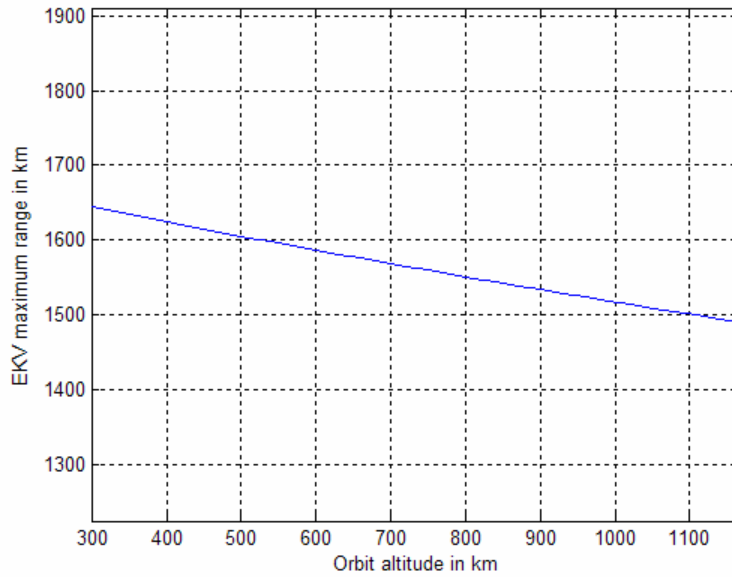


Figure 23. Maximum range of the EKV during a maximum allowable period of 2 minutes and 45 seconds

The maximum range of the EKV decreases as the orbit altitude increases because the initial velocity of the EKV decreases as the altitude decreases, which is indicated by (3.3).

We used the same motion modeling method described in Chapter II to determine the maximum range of the EKV. The ICBM launched from Iran has the minimum altitude at the end of the boost-phase, as shown in Figure 24. This altitude is the lower bound, which will require the EKV to travel the maximum range. The altitude of this ICBM three minutes and 15 s after the launch is 213 km. The geometry of the trajectories of all three ICBMs are shown in Figure 7 in Chapter II.

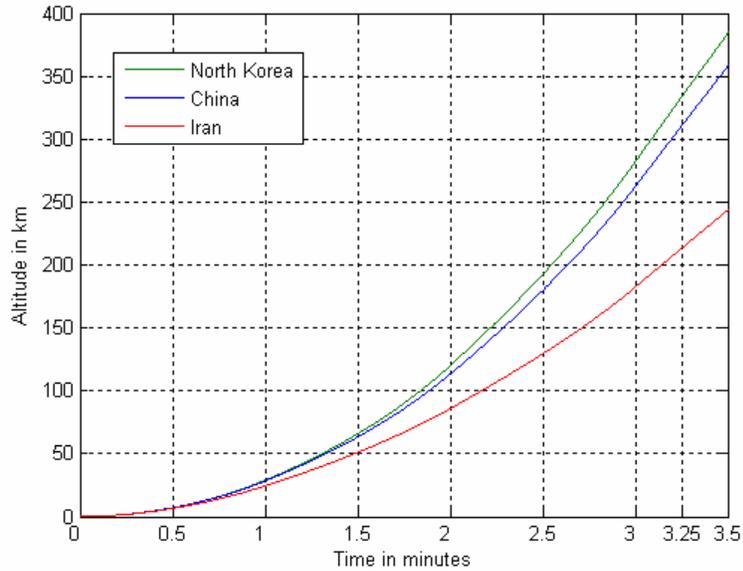


Figure 24. The altitudes of the ICBMs at the end of boost-phase.

The altitude of the orbit and the maximum range of the EKV together determine the down-look launch angle ξ and the coverage angle α as shown in Figure 25. Here we assume that the EKV cannot achieve a successful intercept after it passes over the desired intercept point due to its huge initial velocity in the direction of the orbit.

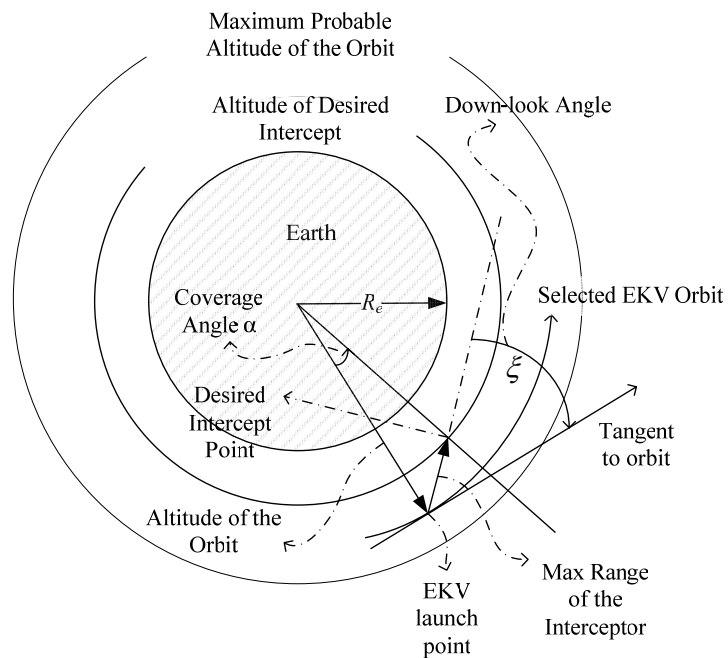


Figure 25. Orbital plane and the intercept geometry.

The maximum probable orbit altitude is determined by the mass of the payload and the capacity of Titan IV together, as shown in Figure 22. The down-look launch angle ξ is calculated using the geometry in Figure 25 and is shown in Figure 26 as a function of orbit altitude.

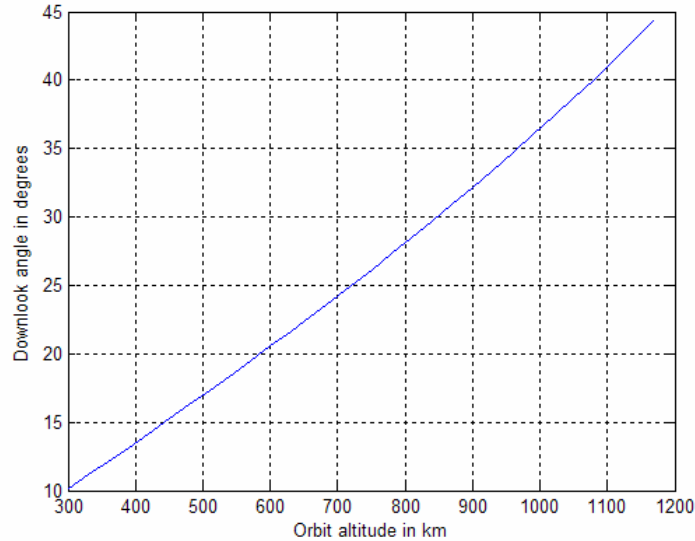


Figure 26. The down-look launch angle as a function of the orbit altitude.

The coverage angle α is measured at the center of the earth from the EKV position vector to the desired intercept point as shown in Figure 25. The coverage angle is calculated using the geometry in Figure 25 and is shown in Figure 27 as a function of orbit altitude.

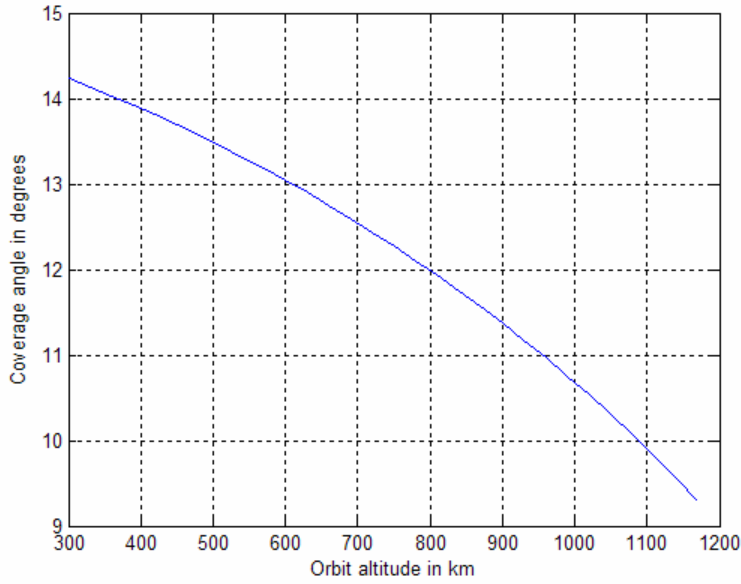


Figure 27. Maximum coverage angle as a function of orbit altitude.

The coverage angle of the EKV decreases as the altitude increases, which makes us choose a lower altitude orbit. The total mass of the system is 2000 kg, which dictates that the maximum orbit altitude be 1000 km due to space launch vehicle limitations, as shown in Figure 22. For an orbit altitude of 1000 km, a coverage angle of approximately 10.6 degrees results, as shown in Figure 27. Consequently, to cover 360 degrees requires $\lceil 360/10.6 \rceil = 34$ launchers.

Now we defined the required orbit and its elements as a circular orbit with an altitude of $r_a = 1000$ km, an inclination angle of $i = 43.52^\circ$ and a right-ascension angle of $\Omega = 15.28^\circ$. Since the orbit is circular, the eccentricity is approximately zero and the semi-major axis and semi-minor axis are both equal to the sum of the radius of the earth and the altitude of the orbit. Next we will derive the orbital parameters in the ECEF coordinate system and implement this orbit in the model we developed.

2. Numerical Implementation of the Selected Orbit

Since the orbit is defined in its own specific elements, we need to define it in the ECEF coordinate system to integrate with the model we have developed. First we will calculate spherical coordinates of the orbit and then transform them into the ECEF coordinate system.

dinate system. The spherical coordinate angles, the ECEF coordinate system and the orbit parameters are illustrated in Figure 28.

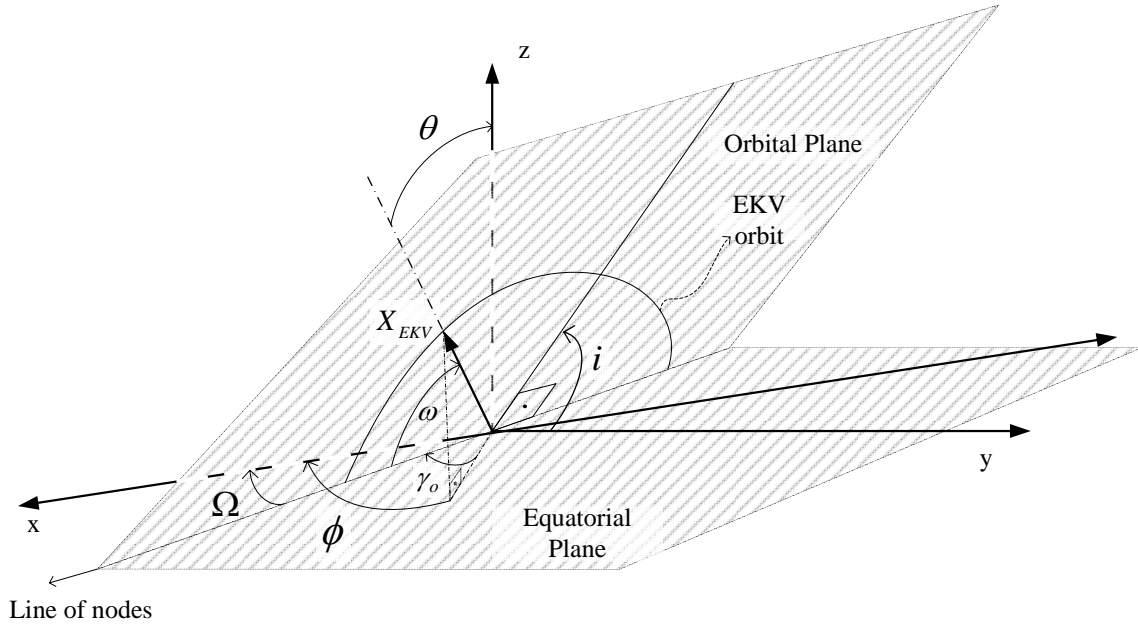


Figure 28. The orbit parameters in the ECEF and spherical coordinate systems.

In Figure 28, X_{EKV} is the current position of the EKV, Ω is the right-ascension of the ascending node and γ_o is measured from the projection of X_{EKV} on the equatorial plane to the line of nodes. The length of the X_{EKV} is the sum of the orbit altitude and the radius of the earth. The spherical angles θ and ϕ are also shown in Figure 28. The mean anomaly ω is measured from the ascending node at a given time. The time starts when the EKV crosses the ascending node and the mean anomaly as a function of time is given by

$$\omega = nt \quad (3.13)$$

After some geometry, we calculated the spherical angles as a function of inclination angle and the mean anomaly and tabulated them in Table 6.

Table 6. Spherical coordinates calculation for EKV at a given time.

Spherical Coordinates			
	θ (rad)	ϕ (rad)	$r = r_a + R_e$
$0 < \omega \leq \frac{\pi}{2}$	$\frac{\pi}{2} - \cos^{-1}\left(\sqrt{\cos^2 \omega + \sin^2 \omega \cdot \cos^2 i}\right)$	$\Omega + \tan^{-1}(\tan \omega \cdot \cos i)$	7371 km
$\frac{\pi}{2} < \omega \leq \pi$	$\frac{\pi}{2} - \cos^{-1}\left(\sqrt{\cos^2 \omega + \sin^2 \omega \cdot \cos^2 i}\right)$	$\Omega + \pi - \tan^{-1}(-\tan \omega \cdot \cos i)$	7371 km
$\pi < \omega \leq 3\frac{\pi}{2}$	$\frac{\pi}{2} + \cos^{-1}\left(\sqrt{\cos^2 \omega + \sin^2 \omega \cdot \cos^2 i}\right)$	$\Omega + \pi + \tan^{-1}(\tan \omega \cdot \cos i)$	7371 km
$3\frac{\pi}{2} < \omega \leq 2\pi$	$\frac{\pi}{2} + \cos^{-1}\left(\sqrt{\cos^2 \omega + \sin^2 \omega \cdot \cos^2 i}\right)$	$\Omega + 2\pi - \tan^{-1}(-\tan \omega \cdot \cos i)$	7371 km

After calculating the spherical coordinates, the EKV position vector is converted to the ECEF coordinate system as given by [25]

$$X_{EKV} = \begin{bmatrix} r \sin \theta \cos \phi \\ r \sin \theta \sin \phi \\ r \cos \theta \end{bmatrix}_{ECEF} \quad (3.14)$$

The above calculations are implemented and simulated in MATLAB[®] with the given conditions of ω . The orbit and the target ICBM locations are shown in Figure 29. This numerical computation of the orbit is used later to calculate the initial launch parameters of the EKV against the ICBMs that are launched from North Korea, China or Iran.

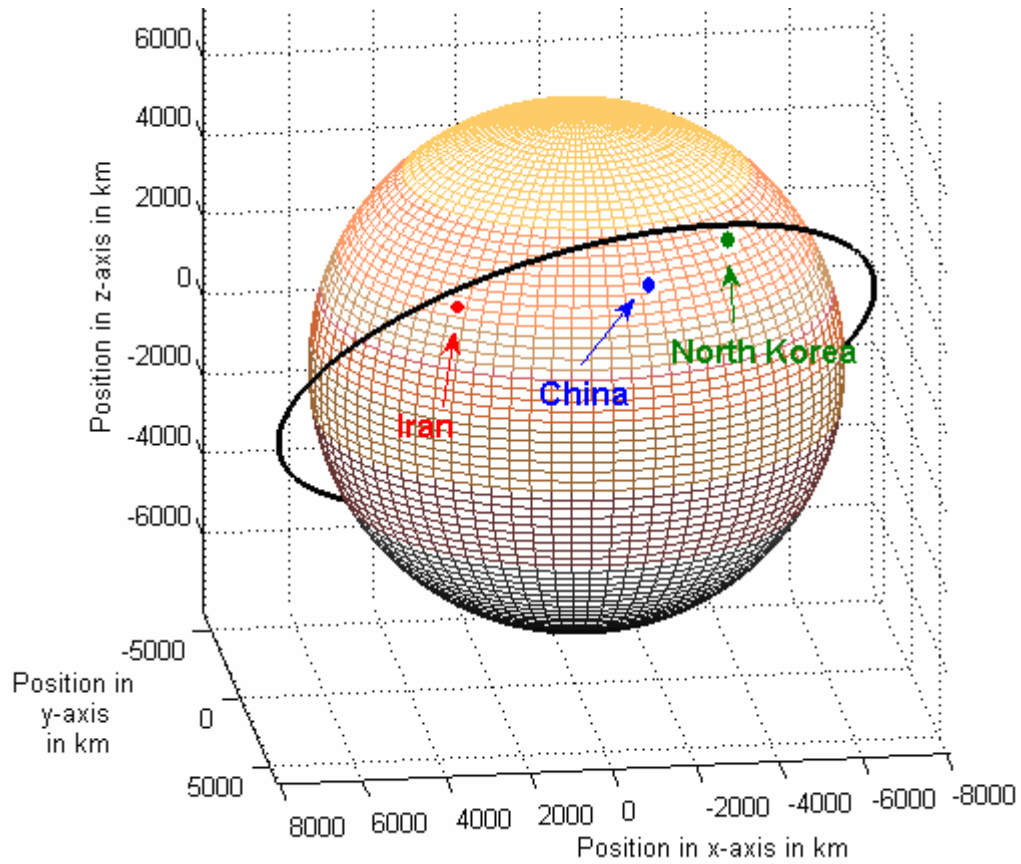


Figure 29. The orbit of the EKV and the target ICBM locations.

E. SUMMARY

In this chapter, an orbit is derived to cover the three example ICBM launch sites uniformly and continuously. The lifetime of the space system, the capabilities of the EKV and the space launch vehicle (Titan IV) are taken into account in deriving the required orbit. After selecting the orbit, it is simulated in MATLAB[®].

IV. EKV GUIDANCE METHODS

This chapter will investigate different guidance rules for space-based interception of hostile ICBMs launched from North Korea, China or Iran. The pursuit guidance (PG), proportional navigation guidance (PNG) and bang-bang guidance (BBG) rules will be introduced and a three-dimensional implementation will be presented. The total commanded acceleration, intercept time, and miss distance generated by these guidance rules for the given scenario will be the major parameters considered to select one of them or combine them properly.

A. DESCRIPTION OF THE SCENARIO

The interceptor missile is a one-stage, boosted, exo-atmospheric kill vehicle (EKV) orbiting in a circular LEO orbit with an inclination angle of $i = 43.52^\circ$, a right-ascension angle of $\Omega = 15.28^\circ$ and an altitude of $r_a = 1000$ km. The target ICBMs are coming from North Korea, China and Iran. The coordinates of these launch sites are N49-E129, N36-E101 and N29-E51, respectively. The ICBMs are targeting the city of San Francisco, California.

B. COORDINATE SYSTEMS AND COORDINATE CONVERSIONS

In this chapter, three different coordinate systems will be introduced. First, the common coordinate system that will be used in the calculations will be the Earth-centered Earth-fixed (ECEF) coordinate system (X_E, Y_E, Z_E). The ECEF coordinate system is a three-dimensional orthogonal Cartesian coordinate system with the origin at earth's center. The x-axis passes through Greenwich (E0), the y-axis passes through E90 and the z-axis passes through the North Pole. The spherical earth rotates about z-axis. We assume that the earth is a perfect sphere and the angular rotation of the earth will be involved in the computations. The second coordinate system is the Airframe Body Coordinates (ABC), which is a rotating system with the airframe of the vehicle (X_M, Y_M, Z_M for EKV or X_T, Y_T, Z_T for ICBM). The x-axis of this coordinate system lies within the velocity vector of the vehicle, assuming that the velocity vector and the missile body are aligned. The y-axis is the left wing of this vehicle and the z-axis is orthogonal to the x and y-axes complying with the right hand rule [29]. The third coordinate system is the line of sight coordinate system (LOS). This is a two-dimensional coordinate system, which can also

be referred to as the LOS plane (Y_L, Z_L). The EKV position relative to the ICBM is defined by using this coordinate system. The distance Y_L is the LOS vector projected on the equatorial plane and the distance Z_L is the LOS vector projected on the z-axis of the ECEF coordinate system [30]. The LOS plane and the ECEF coordinate system are illustrated in Figure 30.

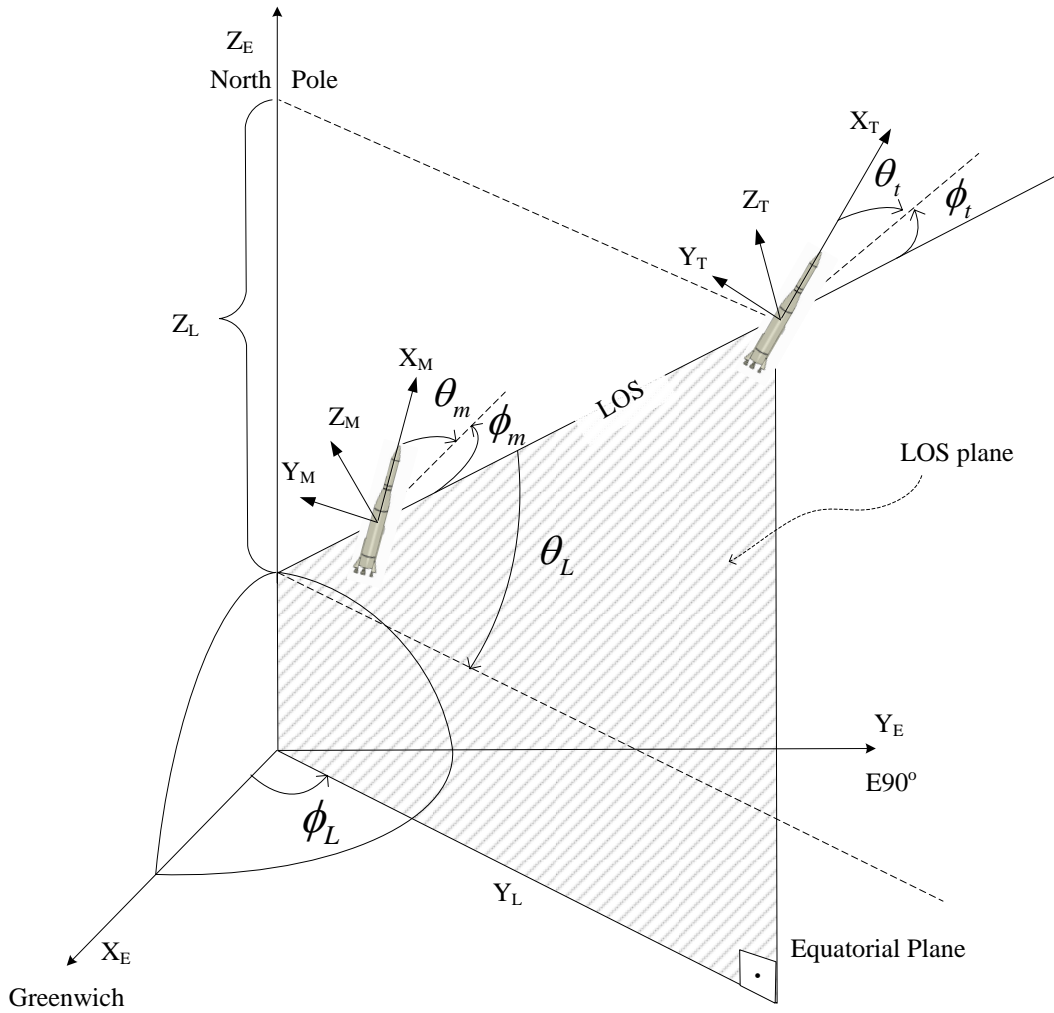


Figure 30. Guidance coordinates geometry: ECEF coordinate system, LOS plane, ABC system.

The missile and target parameters, such as velocity and acceleration, are defined in the ABC coordinate system, and the computations are conducted in the common coordinate system (ECEF). Hence, we need to define and calculate the coordinate conversions to transform all the coordinates to the ECEF coordinate system.

The acceleration command will be applied to the yaw and pitch axes of the EKV, which are represented by X_M and Y_M , respectively. In order to represent these acceleration forces in the ECEF coordinate system, we have to rotate the coordinate system about the rotating axis. The angles resulting from these rotations are called the Euler angles [31]. The rotation matrix about the x-axis by angle ψ can be written as

$$\Psi = \begin{bmatrix} 1 & 0 & 0 \\ 0 & \cos \psi & \sin \psi \\ 0 & -\sin \psi & \cos \psi \end{bmatrix} \quad (4.1)$$

The rotation matrix about the y-axis by the angle θ can be written as

$$\Theta = \begin{bmatrix} \cos \theta & 0 & -\sin \theta \\ 0 & 1 & 0 \\ \sin \theta & 0 & \cos \theta \end{bmatrix} \quad (4.2)$$

The rotation matrix about the z-axis by the angle ϕ can be written as

$$\Phi = \begin{bmatrix} \cos \phi & \sin \phi & 0 \\ -\sin \phi & \cos \phi & 0 \\ 0 & 0 & 1 \end{bmatrix} \quad (4.3)$$

For consecutive rotations, we need to multiply the corresponding rotation matrices [32]. In order to transform the ECEF coordinate system into ABC or LOS coordinate systems, we first rotate the EKV about the y-axis by the pitch angle θ . The next necessary rotation is about the z-axis by yaw angle ϕ . The required overall rotation matrix can be generated by multiplying these two rotation matrices as

$$C = \Theta\Phi \quad (4.4)$$

After some matrix algebra and using appropriate angles, we can write the open form of general conversion matrix C as follows

$$C = \begin{bmatrix} \cos \theta \cos \phi & \cos \theta \sin \phi & \sin \theta \\ -\sin \phi & \cos \phi & 0 \\ -\sin \theta \cos \phi & -\sin \theta \sin \phi & \cos \theta \end{bmatrix} \quad (4.5)$$

Using (4.5), we can now derive the transformation vectors for the defined coordinate systems. First, we define coordinate transformation from the ECEF coordinate system to the LOS coordinate system as [30]

$$\begin{bmatrix} i_L \\ j_L \\ k_L \end{bmatrix} = C_L \begin{bmatrix} i_I \\ j_I \\ k_I \end{bmatrix} \quad (4.6)$$

where i, j and k represent the unit vectors in x, y and z axes, respectively, in the corresponding coordinate system. The conversion matrix C_L is defined as a function of θ_L and ϕ_L angles, which are shown in Figure 30 and represent the appropriate Euler angles [30]. The subscripts I, L and M represent the ECEF coordinate system, the LOS coordinate system and the ABC system, respectively. The coordinate conversion from the LOS coordinate system to the ABC system using (4.5) is defined as

$$\begin{bmatrix} i_M \\ j_M \\ k_M \end{bmatrix} = C_m \begin{bmatrix} i_L \\ j_L \\ k_L \end{bmatrix} \quad (4.7)$$

The conversion matrix C_m is defined as a function of θ_m and ϕ_m angles, which are shown in Figure 30. The θ_M and ϕ_M angles are the spherical coordinate angles for the velocity vector of the missile:

$$\begin{aligned} \theta_m &= \theta_M - \theta_L \\ \phi_m &= \phi_M - \phi_L \end{aligned} \quad (4.8)$$

C. PURSUIT GUIDANCE

The aim of the pursuit guidance, also referred to as beam rider guidance, is to keep the EKV velocity vector on the target and to finally hit the target. The pursuit guidance is very simple to implement and does not require a complicated seeker design. It requires a velocity and geometry advantage to perform a successful intercept. This guidance rule performs better in tail aspect intercepts with a velocity overtake. It has some deficiencies for cross-range collision geometries [14].

1. Principals of Pursuit Guidance

The seeker of the missile is required to produce only a line of sight angle for the pursuit guidance. Since the EKV has very efficient infrared sensors on board, the line of sight angle can be measured very accurately in the end game. Pursuit guidance also requires the measurement of the angle of the missile velocity vector. Both the line of sight angle and the missile velocity vector angle should be referred to the same fixed plane, which is the equatorial plane in this study. The seeker measures the line of sight angle in the ABC and is then converted to the ECEF coordinate system. The inertia navigation system (INS) will also measure the missile velocity vector angle in ABC and is then converted to the ECEF coordinate system.

The angle error is generated by taking the difference between the LOS angle and missile heading, as shown in Figure 31. After capturing the angle error, the acceleration command is generated from this error and guidance gain K . The command acceleration is filtered by the $T(s)$ and the missile dynamics uses this acceleration to change the course of the missile by applying the thrusters. Since the interception will take place in space, the guidance maneuver will be accomplished using thrusters instead of aerodynamic surfaces.

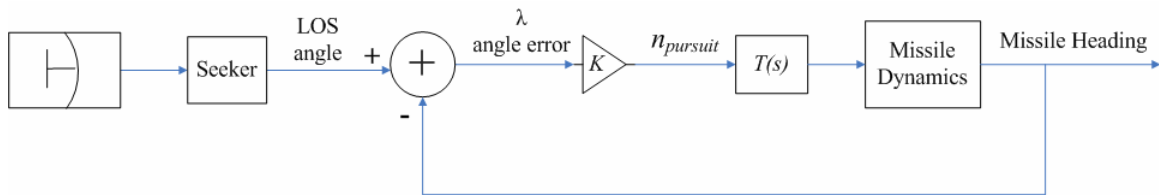


Figure 31. Pursuit guidance flow chart.

2. Three-Dimensional Implementation of the Pursuit Guidance

Since the IR seeker of the EKV measures angles very accurately, we can assume an exact measurement of the target position. For the pursuit guidance, the seeker is required to provide the guidance system with the LOS angle. The seeker will measure the yaw and pitch angles of the EKV relative to the ICBM within its spherical ABC system. These yaw and pitch angles are represented by ϕ_m and θ_m , respectively (see (4.8)). Before defining the yaw and pitch angles, we first need to define the LOS vector. The LOS

vector can be calculated by vector subtraction of the target and missile position vectors.

The target and missile state vectors are defined as

$$\begin{aligned} X_T &= [x_t \quad y_t \quad z_t \quad \dot{x}_t \quad \dot{y}_t \quad \dot{z}_t]^T \\ X_M &= [x_m \quad y_m \quad z_m \quad \dot{x}_m \quad \dot{y}_m \quad \dot{z}_m]^T \end{aligned} \quad (4.9)$$

Using (4.9), we can define the LOS vector as

$$X_L = X_T(1:3) - X_M(1:3) = \begin{bmatrix} x_l \\ y_l \\ z_l \end{bmatrix} = \begin{bmatrix} x_t - x_m \\ y_t - y_m \\ z_t - z_m \end{bmatrix} \quad (4.10)$$

The line of sight (LOS) angles θ_L and ϕ_L are derived as given by

$$\begin{aligned} \theta_L &= \tan^{-1} \left(\frac{z_l}{\sqrt{x_l^2 + y_l^2}} \right) \\ \phi_L &= \tan^{-1} \left(\frac{y_l}{x_l} \right) \end{aligned} \quad (4.11)$$

The missile heading is computed by using the velocity vector of the missile, which is defined in the state vector, assuming that the missile body coincides with the velocity vector. The velocity vector contains the last three components of the state vector.

The missile heading angles θ_M and ϕ_M are computed by

$$\begin{aligned} \theta_M &= \tan^{-1} \left(\frac{\dot{z}_m}{\sqrt{\dot{x}_m^2 + \dot{y}_m^2}} \right) \\ \phi_M &= \tan^{-1} \left(\frac{\dot{y}_m}{\dot{x}_m} \right) \end{aligned} \quad (4.12)$$

Now we can define the yaw and pitch angles as a function of LOS angles and the missile heading. The yaw and pitch angles are shown in Figure 30.

These θ_m and ϕ_m angles represent the missile heading error. Pursuit guidance attempts to zero this error that will guide the EKV to the ICBM. The acceleration command is produced for both yaw and pitch axes to correct this angle error. The yaw and pitch angle deflections are converted to ECEF components as [33]

$$\begin{aligned}
\lambda_x &= \phi_m \sin \theta_L \\
\lambda_y &= -\theta_m \\
\lambda_z &= \phi_m \cos \theta_L
\end{aligned} \tag{4.13}$$

where λ represents the angular error. The guidance commands are applied to be perpendicular to the LOS vector. However, we can only apply acceleration commands perpendicular to the EKV body because of fixed thruster orientation. Hence, using the equations (4.6) thru (4.7), we define the yaw and pitch turn rate commands for pursuit guidance as (After [33])

$$\begin{aligned}
\omega_{yaw} &= K \lambda_y \sin \theta_m \sin \phi_m - K \lambda_z \cos \theta_m \quad (\text{rad/s}) \\
\omega_{pitch} &= K \lambda_y \cos \phi_m \quad (\text{rad/s})
\end{aligned} \tag{4.14}$$

where K is the guidance gain. Increasing the guidance gain will increase the turn rate, which will make the guidance more responsive. However, it will also make the guidance more susceptible to saturation. Hence, the selection of the guidance gain is a trade off between agility and stability.

Definition (4.14) yields the turn rate commands, but we still need the acceleration command to apply to the thrusters of the EKV. The acceleration command is evaluated using coordinated turn definitions, which is sketched in Figure 32 [19].

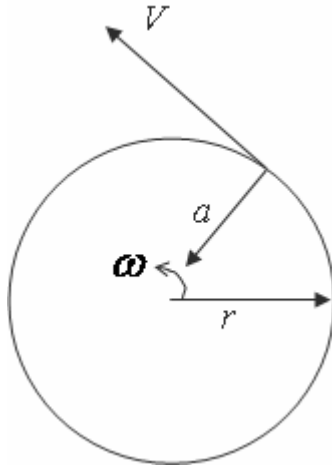


Figure 32. Coordinated turn schematic (After [34]).

The acceleration is defined as a function of velocity and the radius of the turn circle [15]:

$$a = \frac{V^2}{r} \quad (\text{m/s}^2) \quad (4.15)$$

where a is the acceleration that is normal to the velocity vector, V is the tangential velocity and r is the radius of the turn circle. The turn rate can be defined as the total angle traveled over the time. The total angle traveled in a complete turn is 2π radians and the time to travel this angle is

$$t = \frac{2\pi r}{V} \quad (\text{s}) \quad (4.16)$$

Hence, we can write the turn rate as

$$\omega = \frac{2\pi}{2\pi r / V} = \frac{V}{r} \quad (\text{rad/s}) \quad (4.17)$$

Substituting (4.17) into (4.15), we can define the relationship between the acceleration and the turn rate as

$$a = \omega V \quad (\text{m/s}^2) \quad (4.18)$$

Now we can write acceleration commands instead of turn rate commands as (After [30])

$$\begin{aligned} n_{yaw} &= KV_M \lambda_y \sin \theta_m \sin \phi_m - KV_M \lambda_z \cos \theta_m \quad (\text{m/s}^2) \\ n_{pitch} &= KV_M \lambda_y \cos \phi_m \quad (\text{m/s}^2) \end{aligned} \quad (4.19)$$

The yaw and pitch acceleration commands should be expressed in the ECEF coordinate system to be implemented in the simulation. Using the unit vector representation, we write the resultant acceleration command in ABC as

$$n_{pursuit} = \begin{bmatrix} 0 & n_{yaw} & n_{pitch} \end{bmatrix} \begin{bmatrix} i_M \\ j_M \\ k_M \end{bmatrix} \quad (4.20)$$

where $n_{pursuit}$ is the acceleration command vector in ABC. Using (4.7), we convert this acceleration command into LOS coordinates as follows

$$n_{pursuit} = \begin{bmatrix} 0 & n_{yaw} & n_{pitch} \end{bmatrix} C_m \begin{bmatrix} i_L \\ j_L \\ k_L \end{bmatrix} \quad (4.21)$$

Finally, substituting (4.6) into (4.21), we define the acceleration command in the ECEF coordinate system as

$$n_{pursuit} = \begin{bmatrix} 0 & n_{yaw} & n_{pitch} \end{bmatrix} C_m C_L \begin{bmatrix} i_I \\ j_I \\ k_I \end{bmatrix} \quad (4.22)$$

Latencies in the seeker measurements and latencies in applying the acceleration command are two dominant factors that are affecting the intercept capability of the guidance. These two factors are modeled in this study by using a third order transfer function. These latencies will cause a significant miss distance, which would not take place if there were no latencies [35]. The transfer function is defined in the Laplace domain as [9]

$$T(s) = \frac{1}{\left(1 + \frac{\tau}{n}s\right)^n} \quad (4.23)$$

where n is the order of the transfer function and τ is the time constant in seconds. The time constant can vary from 0.5 s to 2 s depending on the agility of the missile [15]. The intercept geometry for space-based intercept of an ICBM generally has a head-on aspect. This geometry results in very high closing velocities and requires a highly responsive EKV. The EKV that is modeled in this study is a hypervelocity advanced missile with a time constant of 0.5 s. The transfer function for $\tau = 0.5$ s can be derived as

$$T(s) = \frac{216}{s^3 + 18s^2 + 108s + 216} \quad (4.24)$$

The time domain response is derived by taking the inverse Laplace transform of $T(s)$ and is given by

$$y(t) = \mathcal{L}^{-1} \left\{ \frac{T(s)}{s} \right\} = 1 - (18t^2 + 6t + 1)e^{-6t} \quad (4.25)$$

The time domain response is computed using MATLAB[®] and the resulting plot is shown in Figure 33.

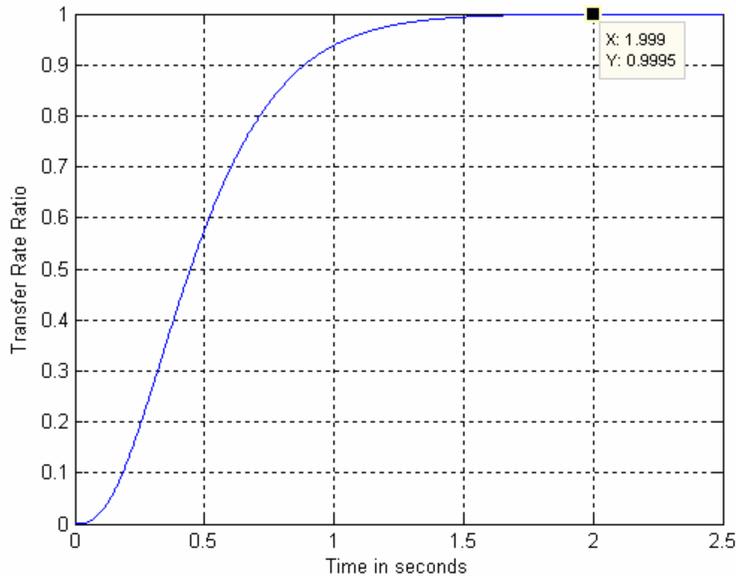


Figure 33. Time domain response of the EKV guidance system.

As a rule of thumb, four times the time constant shows us when the transition will end and the command will be fully applied [15]. Here the time constant is 0.5 s, so the transition should die out in 2 s. As shown in Figure 33, the time domain response reaches 0.9995 at 2 s, which can be considered the end of the transition.

D. PROPORTIONAL NAVIGATION GUIDANCE

The Proportional Navigation Guidance (PNG) produces a perpendicular acceleration that is a function of the LOS angle rate $\dot{\theta}_L$, the closing velocity V_c and the proportional navigation constant N . The turn rate command is generated proportional to the angular velocity of the LOS [36]. The EKV seeker provides an accurate LOS angular velocity measurement, which will increase the performance of the intercept in our model. The idea is to guide the EKV directly to the collision point by leading the target, so the EKV can intercept the ICBM at an optimum time and with minimum command effort. The PNG is well known for minimizing the total control effort. Theoretically, the guidance command should be applied perpendicular to the LOS. However, in practice we can only apply the guidance command perpendicular to the missile body [33]. The guidance com-

mand derived below assumes that EKV is launched towards the missile, but we will see that it is still optimal when the scenario does not meet this requirement.

First, we will discuss the PNG in two-dimensions to have a better understanding of the theory. The scenario is defined in Figure 34 for the two-dimensional geometry. The geometry assumes a constant speed impulsive target and a constant speed impulsive interceptor. The collision flight path is defined from the interceptor's initial launch point to the intercept point. Note that the LOS angle remains unchanged on this collision flight path. The PNG aims to keep the missile on this path by producing acceleration commands. These acceleration commands should also assure that the LOS angular velocity stays zero. For the scenario given above, the PNG is the optimal guidance. It will become sub-optimal with an accelerating target or an accelerating interceptor. PNG can still be effective enough by varying the guidance coefficient, which is discussed below.

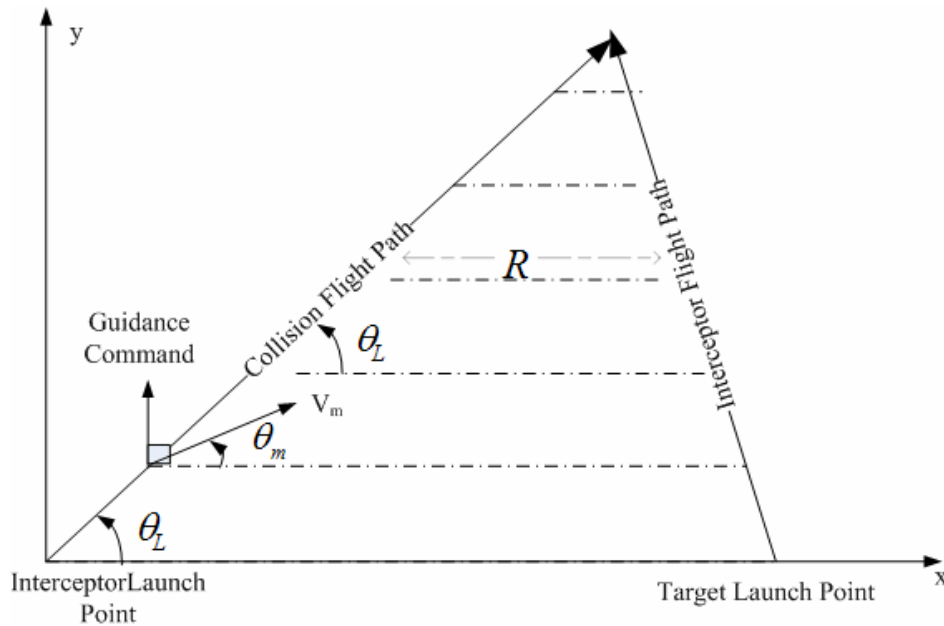


Figure 34. PNG collision geometry.

The LOS angular rate $\dot{\theta}_L$ is measured by the seeker. The closing velocity V_c is the inverse of the time derivative of the distance between the interceptor and the target R . The PNG acceleration command perpendicular to LOS is [9]

$$n_c = NV_c \dot{\theta}_L \quad (4.26)$$

Note that the acceleration command derived above is perpendicular to the LOS vector. However, we can only apply command forces perpendicular to the missile body. The component of this command perpendicular to the missile body is derived assuming that the missile velocity vector is aligned with the missile body [37] as follows

$$n_c = \frac{NV_c \dot{\theta}_L}{\cos \theta_m} \quad (4.27)$$

1. Closing Velocity Approach

The coordinate conversion definitions (4.1) through (4.8) also hold for the PNG, and the geometry is defined in Figure 30. The LOS angular velocity vector Ω_L in three-dimensional geometry is defined by using the coordinate conversion vectors [30]

$$\Omega_L = \begin{bmatrix} \dot{\lambda}_x & \dot{\lambda}_y & \dot{\lambda}_z \end{bmatrix} \begin{bmatrix} i_L \\ j_L \\ k_L \end{bmatrix} \quad (4.28)$$

where $\dot{\lambda}$ is the LOS angular velocity in the corresponding component of the LOS coordinate system [30]. We defined the three components of the LOS angular velocity as

$$\begin{aligned} \dot{\lambda}_x &= \dot{\phi}_L \sin \theta_L \\ \dot{\lambda}_y &= -\dot{\theta}_L \\ \dot{\lambda}_z &= \dot{\phi}_L \cos \theta_L \end{aligned} \quad (4.29)$$

The Euler angles used in (4.29) are presented in Figure 30, and the LOS angular velocities of $\dot{\theta}_L$ and $\dot{\phi}_L$ are in the spherical ECEF coordinate system. The seeker of the EKV is capable of measuring these angles and passing them to the guidance system. The spherical ECEF angles of the LOS vector are derived using (4.11). The angle rates are then given as

$$\begin{aligned} \dot{\theta}_L &= \frac{d\theta_L}{dt} = \frac{d}{dt} \left\{ \tan^{-1} \left(\frac{z_l}{\sqrt{x_l^2 + y_l^2}} \right) \right\} \\ \dot{\phi}_L &= \frac{d\phi_L}{dt} = \frac{d}{dt} \left\{ \tan^{-1} \left(\frac{y_l}{x_l} \right) \right\} \end{aligned} \quad (4.30)$$

where x_l , y_l and z_l are defined in (4.10).

We derive the guidance command perpendicular to the EKV as a function of the closing velocity, angular rates and the proportional navigation constant N as [9], [30]

$$\begin{aligned} n_{PNGyaw} &= -NV_c \dot{\lambda}_y \sin \theta_m \sin \phi_m + NV_c \dot{\lambda}_z \cos \theta_m \\ n_{PNGpitch} &= -NV_c \dot{\lambda}_y \cos \phi_m \end{aligned} \quad (4.31)$$

where N is the guidance coefficient varying from three to five, depending on the maneuverability of the interceptor and the target. We should select a higher guidance coefficient for more agile targets and missiles [9]. The closing velocity is denoted by V_c in the preceding equation and is defined as the time derivative of the distance between the interceptor and the target:

$$V_c = -\dot{R} = \frac{d}{dt} \left\{ \sqrt{x_l^2 + y_l^2 + z_l^2} \right\} \quad (4.32)$$

The acceleration command should be derived in ECEF Cartesian coordinates in order to implement this theory in the simulation. The acceleration command is first calculated in ABC as given by

$$n_{PNG} = \begin{bmatrix} 0 & n_{PNGyaw} & n_{PNGpitch} \end{bmatrix} \begin{bmatrix} i_M \\ j_M \\ k_M \end{bmatrix} \quad (4.33)$$

where n_{PNG} is the acceleration command vector in ABC. Using the method (4.20) through (4.22), the PNG acceleration command is transformed to the ECEF coordinate system:

$$n_{PNG} = \begin{bmatrix} 0 & n_{PNGyaw} & n_{PNGpitch} \end{bmatrix} C_m C_L \begin{bmatrix} i_I \\ j_I \\ k_I \end{bmatrix} \quad (4.34)$$

The block diagram of the PNG implementation is shown in Figure 35.

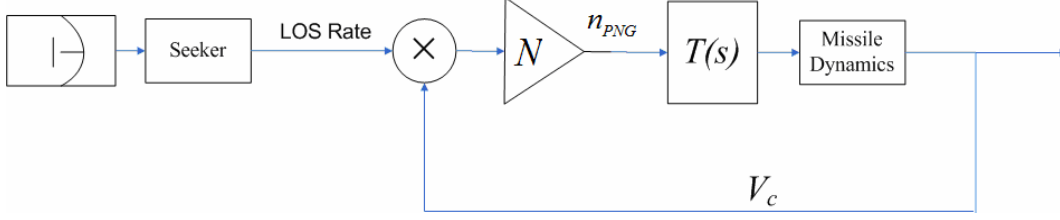


Figure 35. Block diagram of the PNG.

2. Missile Velocity Approach

The angular velocity of the LOS vector is derived using equations (4.28) through (4.30) for missile velocity approach. Blakelock [36] states that the acceleration command generated by the PNG should be proportional to the missile velocity instead of the closing velocity. Blakelock also states that the PNG gain should be greater or equal to one to ensure an intercept. He recommends selecting a PNG constant between two and six for accelerating or maneuvering targets [36]. We will denote the PNG constant with N' to make a distinction between the closing velocity approach.

The acceleration commands for the yaw and the pitch axes of the interceptor is defined in missile body coordinates as [33]

$$\begin{aligned} n_{PNGyaw} &= -N'V_m \dot{\lambda}_y \sin \theta_m \sin \phi_m + N'V_m \dot{\lambda}_z \cos \theta_m \\ n_{PNGpitch} &= -N'V_m \dot{\lambda}_y \cos \phi_m \end{aligned} \quad (4.35)$$

where V_m is the missile velocity, which is measured by the onboard INS or the GPS in the EKV. The acceleration command vector in the ABC system is obtained as [33]

$$n_{PNG} = \begin{bmatrix} 0 & n_{yaw} & n_{pitch} \end{bmatrix} \begin{bmatrix} i_M \\ j_M \\ k_M \end{bmatrix} \quad (4.36)$$

The acceleration command is transformed into the ECEF coordinate system using the method introduced by (4.20) through (4.22):

$$n_{PNG} = \begin{bmatrix} 0 & n_{yaw} & n_{pitch} \end{bmatrix} C_m C_L \begin{bmatrix} i_I \\ j_I \\ k_I \end{bmatrix} \quad (4.37)$$

The block diagram for the PNG law for missile velocity approach is also represented by Figure 35, with N replaced by N' and V_c replaced by V_m .

E. BANG-BANG GUIDANCE

Bang-bang guidance (BBG) is a derivative of proportional guidance. Bang-bang guidance applies the maximum possible acceleration in the direction of the LOS angular velocity. The missiles with thrusters as the control elements apply this guidance very effectively. The guidance command is defined as a function of the LOS angle, the LOS angle rate and the closing velocity [37]

$$n_{bb} = a_m \frac{\text{sgn}(V_c \dot{\theta}_L)}{\cos \theta_L} \quad (4.38)$$

where a_m is the maximum applicable lateral acceleration of the missile.

The BBG produces the maximum maneuver resulting in a large amount of drag. This drag degrades the performance of the interceptor in the atmosphere. Since the EKV is moving in high atmosphere, this drag will not effect the performance of the EKV [38].

Defining the bang-bang acceleration command using the existing derivation for the PNG will make this guidance easier to implement into the model that we developed. The direction of the guidance command perpendicular to the missile body is derived with the same method we used in PNG. The unit vector, which defines the direction of the bang-bang acceleration command, is the same unit vector of the PNG guidance command and is given by

$$\hat{n}_{bb} = \frac{n_{PNG}}{\|n_{PNG}\|} \quad (4.39)$$

where \hat{n}_{bb} is the unit vector of the bang-bang acceleration command. The bang-bang acceleration command is derived using the preceding unit vector as

$$n_{bb} = a_m \hat{n}_{bb} \quad (4.40)$$

Equation (4.39) and (4.40) together define the bang-bang acceleration command along the lines of the same derivation for PNG.

F. SUMMARY

In this chapter, pursuit guidance, proportional navigation guidance and the bang-bang guidance rules are introduced, and a three-dimensional implementation is mathematically modeled. We will compare their performance in the next chapter. Also, a hybrid guidance algorithm that combines the principles of these rules is identified in the next chapter.

V. COMPARISON OF GUIDANCE LAWS

In this chapter the three-dimensional SIMULINK[®] model is developed and the simulation is tested for different scenarios. The performance of the different guidance rules are tested for the North Korea case and then an hybrid guidance (HG) algorithm is developed based on these results. Here the launch delay is assumed to be zero. The hybrid guidance algorithm is then tested against three example ICBM threats with four different EKV launch points for each threat. For all guidance simulations, the ideal seeker is assumed to see the ICBM at all times.

A. SIMULINK[®] SIMULATION MODEL DESCRIPTION

The ICBM dynamics modeled in Chapter II, the EKV dynamics and orbit parameters modeled in Chapter III and the three guidance rules developed in Chapter IV are implemented in a SIMULINK[®] model.

1. Simulation Initialization

The SIMULINK[®] model requires initial parameters of the EKV and the ICBM to run the simulation. These parameters are entered by the user by running *SimulationInit.m* MATLAB[®] file separately. The initial parameters include the EKV launch point on the orbit, the ICBM launch site and the launch delay.

The initial state vector is generated in the code for the initial point of the EKV on the orbit at launch. The user is asked to enter the mean anomaly time, which starts when the EKV passes by the equator from south to north, i.e., time zero for the EKV position starts at the equator. The entered time is used to calculate the position of the EKV on the orbit. The state vector of the EKV is then calculated and passed to the SIMULINK[®] model.

The launch location of the ICBM and the EKV launch delay are also selected by the user. The three choices of launch locations are North Korea, China or Iran. The launch location and the initial launch parameters for a San Francisco attack of the selected ICBM are predetermined. With the parameters above, the initial state vector of the ICBM is calculated and passed to the SIMULINK[®] model. The propellant masses of the

selected ICBM are also predetermined. The MATLAB[®] functions that are used in this model are listed in Table 7.

Table 7. Code listing for the SIMULINK[®] model.

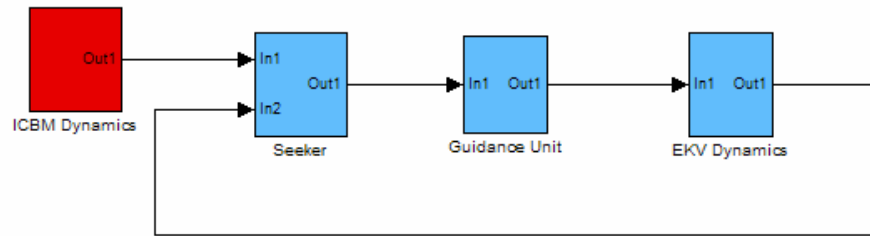
File Name	SIMULINK[®] Block	Comments
SimulationInit.m	N/A	Should be run before simulation
ICBMmotion.m	ICBM Dynamics	Calculates change in ICBM state
Seeker.m	Seeker	Tracks target for LOS rate and V_c
HitDet.m	Seeker	Detects hit or miss and stops simulation
PG.m	Guidance	Calculates PG acceleration command
PNG.m	Guidance	Calculates PNG acceleration command
HG.m	Guidance	Calculates HG acceleration command
Limiter.m	Guidance	Limits the acceleration command
Mag.m	Guidance	Calculates the magnitude of a given vector
EKVmotion.m	EKV Dynamics	Calculates change in EKV state
PlotSimResults.m	N/A	Plots the results that are stored in workspace

2. SIMULINK[®] Model Description

The model incorporates ICBM dynamics, seeker, guidance unit and EKV dynamics in four different subsystems. The overall model is shown in Figure 36. The flow diagram for the model is provided in Appendix A.

WARNING
 This model requires initial parameters
 Initial parameters must be generated by running *SimulationInit.m* separately

CAUTION
 Recommended Configuration Parameters should be used
 to avoid inaccurate calculations
 or
 overloading the memory



This model simulates the Space based interception of the hostile ICBM
 The launch point of the ICBM and the EKV may be selected through *SimulationInit.m*
 The usage details are mentioned in the subsystems
 Double click on the subsystems to see the details

Recommended Configuration Parameters
 (Solver Options)
 Max step size: 0.001
 Min step size: 0.0001
 Solver: ode45(Dormand-Prince)
 Relative tolerance: 1e-6

Figure 36. Overall space-based intercept SIMULINK[®] model for PG, PNG, BBG and HG against North Korean, Chinese and Iranian ICBMs.

This model is capable of running for PG, PNG or HG one at a time. Adding new guidance methods is also possible with a new MATLAB[®] script file for new guidance methods. The model gives three options as the ICBM launch point. The subsystems of the model are ICBM Dynamics, Seeker, Guidance Unit and the EKV Dynamics.

3. ICBM Dynamics Subsystem

The ICBM dynamics subsystem reads the required initial parameters from the lookup tables. The tables read these parameters from the workspace resulting from *SimulationInit.m* file. Initial parameters include the selected launch site, the ICBM initial propellant mass and the ICBM initial state vector.

The subsystem for ICBM dynamics is shown in Figure 37. The *ICBMmotion.m* file calculates the time derivative of the state vector and the propellant mass, and the in-

tegrators within the model integrates these vectors and returns the results back for the next iteration.

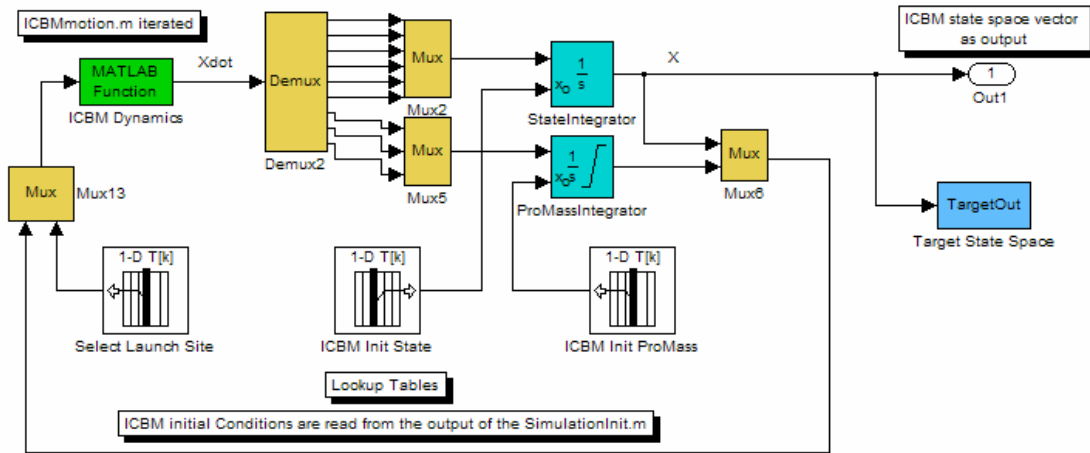


Figure 37. SIMULINK[®] model for ICBM Dynamics.

4. Seeker Subsystem

The seeker provides the guidance unit with ICBM parameters, such as LOS angle, LOS angle rate, off bore sight angles, range and closing velocity. The miss distance is also measured in this unit, and the simulation is terminated upon a hit or miss. The model is shown in Figure 38.

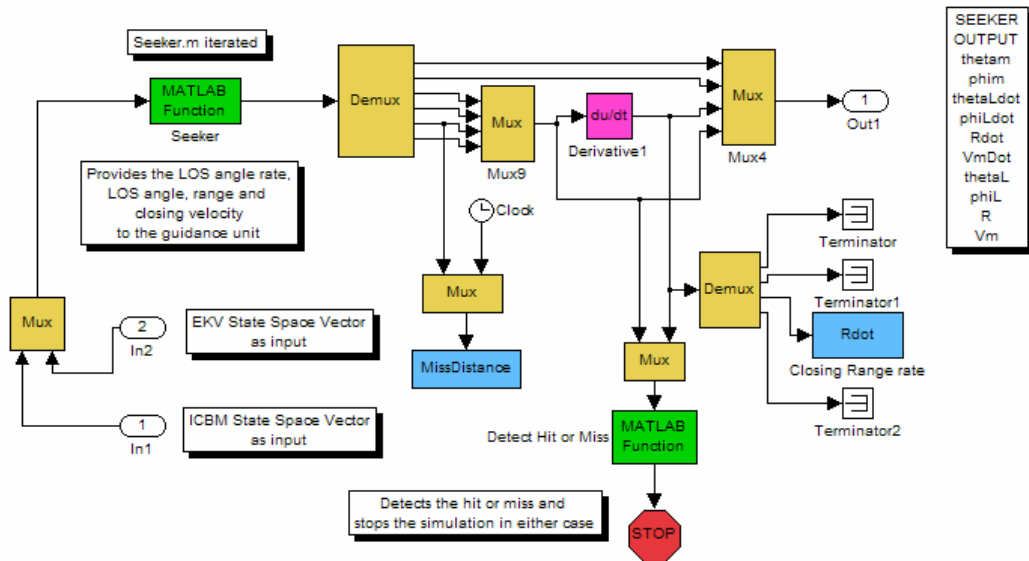


Figure 38. SIMULINK[®] model for Seeker design of the EKV.

5. Guidance Subsystem

The guidance subsystem of the model takes the seeker outputs as the input and uses them to generate the guidance acceleration command. The generated guidance command is filtered by a limiter for maximum acceleration capability of the EKV, and the total system delay is applied by the autopilot $T(s)$. The guidance subsystem model is shown in Figure 39. The EKV parameters of interest are also stored in the workspace variables in this subsystem.

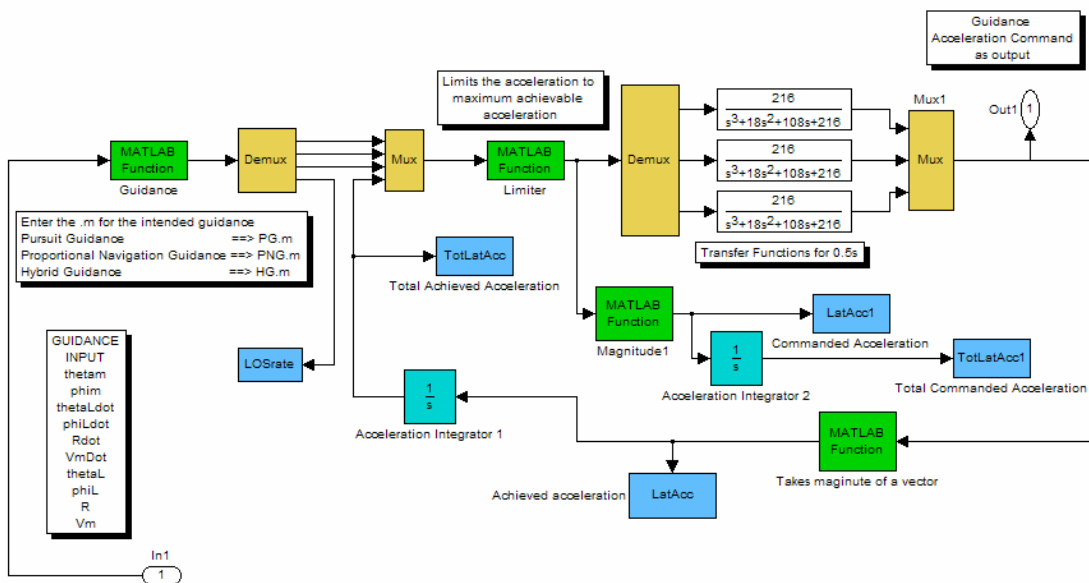


Figure 39. SIMULINK[®] model for Guidance Unit of the EKV.

6. EKV Dynamics Subsystem

EKV Dynamics uses the same method as in ICBM Dynamics. The initial parameters are read from the workspace by the lookup tables. These initial parameters include the initial propellant mass and the initial EKV state vector. The subsystem takes the guidance command input from the guidance unit and applies it to EKV Dynamics. The EKV dynamics subsystem moves and steers the EKV towards the ICBM during its flight and returns an EKV state vector as the output. This output is also carried to the seeker subsystem by a feedback loop in order to model the INS/GPS unit of the EKV.

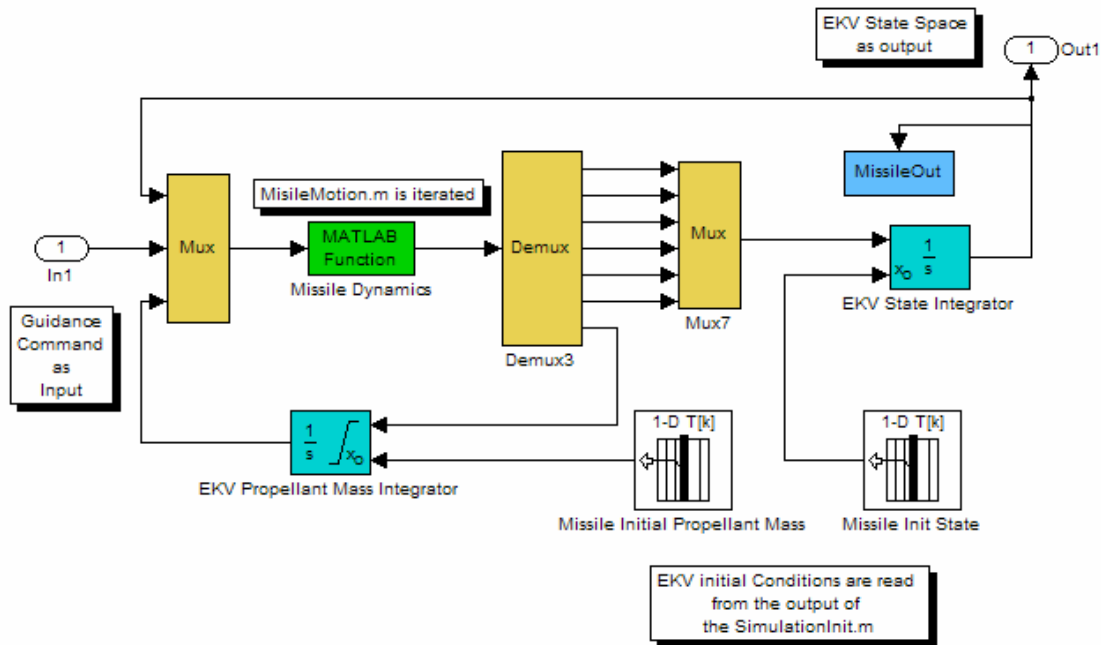


Figure 40. SIMULINK[®] model for EKV Dynamics.

The flow chart of the SIMULINK[®] model and the MATLAB[®] functions are provided in Appendix A.

B. SIMULATION RESULTS FOR PURSUIT GUIDANCE

For all guidance laws, the intercept is tested for North Korea in order to develop an optimum algorithm. This algorithm is then tested for all launch sites of interest. The SIMULINK[®] model is set for pursuit guidance against a North Korean ICBM. The acceleration limiter is set to 500 m/s^2 . The altitude of the EKV is 1000 km and has a maximum range of 1520 km (see Figure 23). With these parameters, it is predicted that if the EKV lies within a coverage angle of 10.6° about the launch site (see Figure 25 and Figure 27) it will be able to hit the ICBM successfully. This maximum coverage constraint will be met if the EKV is launched where the mean anomaly (angle from equator) of the orbit is 98.6° . This angle is the position of the EKV carrier on the selected orbit. This position of the EKV carrier corresponds to 1725 s after its pass by the ascending node and lies at the edge of the coverage region. The initial velocity of the EKV is determined by the angular velocity of the EKV carrier on the orbit (7.35 km/s) and it is tan-

gent to the orbit at the given launch time. The initial ($t = 0$) state vector of the EKV is calculated for the parameters above as

$$X_M(0) = \begin{bmatrix} x_M \\ y_M \\ z_M \\ \dot{x}_M \\ \dot{y}_M \\ \dot{z}_M \end{bmatrix} = \begin{bmatrix} -2456646.97 \\ 4807702.67 \\ 5018218.97 \\ -6436.30 \\ 876.06 \\ 3447.19 \end{bmatrix}_{ECEF} \quad (4.41)$$

The initial state vector of the target ICBM is defined by its launch location and the silo exit velocity. The silo exit velocity of the ICBM is 18 m/s [6]. The location of the North Korean ICBM is N41-E129 (see Table 3 for initial launch parameters). Using the required conversions, the initial ($t = 0$) state vector of the ICBM is obtained as

$$X_T(0) = \begin{bmatrix} x_T \\ y_T \\ z_T \\ \dot{x}_T \\ \dot{y}_T \\ \dot{z}_T \end{bmatrix} = \begin{bmatrix} -3025932.75 \\ 3736715.75 \\ 4179752.07 \\ -8.76 \\ 9.48 \\ 12.54 \end{bmatrix}_{ECEF} \quad (4.42)$$

The EKV and ICBM dynamics are simulated as discussed in Chapter II. The ICBM is a three-stage missile targeting San Francisco, California. The ICBM reaches a velocity of ~ 6.5 km/s and an altitude of 182 km of altitude at the end of the boost-phase (three minutes). The EKV is a single stage kill vehicle with control thrusters that has an initial velocity of ~ 7.35 km/s and altitude of 1000 km. The EKV guidance coefficient K is set to 3, which will introduce the least amount of oscillations in the acceleration command while keeping the EKV agile.

The three-dimensional encounter geometry is shown in Figure 41. It is shown in the geometry that the EKV falls behind the ICBM, which is the nature of the pursuit guidance. After falling behind the ICBM, the EKV uses its velocity advantage to overtake and catch the ICBM at the intercept point.

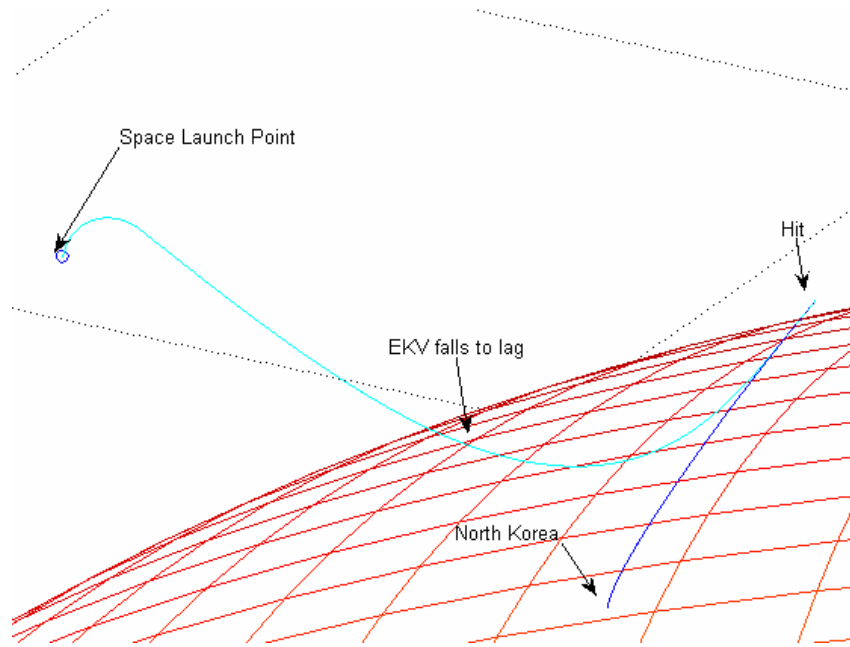


Figure 41. The intercept geometry for PG with $K = 3$.

Figure 42 shows the miss distance for the PG intercept scenario as a function of time with $K = 3$. The minimum miss distance of this interception is 0.04 m. The minimum miss distance is small enough to consider this intercept as a hard-kill-hit because the diameter of the ICBM is 2.3 m [6]. Figure 44 shows the altitude of the EKV as a function of scenario time for PG with $K = 3$. The EKV falls behind the ICBM during the scenario and can be observed in Figure 43, where the EKV altitude is below the ICBM altitude. The interception time is read from Figure 42 as 3.93 minutes, which is greater than our assumption, which was 3.0 to 3.25 minutes, i.e., the RVs have already been launched prior to the intercept. This latency is mostly caused by the lagging trajectory of the EKV, which causes it to travel a greater distance than expected. The altitude of the EKV increases at the beginning of the scenario because it does not point to the ICBM at the launch time, but the pursuit guidance succeeds in providing a positive closing velocity after ~ 0.3 minutes, and the EKV starts descending toward the ICBM.

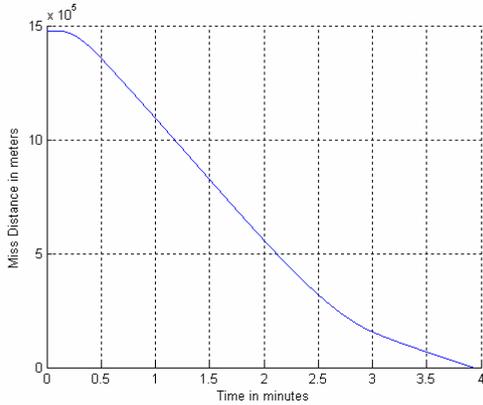


Figure 42. Miss distance for pursuit guidance with $K = 3$.

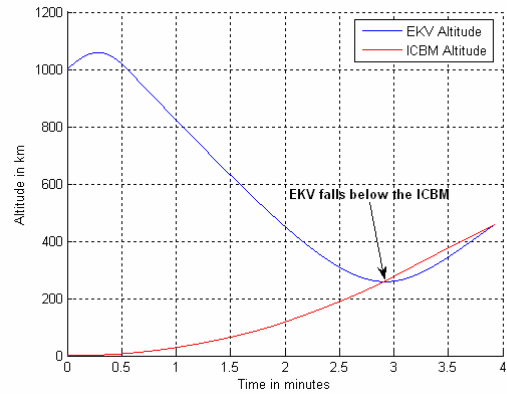


Figure 43. Altitude of the EKV and the ICBM for pursuit guidance with $K = 3$.

The performance of the pursuit guidance is not satisfactory mainly due to the extra distance the EKV travels under PG. Figure 44 shows the instantaneous acceleration applied by the EKV under PG with $K = 3$. Figure 45 shows the cumulative acceleration. The instantaneous acceleration command reaches the maximum applicable value (500 m/s^2) at the beginning of the interception in order to point the EKV towards the ICBM, as shown in Figure 44. This maximum acceleration continues for 30 s until the EKV starts pointing towards the ICBM. The total acceleration command effort applied to the EKV can be read from Figure 45 as $33,000 \text{ m/s}^2$. This total acceleration command gives an idea about the total effort used by the EKV to hit the ICBM. Minimizing this total command effort will decrease the cost proportionally [39]. The EKV begins to fall behind the ICBM $\sim 130 \text{ s}$ after the launch and starts to apply more acceleration command to make the EKV point to the ICBM again. Here, acceleration command increases gradually and reaches 212 m/s^2 . The total acceleration command increases linearly up to 30 s, when the maximum acceleration command is applied continuously, as shown in Figure 45. The oscillations observed in the instantaneous acceleration are the result of the autopilot $T(s)$.

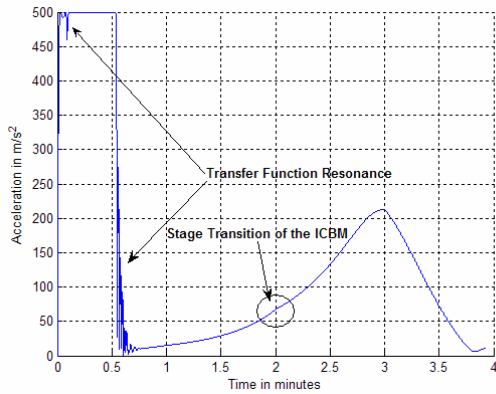


Figure 44. Instantaneous acceleration applied on the EKV for pursuit guidance with $K = 3$.

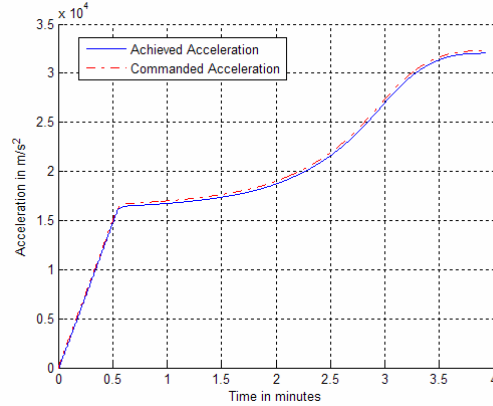


Figure 45. Cumulative acceleration applied on the EKV for pursuit guidance with $K = 3$.

Figure 46 shows the speed of the EKV under PG and the speed of the ICBM. Figure 47 shows the closing velocity. The initial velocity of the EKV is a result of the orbital angular velocity and gives an advantage to the EKV for this scenario, where the initial velocity points in the direction of the ICBM within $\sim 60^\circ$. The velocity of the EKV starts to decrease, as shown in Figure 46, due to gravitational forces. After the EKV starts to point to the ICBM, the velocity of the EKV starts to increase again due to the booster thrust. The rapid increase in velocity stops when the booster fuel is expended, but the increase in velocity is sustained due to gravitational forces. The EKV falls behind the ICBM ~ 130 s after the launch because of the nature of the pursuit guidance. Hence, the velocity of the EKV starts to decay because it starts to move against the gravitational forces after this point, while the ICBM continues accelerating.

The closing velocity of the EKV to the ICBM is negative at the beginning because the initial velocity of the EKV is not pointing to the ICBM due to the orbital angular velocity vector at launch. The pursuit guidance commands the missile to turn towards the ICBM, which results in a rapid increase in the closing velocity (as shown in Figure 47) because of the favorable interception geometry. The closing velocity gradually increases until the EKV falls behind the ICBM and rapidly decreases until the end of the boost-phase of the ICBM.

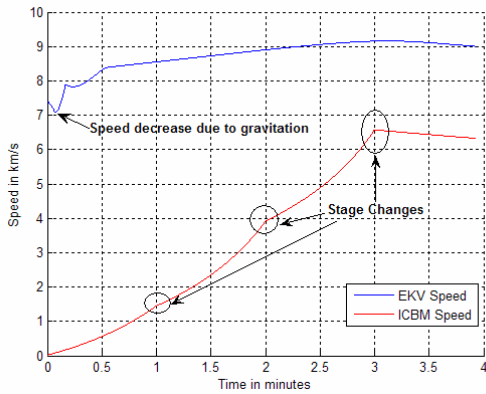


Figure 46. Speeds of the EKV under PG with $K = 3$ and the speed of the ICBM.

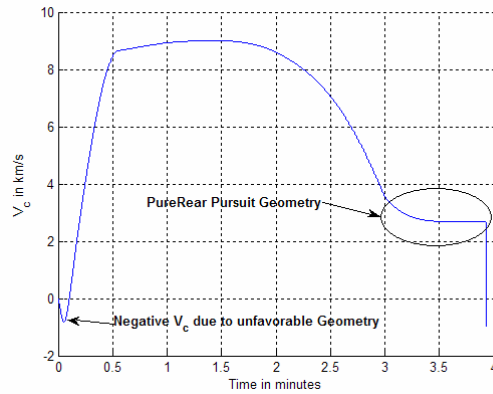


Figure 47. Closing velocity of the EKV to the ICBM for PG with $K = 3$.

The performance of the pursuit guidance can be increased by increasing the guidance coefficient, which might yield a smaller miss distance and intercept time. However, increasing the guidance coefficient will also increase the total commanded acceleration and cause an increase in the acceleration oscillation, making the EKV unstable.

C. SIMULATION RESULTS FOR PROPORTIONAL NAVIGATION GUIDANCE

In this section, the simulation results for PNG are analyzed. The first set of results are recorded when the acceleration command is calculated using the closing velocity. The second set of results are recorded when the acceleration command is calculated using the EKV velocity.

1. Simulation Results for the Closing Velocity Approach

The simulation is initialized with the same initial positions as the pursuit guidance in order to be able to make a fair comparison. The guidance coefficient N is selected as 5 because both missiles have high acceleration forces acting on them. The acceleration limiter is set to 500 m/s^2 to prevent applying forces that the EKV cannot hold. The velocity vector of the EKV at the beginning of the interception is not towards the ICBM, which results in an unfavorable closing velocity. Hence, we picked an initial value for the closing velocity as 6 km/s until the PNG steers the EKV towards the ICBM.

The three-dimensional interception geometry for PNG with $N = 5$ is shown in Figure 48. The EKV flies nearly directly to the collision point and hits the target. The EKV travels a curved trajectory at the beginning, which can be considered undesirable. In addition, the trajectory in endgame phase is also slightly curved due to the high acceleration of the ICBM.

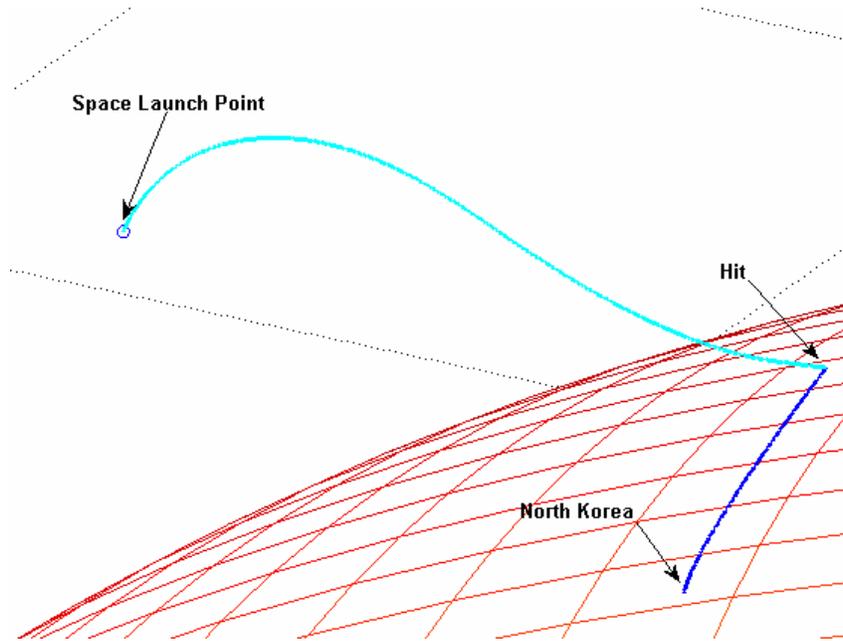


Figure 48. Intercept geometry for PNG with $N = 5$.

Figure 49 shows the miss distance for PNG with $N = 5$ as a function of scenario time. Figure 50 shows the altitudes of the EKV and ICBM. The minimum miss distance of this interception is 0.0182 m, which can be read from Figure 49. The minimum miss distance is clearly improved by using the PNG. The EKV altitude is always above the ICBM altitude, which gives an advantage to the EKV, as shown in Figure 50. Staying above the ICBM altitude provides the EKV with a kinematical advantage over the ICBM, enabling the EKV to react to the ICBM's evasive maneuvers. The interception time is read from Figure 49 as 3.25 minutes, which is within our intercept time window. The altitude of the EKV increases at the beginning, as shown in Figure 50, because of the initial angular velocity of the orbit, but the PNG starts steering the EKV downwards after ~ 0.7 minutes. Note that this time was lower for the pursuit guidance.

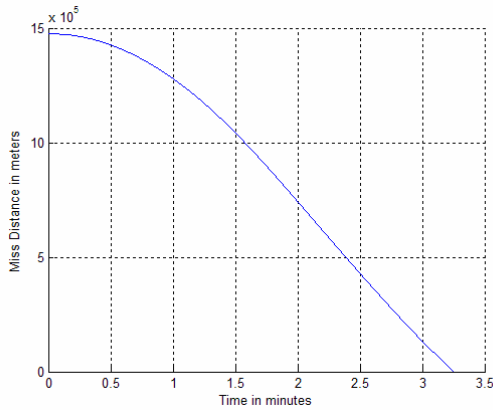


Figure 49. Miss distance for PNG with $N = 5$.

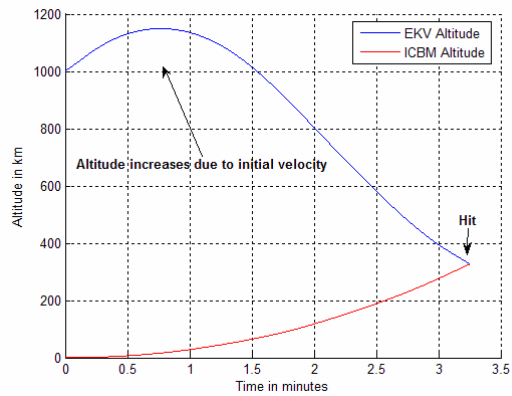


Figure 50. Altitude of the EKV and the ICBM for PNG with $N = 5$.

The minimum miss distance and the intercept time improved, but we have to question if we are reaching these results effectively. Hence, we also need to examine the total command effort used for the intercept. Figure 51 shows the instantaneous acceleration command of EKV as a function of scenario time under PNG with $N = 5$. Figure 52 shows the cumulative acceleration. The instantaneous acceleration command reaches 169 m/s^2 at the beginning of the intercept in order to put the EKV on the collision path, as shown in Figure 51. This acceleration decreases gradually as the EKV trajectory coincides with the collision path. The instantaneous acceleration presents a discontinuity at $t = 57 \text{ s}$ since it switches from the initial velocity value to the actual closing velocity to calculate the guidance command. The acceleration starts increasing at this point as a result of the change in the prediction of the collision path. The stage transitions can also be observed from the acceleration command of the EKV, as shown in Figure 51. Three minutes into the scenario, the guidance acceleration drops rapidly because the ICBM stops boosting and accelerating. The total acceleration command applied on the EKV can be read from Figure 52 as 21980 m/s^2 , which is considerably lower compared to the pursuit guidance. The oscillations observed in the instantaneous acceleration are a result of the autopilot.

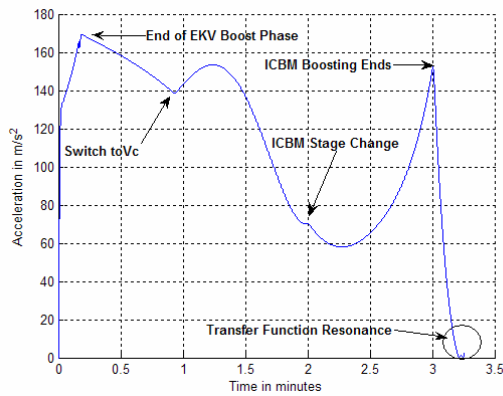


Figure 51. Instantaneous acceleration applied on the EKV for PNG with $N = 5$.

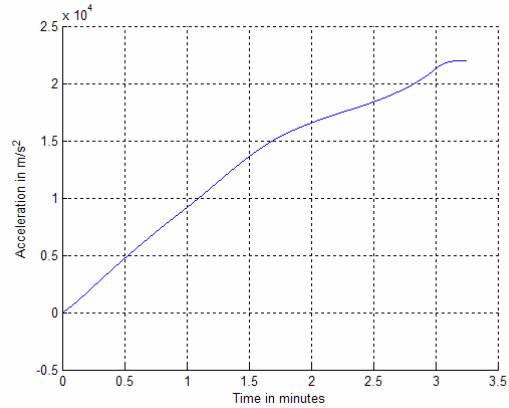


Figure 52. Cumulative acceleration applied on the EKV for PNG with $N = 5$.

The velocities of both the EKV and the ICBM are shown in Figure 53. The velocity of the EKV increases for 10 s as a result of the single stage boosting. After the boost-phase, the velocity decreases slightly due to gravitational forces, until the EKV turns downwards, where the gravitational forces start acting in its favor. The velocity keeps increasing until the hit because the EKV always stays above the ICBM altitude pointing downwards.

Figure 54 shows the closing velocity of the EKV to the ICBM as a function of scenario time for PNG with $N = 5$. The closing velocity of the EKV to the ICBM is small at the beginning of the intercept because the initial velocity vector of the EKV is not pointing to the ICBM. The PNG steers the missile towards the ICBM, which results in a rapid increase in the closing velocity, as shown in Figure 54. The closing velocity decreases slightly as the ICBM velocity increases while boosting. The closing velocity stays constant after the third minute of the interception because the ICBM boost-phase ends.

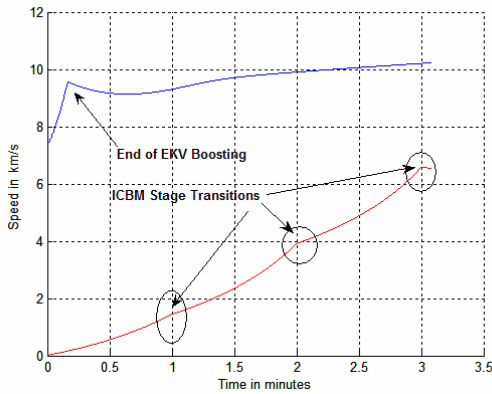


Figure 53. Speeds of the EKV and the ICBM for PNG with $N = 5$.

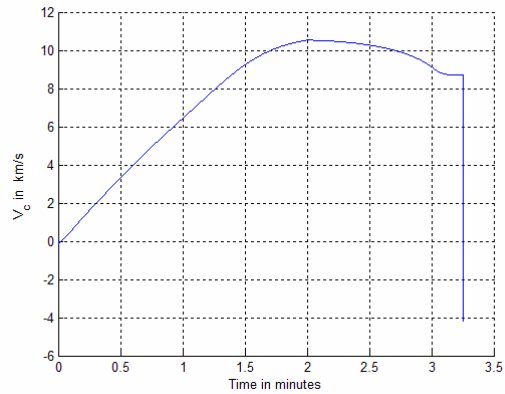


Figure 54. Closing velocity of the EKV to the ICBM for PNG with $N = 5$.

The PNG improves the intercept time with a significantly smaller amount of command effort, but it does not provide an optimum guidance at the beginning when we want the EKV to turn into the collision path as soon as possible. We will address this problem in the following sections.

2. Simulation Results for Missile Velocity Approach

The initial states of the EKV and the ICBM are the same as before for this simulation. We only alter the guidance calculation to use EKV velocity. For the missile velocity approach, the seeker is not required to measure the closing velocity. The guidance gain is set to 6 due to high acceleration of the EKV and the ICBM.

The three-dimensional intercept geometry for PNG with $N' = 6$ is shown in Figure 55. The initial performance is improved when compared to the closing velocity approach. The EKV turns towards the ICBM faster, and the curvature at endgame phase is decreased, which in turn decreases the intercept time.

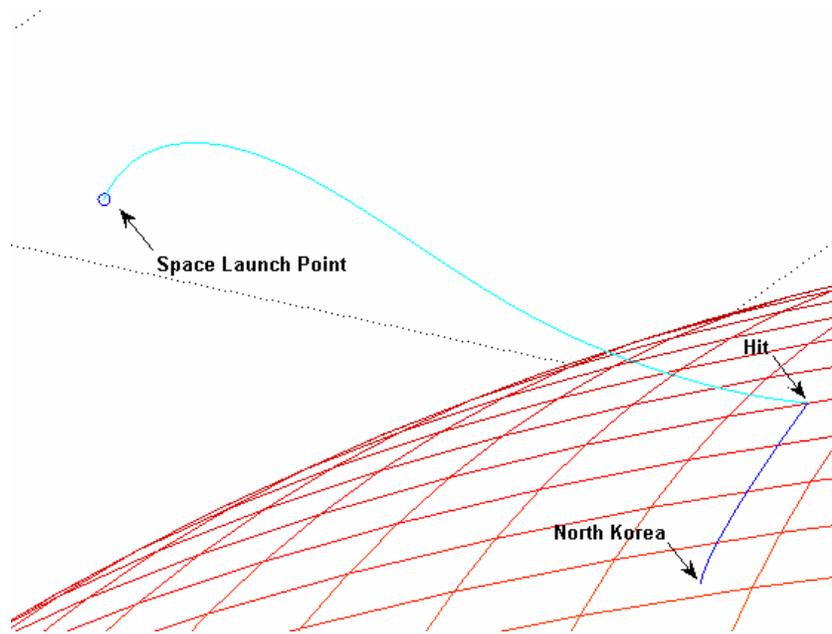


Figure 55. Intercept geometry for PNG with $N' = 6$.

Figure 56 shows the miss distance for PNG with $N' = 6$ as a function of scenario time. Figure 57 shows the altitudes of the EKV and the ICBM. The minimum miss distance for this simulation is 0.00095 m, which is a very successful result for a hit-to-kill intercept. The intercept time is decreased to 172 s and is within the 3.25 minutes window, which makes a 23.4 s improvement when compared to the closing velocity approach. The altitude of the EKV still increases before it compensates for the unfavorable initial velocity vector, but this loss is also improved with the EKV velocity approach of PNG. The intercept takes place at an altitude of 250 km as shown in Figure 57.

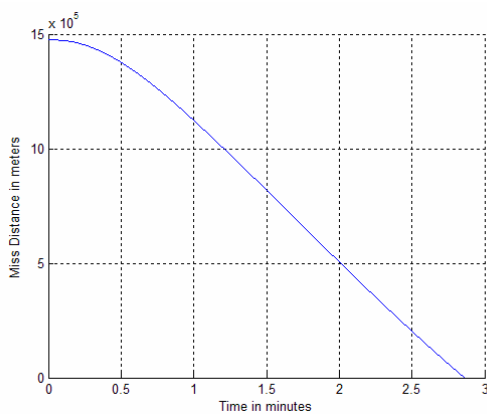


Figure 56. Miss distance for PNG with $N' = 6$.

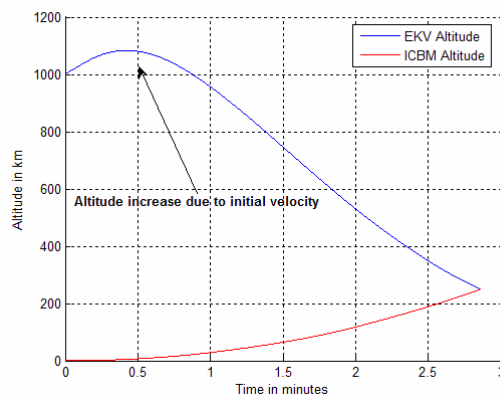


Figure 57. Altitudes for PNG with $N' = 6$.

Figure 58 shows the instantaneous acceleration applied to the EKV under PNG with $N' = 6$. Figure 59 shows the cumulative acceleration. The initial acceleration increases to 325 m/s^2 , which puts the EKV on the collision path more effectively. The ICBM stage changes can also be observed from the EKV instantaneous acceleration chart. The PNG exerts more command effort on the EKV at the beginning of the intercept, which puts the EKV on the collision path faster, prevents extensive future guidance effort and decreases the intercept time. The total command effort is read from Figure 59 as 21410 m/s^2 , which is a 580 m/s^2 , improvement when compared to the PNG with the closing velocity approach.

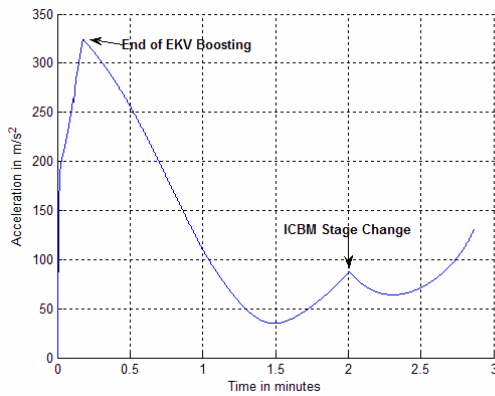


Figure 58. Instantaneous acceleration for PNG with $N' = 6$.

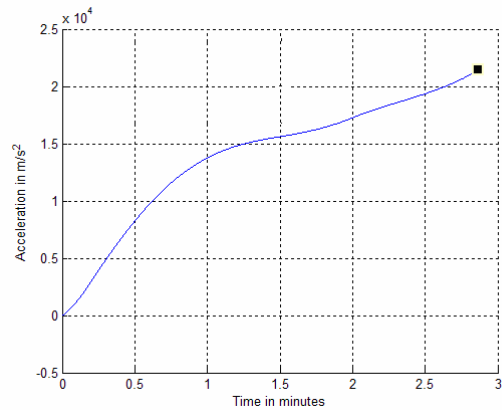


Figure 59. Total acceleration command for PNG with $N' = 6$.

Figure 60 shows the speed of the EKV under PNG with $N' = 6$ and the speed of the ICBM as a function of scenario time. Figure 61 shows the closing velocity. The velocity vector of the EKV is shown in Figure 60 and is very similar to the velocity in PNG with the closing velocity approach. The closing velocity increases faster when compared to the PNG with the closing velocity approach because the EKV turns more rapidly towards the ICBM. The maximum closing velocity is $\sim 10.5 \text{ km/s}$ for both PNG calculations, but the EKV velocity approach reaches this velocity in 1 minute, where the closing velocity approach reaches this velocity in 1.7 minutes.

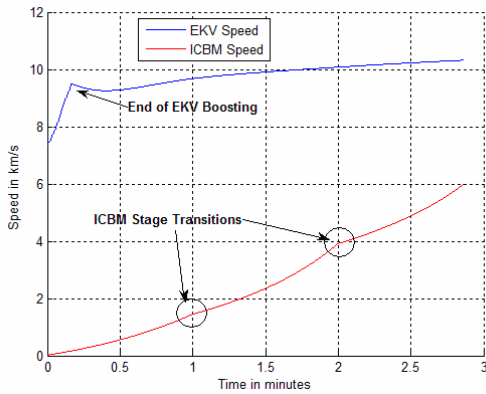


Figure 60. Velocities for PNG with $N' = 6$.

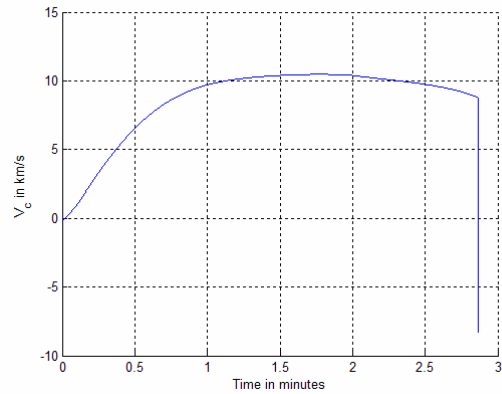


Figure 61. Closing velocity for PNG with $N' = 6$.

We have shown that the PNG using the EKV velocity approach performs better than the closing velocity approach. However, when we look at guidance unit's performance at the beginning of the intercept, we see that it still can be improved. The EKV is launched at an unfavorable attitude. By putting the maximum available acceleration command effort at the beginning of the scenario, the interception can be improved. Note that the current scenario is the most favorable we can achieve. We will face more unfavorable launch conditions when we have to launch the EKV at a later orbit time. We will address this problem in the next section.

D. SIMULATION RESULTS FOR THE HYBRID GUIDANCE

The proportional navigation guidance performs in the near optimal region for the window where the EKV is pointing toward the ICBM. The only non-optimal region is where the EKV is in an unfavorable attitude due to initial orbital velocity. We need to steer the EKV towards the ICBM as soon as possible after the launch. To accomplish this goal, we will introduce the bang-bang guidance (BBG) method at the beginning of the intercept. BBG will be used until the ICBM enters the seeker's gimble limit. The gimble limit of the EKV seeker is assumed to be 4.38 steradians. The guidance unit switches to the PNG after this point. This Hybrid Guidance (HG) method will provide the missile with a quick correction of the initial unfavorable attitude.

The hybrid guidance simulation is run for the same conditions as the PNG, and the most significant improvement is achieved in the total command effort. The minimum

miss distance is 0.02854 m, the total intercept time is 170 s and the total command effort is 20,090 m/s² for the HG simulation. Note that the intercept time is improved by 2 s and the total command effort is improved by 1320 m/s² when compared to PNG with the missile velocity approach.

Since we have reached the best guidance method that we can achieve for the given scenario, we will run this simulation for several EKV initial conditions and different ICBM launch points. In addition, there will be a launch delay due to target detection, launch decision and human interface delays as given by

$$\tau_l = \tau_{dt} + \tau_{dc} + \tau_h \quad (4.43)$$

where τ_l is launch delay, τ_{dt} is detection time, τ_{dc} is the decision time and τ_h is the human interface delay time. This is implemented in the simulation by delaying the EKV launch by $\tau_l = 30$ s.

The three launch locations of interest are North Korea, China and Iran respectively. The initial conditions of the ICBM are defined by their initial state vectors. The EKV travels on a circular orbit with an altitude of 1000 km, an inclination angle of 43.52° and a right-ascension angle of 15.28°. The initial state vector of the EKV on this orbit is defined by the mean anomaly ω , which is measured from the ascending node. We will examine the guidance method for four different launch points within the launch range on the orbit.

a) North Korea Case

The initial state space vector of the ICBM is

$$X_T(30) = \begin{bmatrix} x_T \\ y_T \\ z_T \\ \dot{x}_T \\ \dot{y}_T \\ \dot{z}_T \end{bmatrix} = \begin{bmatrix} -3029966.67 \\ 3737980.67 \\ 4186406.53 \\ -279.69 \\ 20.81 \\ 479.46 \end{bmatrix}_{ECEF} \quad (4.44)$$

The minimum ω for an ICBM originating from North Korea is 99.97° for a successful intercept within the desired intercept time window. The maximum ω for the same case is 114.72° . These angle values are determined after running the simulation several times.

Table 8. Orbital launch points for the North Korea case.

Position	A	B	C	D
ω	99.97°	104.89°	109.81°	114.72°

Figure 62 shows the four different intercept geometries against a North Korean ICBM for HG EKV guidance. The coverage angle is measured from point A to point D as 14.75° . A launch between these points on the orbit guarantees a successful hit-to-kill intercept before the ICBM releases its RVs. The intercept geometries of four different launch points are shown in Figure 62. Any EKV carrier between point A and point D is capable of killing the North Korean ICBM. Before the EKV carrier leaves this region from point D, another EKV carrier should enter from point A in order to assure the intercept of any ICBM launched from North Korea. Hence, we need a minimum of $\lceil 360/14.75 \rceil = 25$ EKV carriers in the orbit.

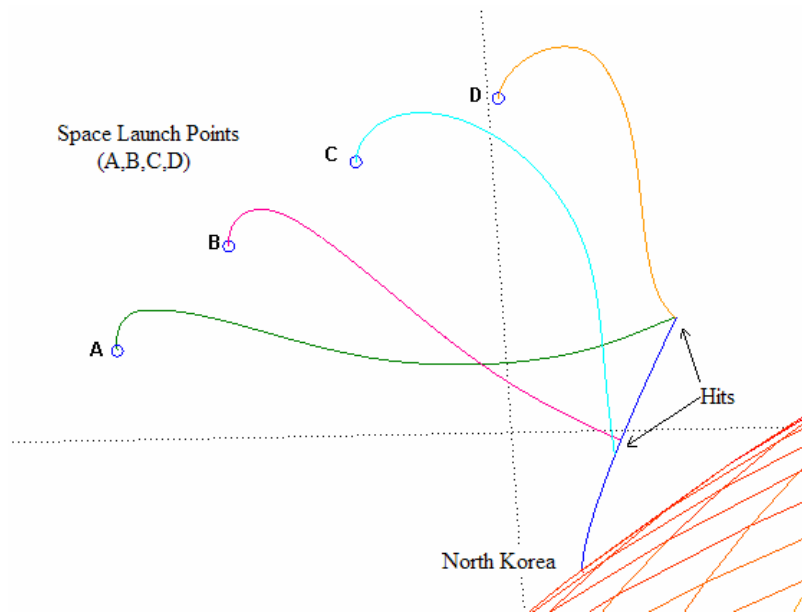


Figure 62. Intercept geometries against North Korean ICBM.

Figure 63 shows the miss distance of four different EKV's under HG as a function of time. Figure 64 shows the altitudes of the EKV's and the ICBM. The minimum miss distance for the EKV launched from point A is 0.01834 m. The EKV hits the ICBM 195 s after the ICBM launch, as shown in Figure 64. The significant improvement in the guidance method at the beginning of the intercept is observed in Figure 64, where the surplus altitude increase of the EKV is minimal compared to PNG results. The minimum miss distances and intercept times for points B, C and D are within the limits of the required constraints. Simulation results are listed in Table 9. Note that the time axes in the following figures start at the ICBM launch.

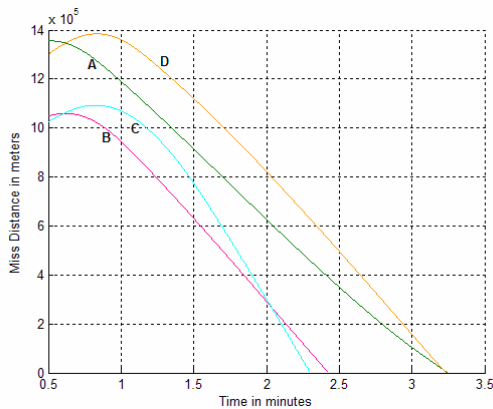


Figure 63. Miss distances with HG for North Korean ICBM defense.

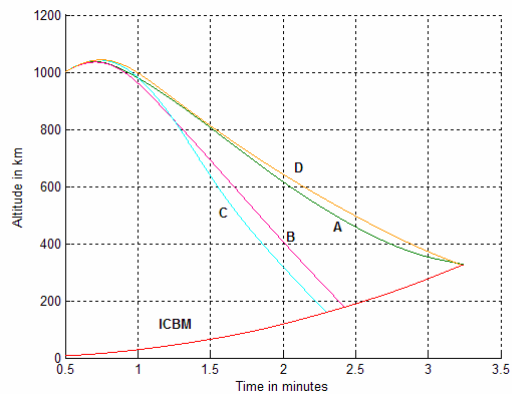


Figure 64. Altitudes of EKV's and North Korean ICBM with HG.

Figure 65 shows the acceleration command exerted on four EKV's under HG as a function of scenario time. Figure 66 shows the cumulative accelerations. At the beginning of the intercept, the EKV uses BBG (as shown in Figure 65) until the ICBM is within the gimble limit of the EKV, which steers the EKV to the collision path as soon as possible. The linear increase region in the cumulative lateral acceleration is observed where the BBG is applied. The BBG is applied where the EKV is not pointing to the ICBM. Hence, the shorter the BBG applied, the better the Launch point. The preceding statement claims that point A is the most favorable launch point for an EKV against a North Korean ICBM.

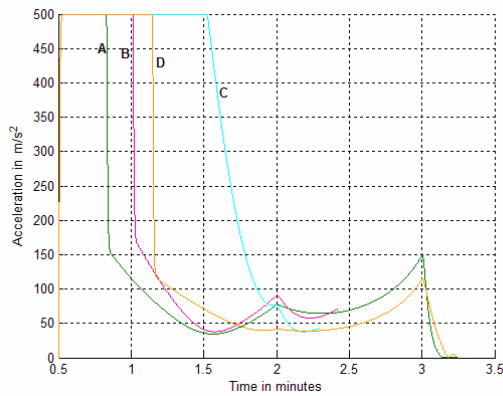


Figure 65. Lateral acceleration exerted by HG on the EKV launched from points A, B, C and D against North Korean ICBM.

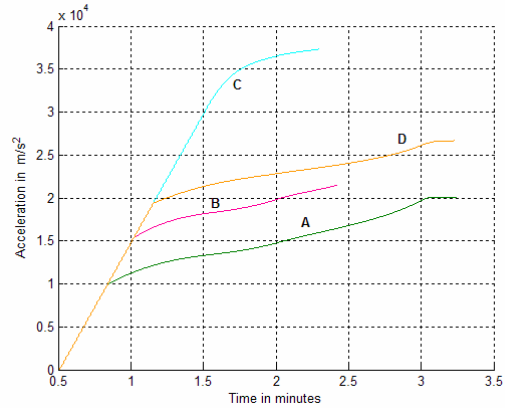


Figure 66. Cumulative acceleration exerted by HG on the EKV launched from points A, B, C and D against North Korean ICBM.

Figure 67 shows the speeds of four EKV under HG as a function of time and speed of the ICBM. Figure 68 shows the closing velocities. Since the EKV are launched with a 30-s delay, the ICBM has already attained a velocity of 555 km/s, which can be calculated using (4.44). The EKV speed increases rapidly for launch point C because the collision path is perpendicular to the earth's surface in this case. This case also introduces a head-on intercept since the EKV is literally right above the ICBM launch point. However, point D does not provide the EKV with an advantageous launch direction. The HG exerts the maximum acceleration command on the EKV for 73 s to steer the EKV towards the ICBM, which causes the high total acceleration command observed in Figure 66. In addition, the closing velocity reaches its maximum value for launch point D because of the head-on intercept geometry.

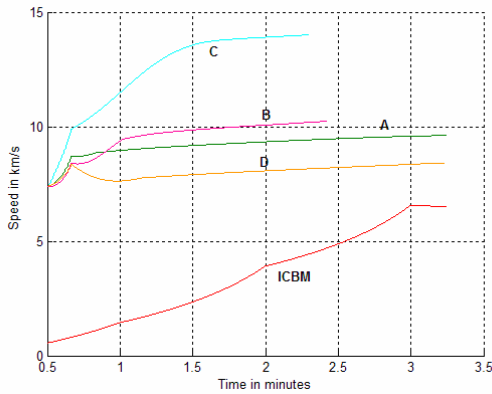


Figure 67. Velocity magnitudes of the EKV launched from points A, B, C, D and the ICBM with HG.

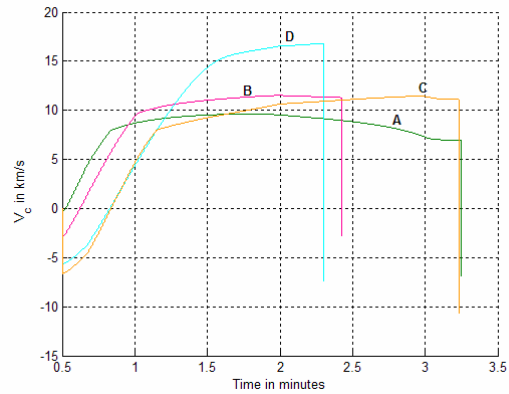


Figure 68. Closing velocity of the EKV to the ICBM for launch points A, B, C and D with HG.

The minimum miss distance, intercept time, intercept altitude and total command acceleration values are listed in Table 9; the intercept time is measured starting from the ICBM launch. The minimum miss distances are small enough for a hit-to-kill intercept. All the intercept times are before the ICBM delivers its RVs, and EKV is launched between point A and point D with a maximum launch delay of 30 s.

Table 9. Simulation results for North Korean ICBM intercept with HG.

	Point A	Point B	Point C	Point D
Miss Distance (m)	0.01834	0.01228	0.0839	0.1644
Intercept Time (s)	195	145.68	138.06	194.16
Intercept Altitude (km)	326.8	177.8	159.1	324.1
Total Acceleration (m/s^2)	20110	21500	37330	26670

The LOS angular velocities for different launch points are shown in Figure 69. The LOS angular velocity is proportional to the command acceleration where the PNG is applied. This proportionality proves the correct implementation of the PNG law.

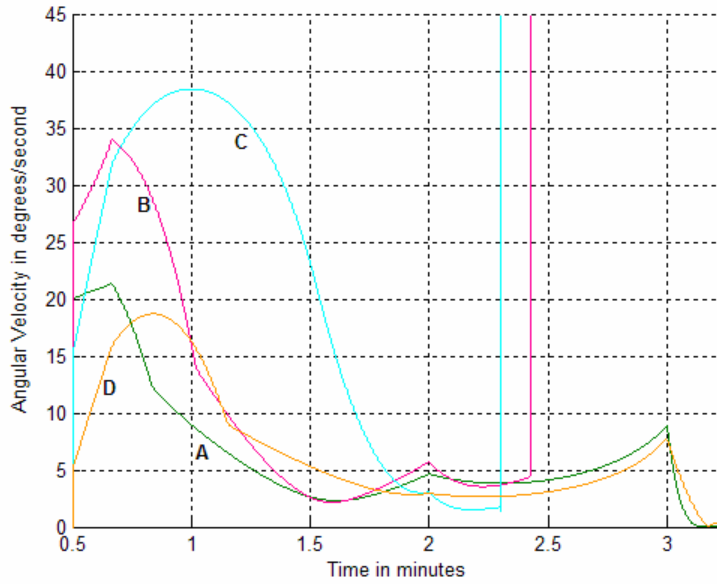


Figure 69. LOS angular velocity magnitudes for points A, B, C and D with HG.

b) China Case

The initial state vector of the ICBM is

$$X_T(30) = \begin{bmatrix} x_T \\ y_T \\ z_T \\ \dot{x}_T \\ \dot{y}_T \\ \dot{z}_T \end{bmatrix} = \begin{bmatrix} -985516.77 \\ 5062656.41 \\ 3751990.63 \\ -153.30 \\ 147.52 \\ 533.47 \end{bmatrix}_{ECEF} \quad (4.45)$$

The minimum ω for an ICBM originating from China is 78.82° for a successful intercept within 3.25 minutes after ICBM launch. The maximum ω for the same case is 84.25° .

Table 10. Orbital launch points for the China case.

Position	A	B	C	D
ω	78.82°	80.64°	82.44°	84.25°

The coverage angle from point A to point D is 5.43° . A launch between these points on the orbit guarantees a successful hit-to-kill intercept before the Chinese

ICBM delivers its reentry vehicles (RVs). The intercept geometries of four different launch points are shown in Figure 70. Any EKV carrier that is present between point A and point D is capable of killing the Chinese ICBM. In this case, the minimum required number of EKV carriers is 67.

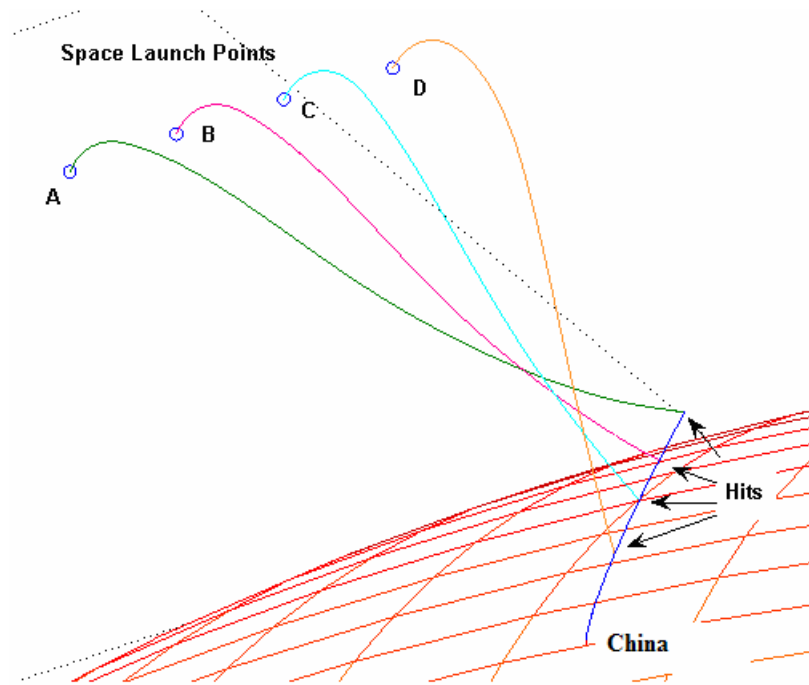


Figure 70. Intercept geometries against Chinese ICBM.

Figure 71 shows the miss distance for four EKV's under HG as a function of time. Figure 72 shows the altitudes of the EKV's and the ICBM. The minimum miss distance for the EKV launched from point A is 0.08915 m. The EKV hits the ICBM 190 s after the ICBM is launched, as shown in Figure 71. The minimum miss distances and intercept times for points B, C and D are within the limits of the required constraints. The EKV hits the ICBM at an altitude of 287 km, as shown in Figure 72. Simulation results are listed in Table 11. Note that the time axes of the following figures start at the ICBM launch.

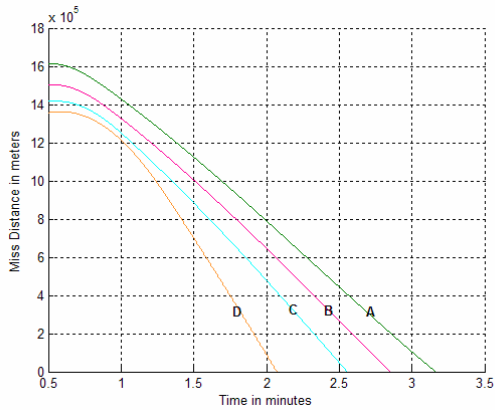


Figure 71. Miss distances with HG for Chinese ICBM defense.

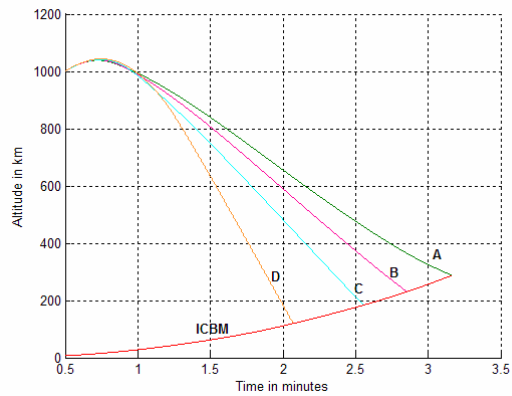


Figure 72. Altitudes of EKV and Chinese ICBM with HG.

Figure 73 shows the acceleration command applied on the EKV under HG as a function of scenario time. Figure 74 shows the cumulative accelerations. At the beginning of the intercept, the guidance unit exerts the maximum acceleration on the EKV (as shown in Figure 73) until the ICBM is within the gimble limit of the EKV seekers, which steers the EKV to the collision path as soon as possible. Point A is the most favorable launch point for an EKV against a Chinese ICBM. The stage transitions of the ICBM are also observed in instantaneous lateral acceleration command.

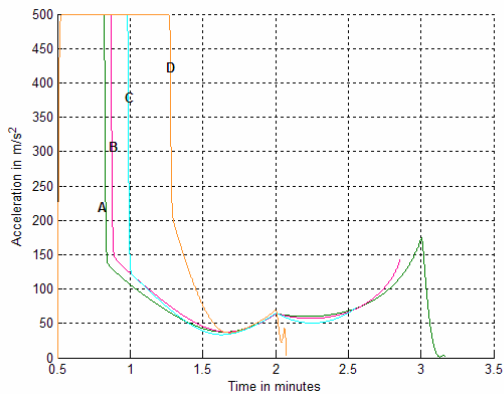


Figure 73. Lateral acceleration exerted by HG on the EKV launched from points A, B, C and D against Chinese ICBM.

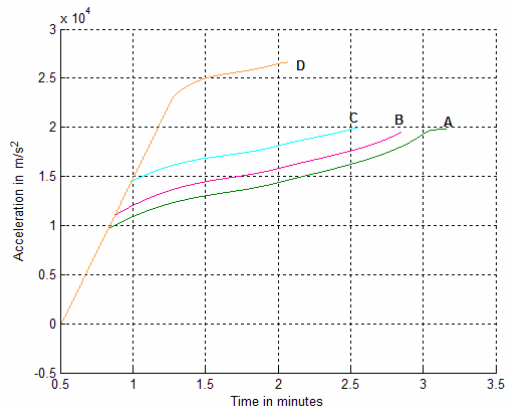


Figure 74. Cumulative acceleration exerted by HG on the EKV launched from points A, B, C and D against Chinese ICBM.

The speeds of the EKV and the ICBM are shown in Figure 75. Since the EKV is launched with a 30-s delay, the ICBM has already attained 574 km/s of velocity, which can be calculated using (4.45). The EKV speed increases rapidly for point D launch, because the collision path is perpendicular to the earth's surface in this case. The HG exerts the maximum acceleration command on the EKV for 76 s to steer the EKV towards the ICBM, which causes the high total acceleration command observed in Figure 74. In addition, the closing velocity reaches its maximum value for launch point D because of the head-on intercept geometry. The closing velocity of the EKV to the ICBM is shown in Figure 76. The closing velocity for point D launch reaches 22 km/s, which is approximately the sum of the EKV speed and the ICBM speed. This shows that the EKV is on a head-on intercept geometry.

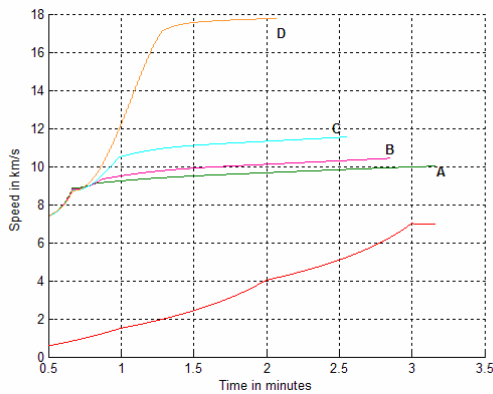


Figure 75. Velocity magnitudes of the EKV launched from points A, B, C, D and the ICBM with HG.

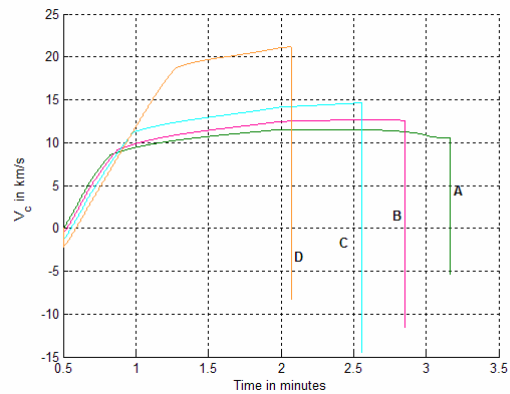


Figure 76. Closing velocity of the EKVs to the ICBM for launch points A, B, C and D with HG.

The simulation results for the Chinese ICBM interception from space launch points A, B, C and D are shown in Table 11; the intercept time is measured from the ICBM launch. The minimum miss distances that are listed in Table 11 are all smaller than the radius of the ICBM, which assures a hit-to-kill intercept. The intercept times show that the kills occur before the ICBM delivers its RVs.

Table 11. Simulation results for Chinese ICBM intercept with HG.

	Point A	Point B	Point C	Point D
Miss Distance (m)	0.08915	0.09718	0.2521	0.2710
Intercept Time (s)	189.96	171.42	153.42	124.26
Intercept Altitude (km)	287.4	230.7	183.7	119.5
Total Acceleration (ms ⁻²)	19780	19560	20010	26630

Figure 77 shows the LOS angle rate as a function of scenario time. The HG guidance decreases the LOS angular rate during the intercept, as shown in Figure 77. If the LOS angular velocity was zero during the entire intercept we could say that the PNG was implemented perfectly. However, such perfect implementation is impossible to achieve for this scenario because the ICBM is accelerating, which is introduced to the guidance as a maneuvering target. Nevertheless, HG guidance performs extremely well and hits the ICBM with a very small miss distance.

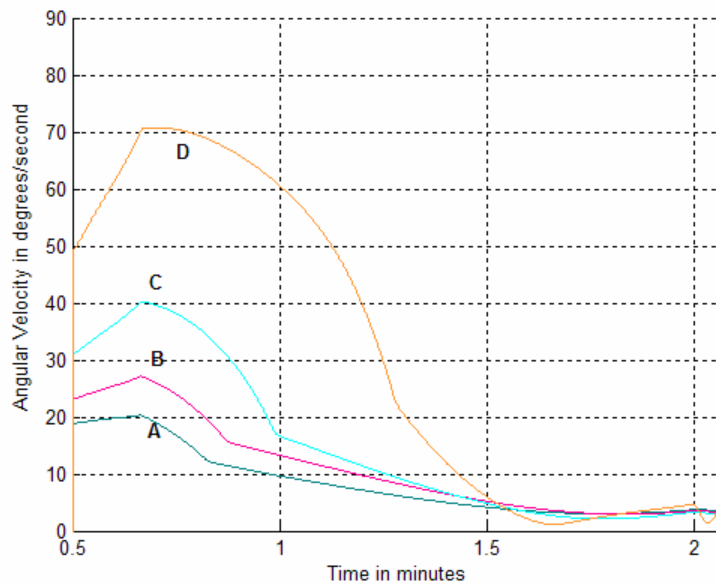


Figure 77. LOS angular velocity magnitudes for points A, B, C and D with HG.

c) **Iran Case**

The initial state vector of the ICBM is

$$X_T(30) = \begin{bmatrix} x_T \\ y_T \\ z_T \\ \dot{x}_T \\ \dot{y}_T \\ \dot{z}_T \end{bmatrix} = \begin{bmatrix} 3510071.07 \\ 4332137.25 \\ 3095896.55 \\ 204.53 \\ 43.94 \\ 540.68 \end{bmatrix}_{ECEF} \quad (4.46)$$

The minimum ω for an ICBM originated from Iran is 38.35° for a successful intercept within the desired intercept time window. The maximum ω for the same case is 47.57° .

Table 12. Orbital launch points for the Iran case.

Position	A	B	C	D
ω	40.01°	41.92°	43.44°	45.73°

The coverage angle from point A to point D is 5.72° . A launch between these points on the orbit guarantees a successful hit-to-kill intercept before the ICBM delivers its reentry vehicles (RVs). The intercept geometries from four different space launch points are shown in Figure 78. Any EKV carrier between point A and point D is capable of killing the Iranian ICBM. In this case, the minimum required number of EKV carriers is 63.

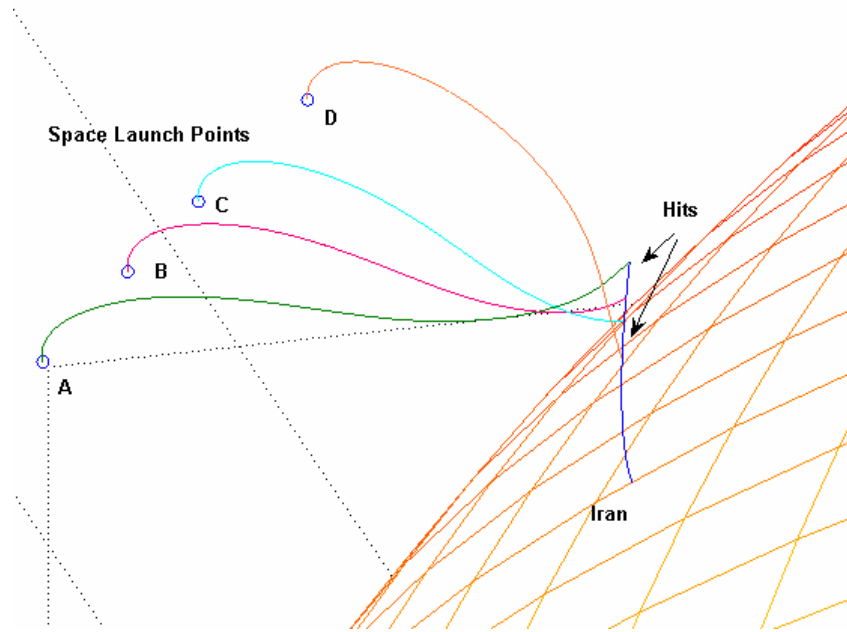


Figure 78. Intercept geometries against Iranian ICBM.

Figure 79 shows the miss distances of four EKV's under HG as a function of scenario time. Figure 80 shows the altitudes of the EKV's and the ICBM. The minimum miss distance for the EKV launched from point A is 0.03729 m. The EKV hits the ICBM 190.5 s after the ICBM is launched, as shown in Figure 79. The EKV hits the ICBM at an altitude of 195.4 km as shown in Figure 80. Simulation results are listed in Table 13. Note that the time axes of the following figures start at the ICBM launch.

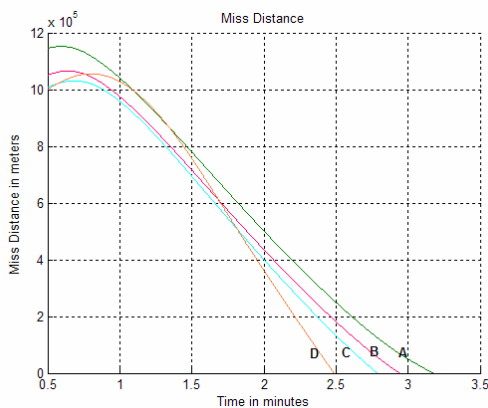


Figure 79. Miss distances with HG for Iran ICBM defense.

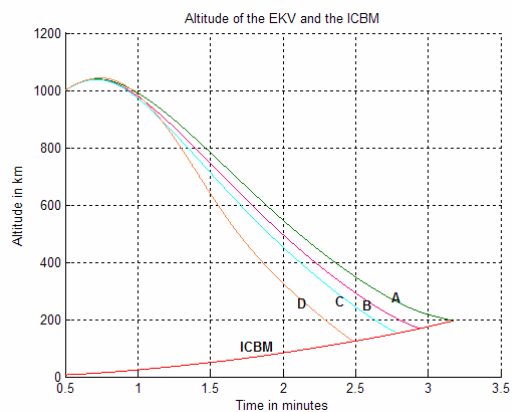


Figure 80. Altitudes of EKV's and Iran ICBM with HG.

Figure 81 shows the instantaneous acceleration command applied to the EKV by the HG as a function of scenario time. Figure 82 shows the cumulative accelerations. The guidance unit applies BBG on the EKV (as shown in Figure 81) until the ICBM is within the gimble limit of the EKV, which steers the EKV to the collision path as soon as possible. Point D holds an unfavorable launch direction for the EKV, which requires it to sustain BBG for 94 s. Point D launch exerts the maximum total acceleration on the EKV as shown in Figure 82. Point A holds the most favorable launch direction for EKV against an Iranian ICBM. The stage transitions of the ICBM are also observed in instantaneous lateral acceleration command.

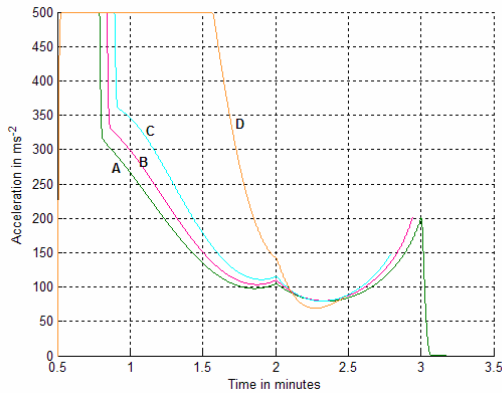


Figure 81. Lateral acceleration exerted by HG on the EKVs launched from points A, B, C and D against Iran ICBM.

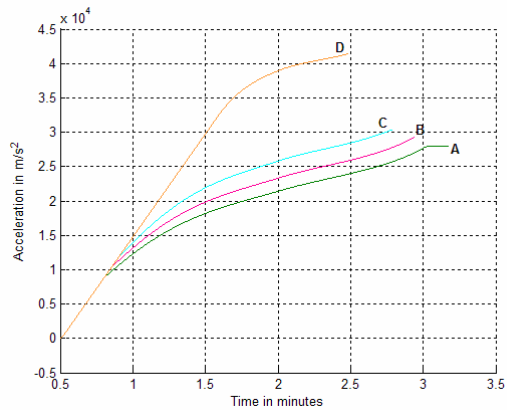


Figure 82. Total cumulative acceleration exerted by HG on the EKVs launched from points A, B, C and D against Iran ICBM.

Figure 83 shows the speeds of four EKVs under HG and the ICBM as a function of time. Figure 84 shows the closing velocities. The HG exerts the maximum acceleration command on the EKV where the ICBM is out of the gimble limit of the seeker, as shown in Figure 83. The EKV moves towards the earth's surface in point D launch, which can be attributed to higher velocity. In addition, the closing velocity reaches its maximum value for launch point D as shown in Figure 84. For point D launch, the intercept geometry is a near head-on approach, which causes this high closing velocity.

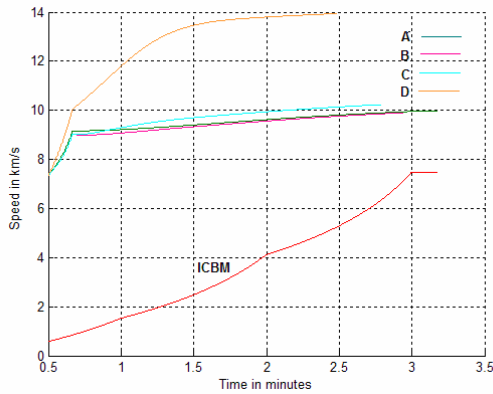


Figure 83. Speeds of the EKVs launched from points A, B, C, D and the ICBM with HG.

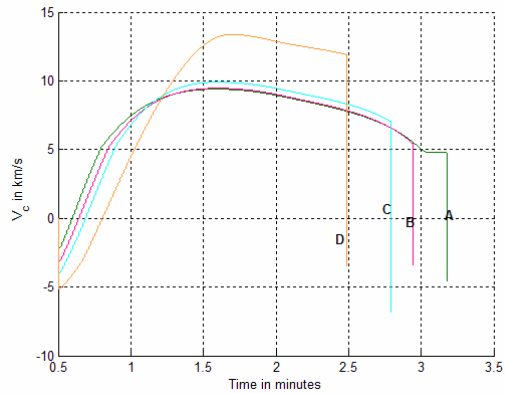


Figure 84. Closing velocities of the EKVs to the ICBM for launch points A, B, C and D with HG.

Simulation results are given in Table 13, where the time is measured starting from the ICBM launch. Note that there is a 30-s launch delay for the EKV launch.

Table 13. Simulation results for Iranian ICBM intercept with HG.

	Point A	Point B	Point C	Point D
Miss Distance (m)	0.03729	0.02465	0.02386	0.008616
Intercept Time (s)	190.5	176.7	167.4	148.7
Intercept Altitude (km)	195.4	168.6	152	123.4
Total Acceleration (m/s^2)	27990	29310	20380	41410

The LOS angular rates are shown in Figure 85 and are proportional to the commanded acceleration where PNG is applied.

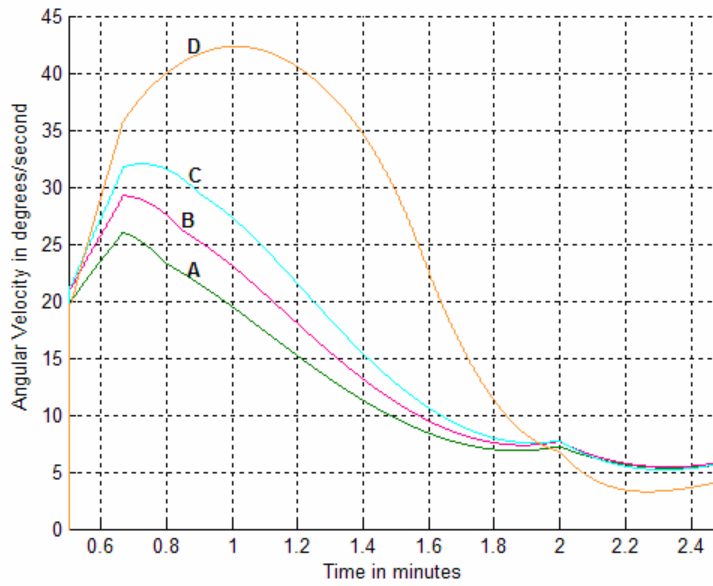


Figure 85. LOS angular velocity magnitudes for points A, B, C and D with HG.

E. SUMMARY

After running the simulation for North Korea, China and Iran, the performances of different guidance rules were analyzed, and a hybrid guidance is utilized for best performance. We showed that the hybrid guidance method performs extremely well for space-based ICBM defense for the scenarios of interest. We also showed that this guidance achieves a hit-to-kill intercept before the ICBM delivers its RVs.

THIS PAGE IS INTENTIONALLY LEFT BLANK

VI. CONCLUDING REMARKS AND FUTURE RECOMMENDATIONS

A. SUMMARY OF THE WORK

This thesis developed a model for space-based, boost-phase interception of ICBMs from three example launch sites, namely North Korea, China and Iran. The ICBM was mathematically modeled and by taking the earth's rotation and the atmospheric drag into account. The required orbit for a successful intercept was derived for the EKV carriers. Finally, a guidance algorithm was designed to achieve the interception for a hit-to-kill mission.

The ICBM was modeled in three-dimensional space in the ECEF coordinate system. The initial launch parameters were calculated for a San Francisco, California attack by using the Lambert guidance. The precise parameters were generated by running a simulation of the developed model several times around the initial parameters.

The orbit was derived to cover the three launch points of interest uniformly from space. The payload capability of the space launch vehicle and the lifetime of the system were also considered. The performance of the orbit was predicted using the maximum range of the EKV and the desired intercept features in the window of opportunity.

The pursuit guidance (PG), proportional navigation guidance (PNG) and bang-bang guidance (BBG) are described and implemented in a three-dimensional model for the given scenario. The guidance rules were analyzed based on the simulation runs and their performances compared. The BBG and PNG were combined to form a hybrid algorithm for the best performance.

B. SIGNIFICANT RESULTS

Significant results obtained in this thesis work include the trajectory and the launch parameters of the example ICBMs, the required orbit for a space-based, boost-phase intercept, and an investigation of different guidance rules for the given scenario.

The mathematical model we developed for the trajectory of the ICBM takes the earth's rotation and the atmospheric drag into account along with the gravitational forces and the thrust acting on the ICBM. Since the ICBM travels in space during its mid-

course, the earth's rotation plays a significant role on its impact point. For example, the impact point of the ICBM launched from North Korea with azimuth launch angle 39.6° and elevation launch angle 85.81° is San Francisco, California. However, if we take earth's rotation out of the calculations, the impact point calculated by the simulation with the same launch parameters is $N47^\circ W 115.5^\circ$. The distance between San Francisco and this location is approximately 780 miles, which is the error if we assume a non-rotating earth.

The orbit we derived covers the three example launch sites. The analysis made in Chapter III showed that the bounding limitation for the orbit altitude was the payload capability of the space launch vehicle within the given scenario. The selected orbit has an inclination angle of $i = 43.52^\circ$, a right-ascension angle of $\Omega = 15.28^\circ$ and an altitude of $r_a = 1000$ km. After running the intercept simulation it is found that the North Korea defense requires 25 EKV carriers in orbit, the China defense requires 67 EKV carriers, and the Iran defense requires 63 EKV carriers. In the interest of providing a common defense system, we have to consider the highest number, so the total required EKV carriers in the orbit is 67.

Pursuit guidance (PG), proportional navigation guidance (PNG) and the bang-bang guidance (BBG) were implemented in a three-dimensional intercept model. The performance of these guidance rules were analyzed by running the SIMULINK[®] simulation for the North Korea case. From this analysis, the best performance was achieved by combining the BBG and the PNG guidance algorithms, which formed the hybrid guidance (HG). The HG is tested for three example launch scenarios, and four different space launch points were chosen for each launch scenario. The simulation results showed that the HG met the requirements of the space-based, boost-phase intercept as shown in Table 9, Table 11 and Table 13.

The most significant problem in the space-based interception is the initial launch direction of the EKV. In most cases, it is not possible to launch the EKV towards the ICBM due to angular velocity of the orbit. The initial launch direction of the EKV is corrected by using the BBG until the EKV pointed towards the ICBM. This method turned the EKV towards the ICBM as soon as possible by applying the maximum applicable

command acceleration and decreased the total command effort for the entire intercept. After ICBM entered the field of view of the EKV seeker, the PNG is used to steer the EKV, which minimized the command effort within the required intercept time.

C. RECOMMENDATIONS FOR FUTURE WORK

In this study, we assumed the earth as a perfect sphere and the ICBM as a point mass. These assumptions lead to inaccuracies in the ICBM trajectory calculation. In a future study, the oblate shape of the earth may be introduced to ICBM dynamics, and a full aerodynamic ICBM model may be considered for more accurate trajectory prediction.

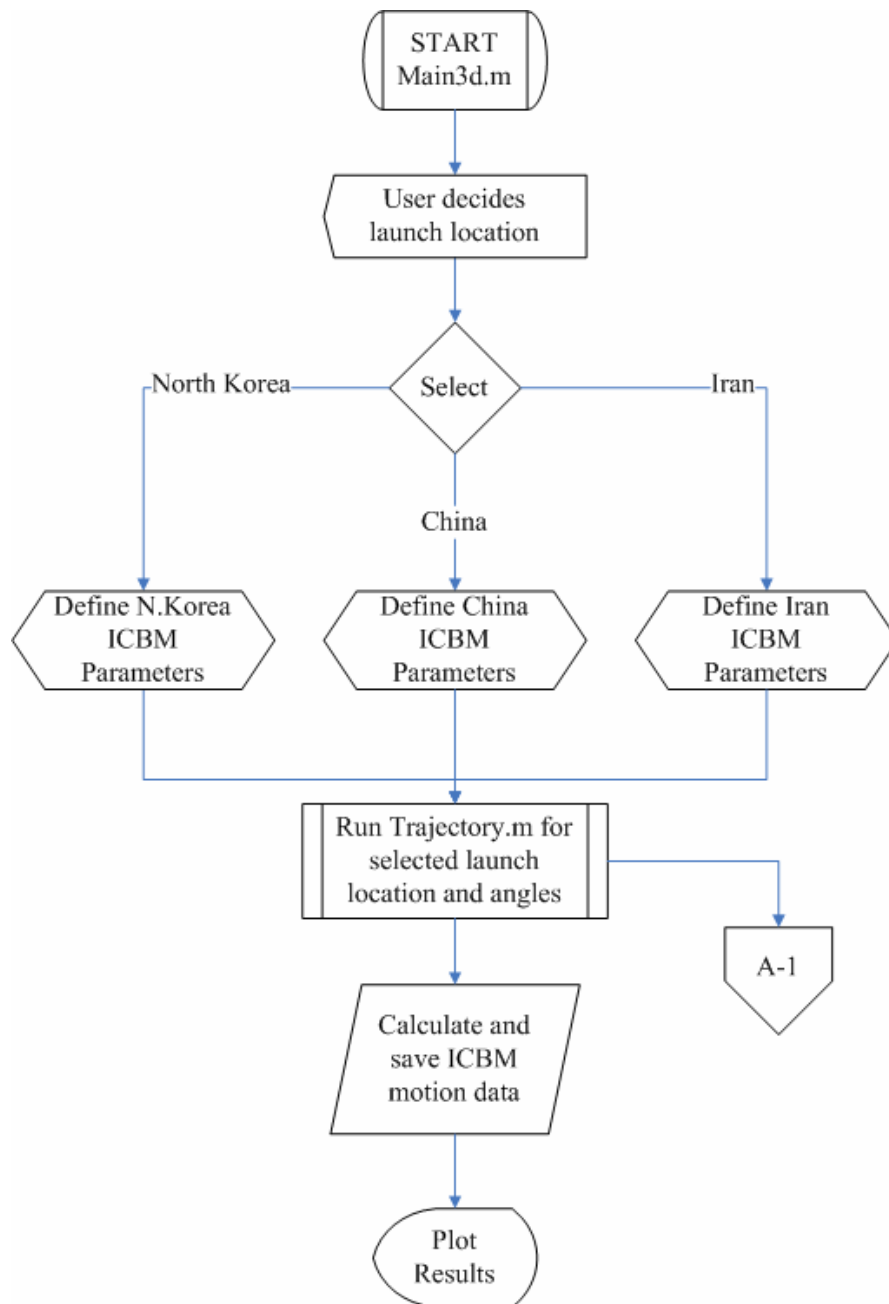
In this work, the EKV seeker is assumed to track the ICBM at all times and without any error. However, the EKV seeker has a limited field of view, so it cannot track the target at all times, especially at the beginning of the intercept. In a future study, the tracking of the ICBM may be supported by the sensor network as illustrated in Figure 1 and investigated in previous studies [3] and [6]. The EKV seeker may also be remodeled by introducing the errors in tracking.

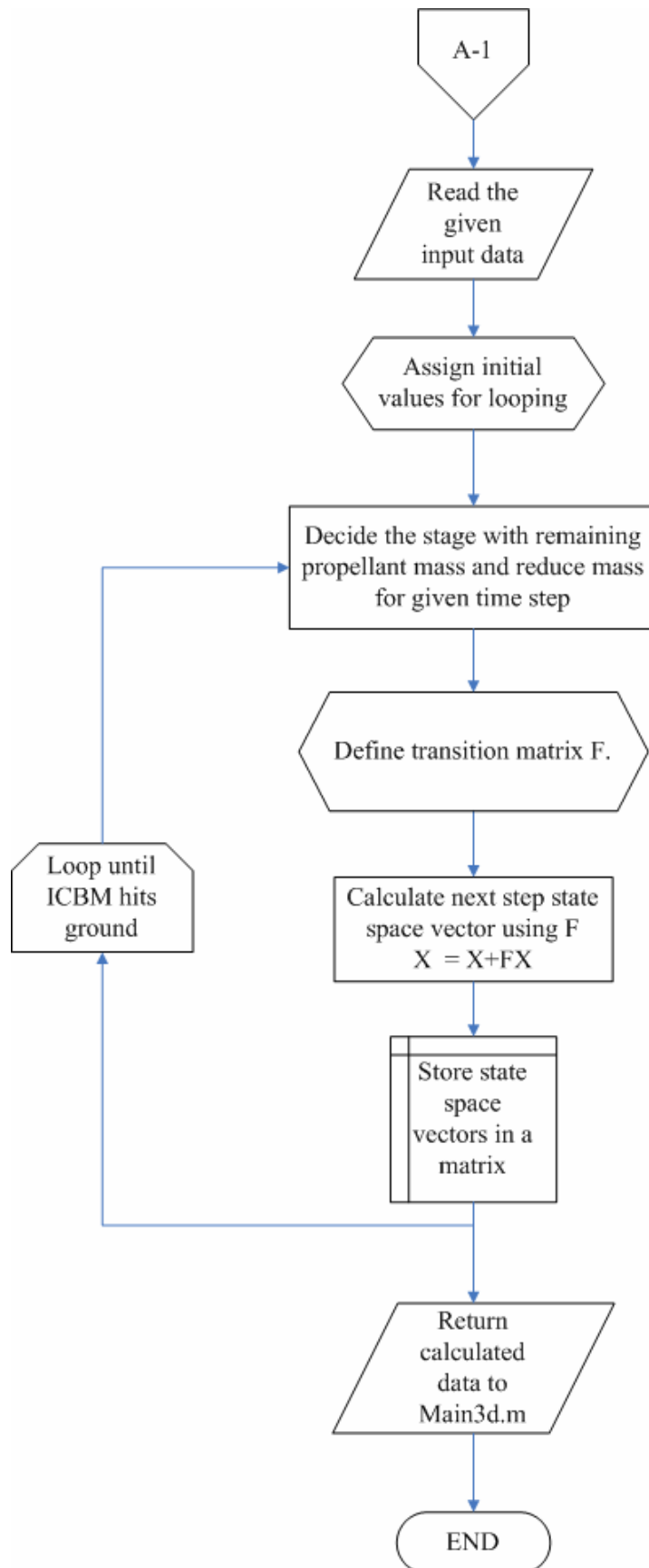
In this thesis, we used the BBG and PNG as the selected guidance rules. Although these guidance rules perform satisfactorily, an optimum guidance algorithm may be investigated in a future study as proposed in [40].

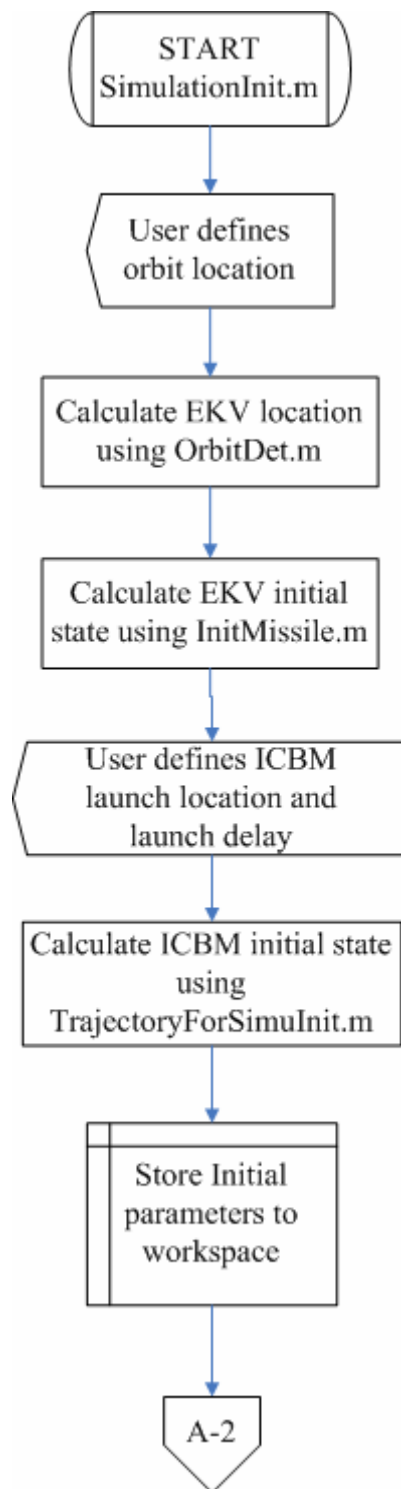
THIS PAGE INTENTIONALLY LEFT BLANK

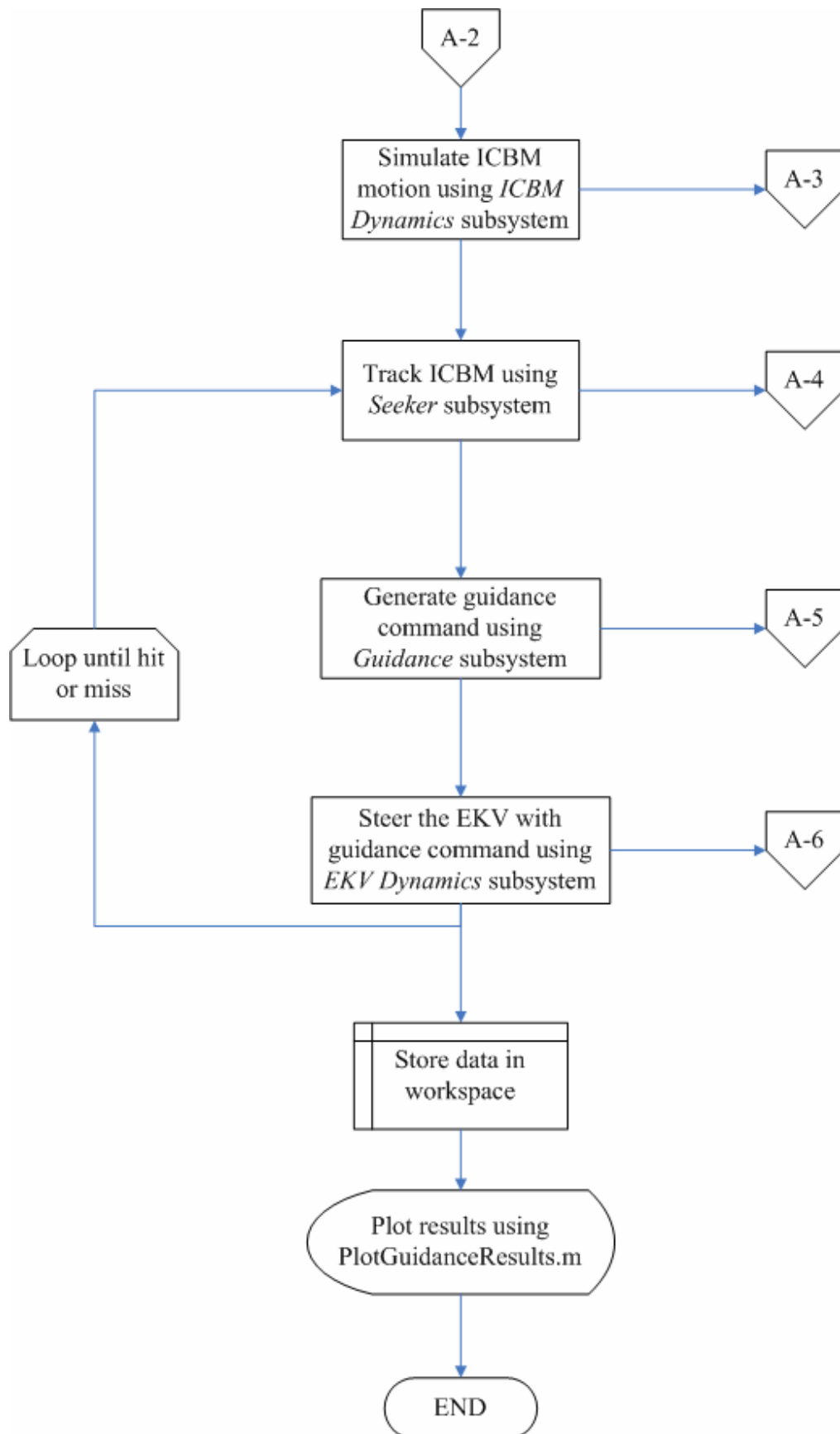
APPENDIX A. CODE FLOW CHART

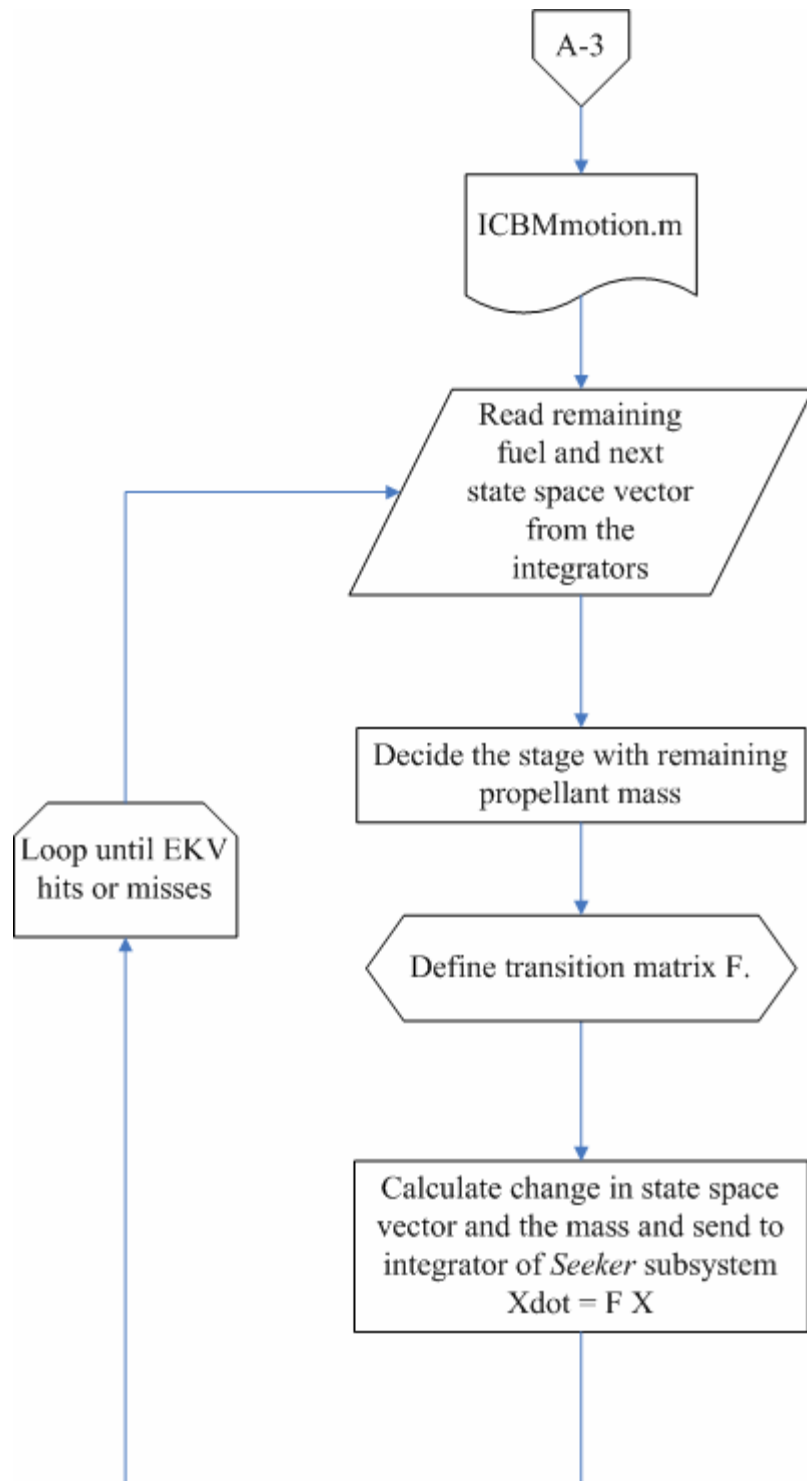
This appendix contains the flow chart of the MATLAB[®] code for the ICBM trajectory prediction and the SIMULINK[®] model for ICBM intercept with different EKV guidance algorithms.

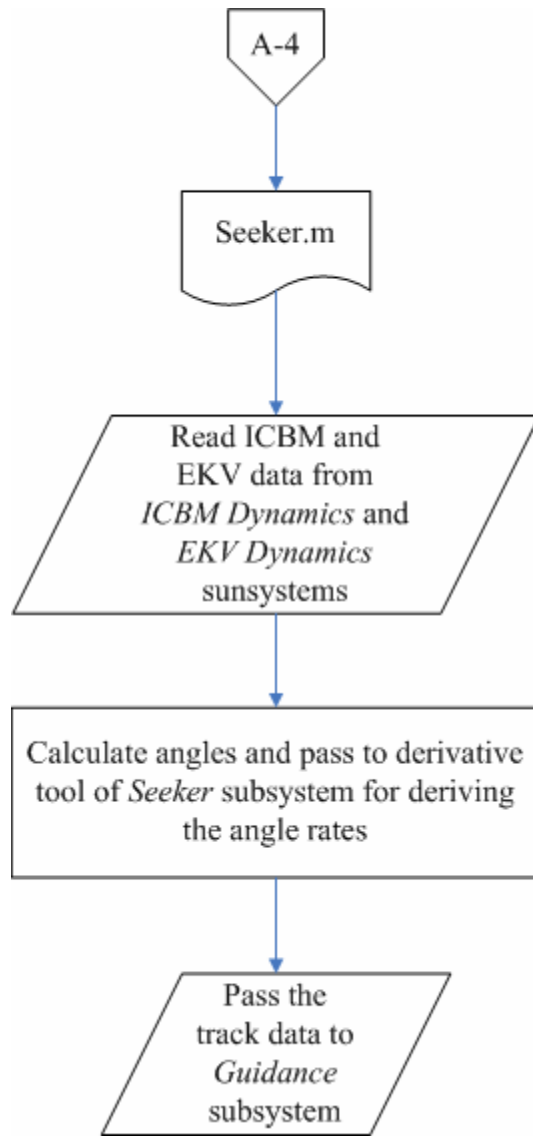


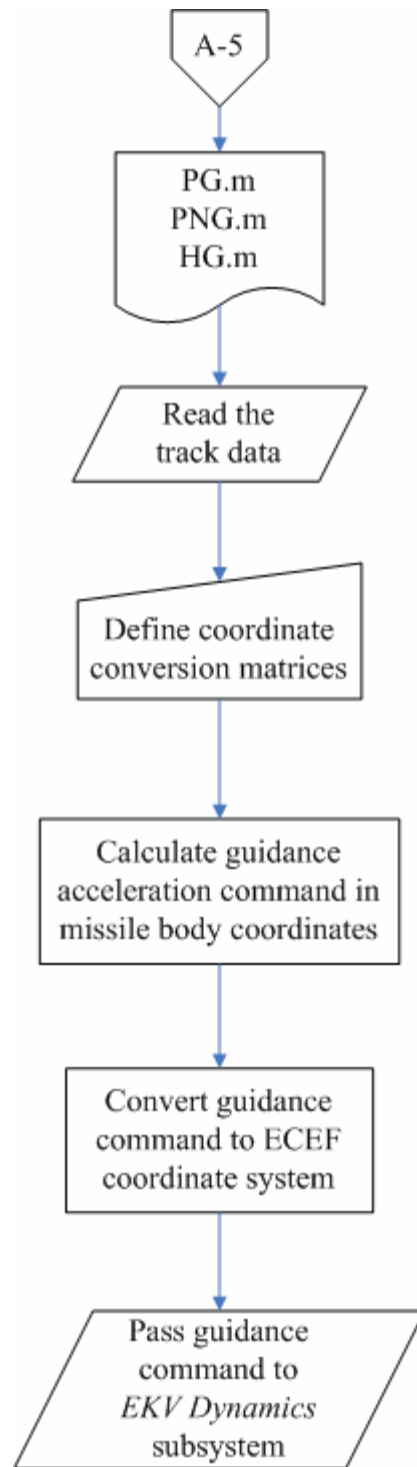


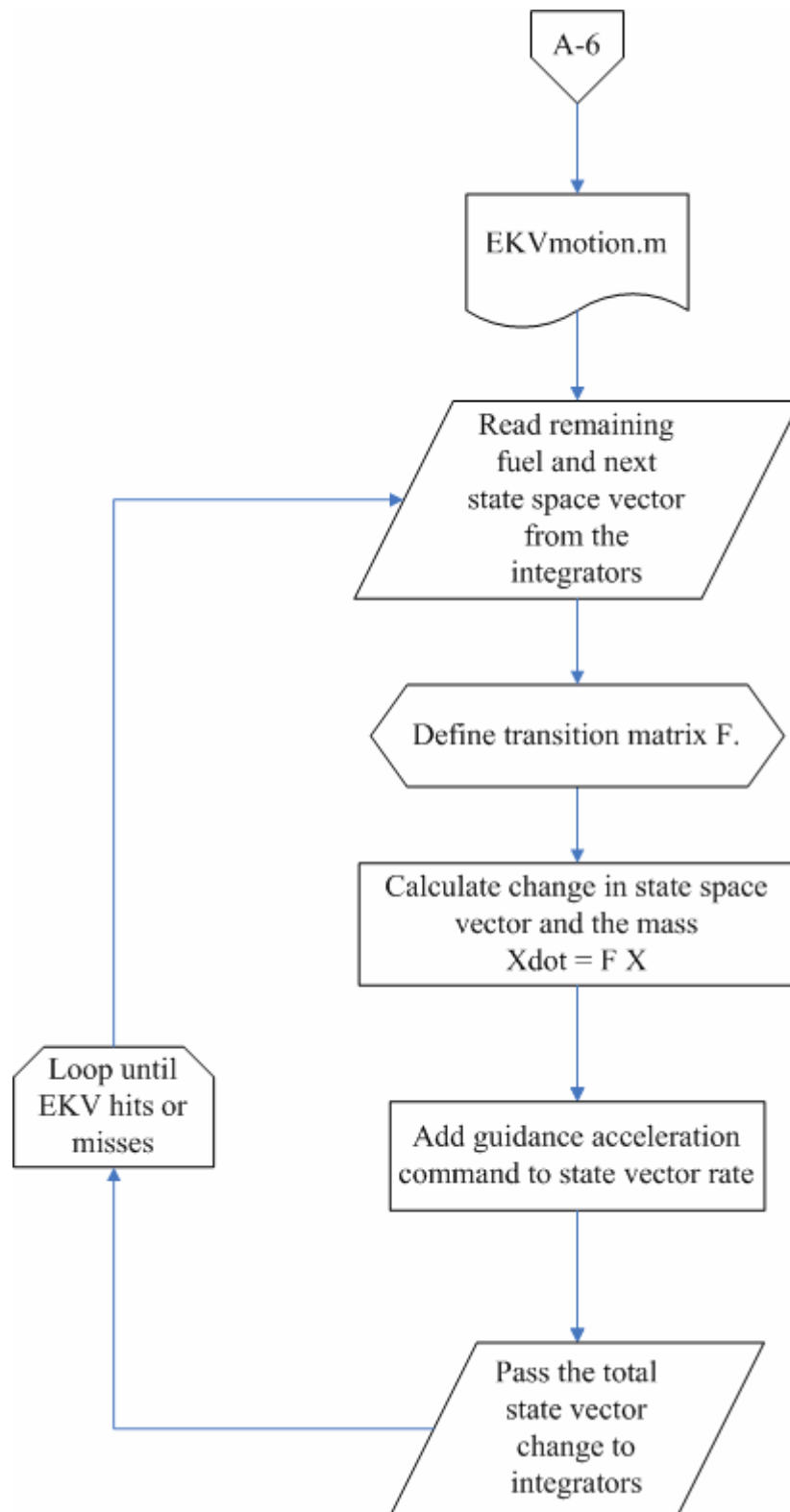












LIST OF REFERENCES

- [1] Dov S. Zakheim, "Old Rivalries, New Arsenals: Should the United States Worry?" *IEEE Spectrum*, Vol. 36, No. 3, p. 31, 1999.
- [2] Commission to Assess the Ballistic Missile Threat to the United States, Report, <http://www.fas.org/irp/threat/missile/rumsfeld/toc.htm>, last accessed 26 July 2005.
- [3] Kursat Yildiz, "Electronic Attack and Sensor Fusion Techniques for Boost-Phase Defense Against Multiple Ballistic Threat Missiles," Master's Thesis, Naval Postgraduate School, June 2005.
- [4] Richard L. Garwin, "Holes in the Missile Shield," *Scientific American*, Vol. 291, Iss. 5, pp. 70 – 79, November 2004.
- [5] John A. Adam, "Star Wars in Transition," *IEEE Spectrum*, Vol. 26, No. 3, pp. 32 – 38, 1989.
- [6] Kubilay Uzun, "Requirements and Limitations of Boost-Phase Ballistic Missile Intercept Systems," Master's Thesis, Naval Postgraduate School, September 2004.
- [7] Gregory H. Canavan, "Space-Based Missile Defense and Stability," *The American Philosophical Society Proceedings*, Vol. 145, No. 3, pp. 270-283, 2001.
- [8] Bruce M. Deblois, Richard L. Garwin, et al., "Star Crossed," *IEEE Spectrum*, Vol. 42, No. 3, pp. 40 – 49, March 2005.
- [9] Paul Zarchan, *Tactical and Strategic Missile Guidance*, American Institute of Aeronautics and Astronautics, Reston, VA, 2002.
- [10] Y. Kashiwagi, "Prediction of Ballistic Missile Trajectories," *Memorandum 37*, Defense Technical Information Center, June 1968.
- [11] M. P. Fitzgerald, T. R. Armstrong, "Newton's Gravitational Constant with Uncertainty Less Than 100 ppm," *IEEE Transactions on Instrumentation and Measurement*, Vol. 44, No. 2, April 1995.
- [12] Dennis Roddy, *Satellite Communications, Third Ed.*, McGraw-Hill, Hightstown, NJ, 2001.

- [13] A. T. Aydin, P.E. Pace, M. Tummala, "Orbit Selection for Space-based Interception of a Select ICBM Case," *IEEE International Conference on Systems, Man and Cybernetics*, HI, to be published in October 2005.
- [14] D. A. James, *Radar Homing Guidance for Tactical Missiles*, Halsted Press, John Wiley & Sons, Inc., New York, 1986.
- [15] Robert Hutchins, Notes for EC4340 (Navigation, Missile, and Avionics Systems for International Students), Naval Postgraduate School, 2005, (unpublished).
- [16] Florios Bardanis, "Kill Vehicle Effectiveness for Boost-phase Interception of Ballistic Missiles," Master's Thesis, Naval Postgraduate School, June 2004.
- [17] Ground-based Midcourse Defense (GMD) System Exo-atmospheric Kill Vehicle (EKV)," <http://www.raytheon.com/products/ekv/> , last accessed 11 Sep 2005.
- [18] George P. Sutton and Oscar Biblarz, *Rocket Propulsion Elements, Seventh Ed.*, pp. 639 – 652, John Wiley & Sons, Inc., New York, 2001.
- [19] Donald T. Greenwood, *Principals of Dynamics Second Edition*, Prentice Hall, Englewood Cliffs, NJ, 1988.
- [20] D. Casey and J. Way, "Orbit Selection for the EOS Mission and Its Synergism Implications," *IEEE Transactions on Geosciences and Remote Sensing*, Vol. 29, No. 6, pp. 822 – 835, November 1991.
- [21] D. Y. Stodden and G. D. Galasso, "Space System Visualization and Analysis Using the Satellite Orbit Analysis Program (SOAP)," *Proceedings of the IEEE Aerospace Applications Conference*, Vol. 1, pp. 369 – 387, February 1995.
- [22] S. D. Tomlin, "Remote Non-Satellite Formation Designs with Orbit Perturbation Corrections and Attitude Control/Propulsion Subsystem Correlation," Master's Thesis, Naval Postgraduate School, June 2000.
- [23] Google Earth 3.0.0336 (beta).
- [24] "Weapons of Mass Destruction," <http://www.globalsecurity.org/wmd/world/iran/bushehr.htm>, last accessed 9 June 2005.

- [25] Fawwaz T. Ulaby, *Fundamentals of Applied Electromagnetic*, Prentice Hall, Upper Saddle River, NJ, 2004.
- [26] “Titan IV-B/Centaur Launch Vehicle,” <http://www.nasa.gov/centers/glenn/about/history/castitan.html>, last accessed 11 June 2005.
- [27] “National Reconnaissance Office,” http://www.nro.gov/PressReleases/prs_rel73.html, last accessed 12 June 2005.
- [28] “Titan IV,” http://www.losangeles.af.mil/SMC/PA/Fact_Sheets/ttn4_fs.htm, last accessed 11 June 2005.
- [29] Brian L. Stevens, Frank L. Lewis, *Aircraft Control and Simulation*, Wiley Interscience, New York, 1992.
- [30] Jae-Hyuk Oh, In-Joong Ha, “Capturability of the 3-Dimensional Pure PNG Law,” *IEEE Transactions on Aerospace and Electronic Systems*, Vol. 35, No. 2, pp. 491 – 503, April 1999.
- [31] P. E. Pace, M. D. Nash, D. P. Zulaica, et al., “Relative Targeting Architectures for Captive-Cary HIL Missile Simulator Experiments,” *IEEE Transactions on Aerospace and Electronic Systems*, Vol. 37, No. 3, July 2001.
- [32] Donald T. Greenwood, *Advanced Dynamics*, Cambridge University Press, 2003.
- [33] Seong-Ho Song, In-Joong Ha, “A Lyapunov-Like Approach to Performance Analysis of 3-Dimensional Pure PNG Laws,” *IEEE Transactions on Aerospace and Electronic Systems*, Vol. 30, No. 1, pp. 238 – 248, January 1994.
- [34] Robert Hutchins, Notes for EC3310 (Optimal Estimation: Sensor and Data Association), Naval Postgraduate School, 2005, (unpublished).
- [35] Ben-Zion Naveh, Ariel Lorber, et al., *Theater Ballistic Missile Defense*, American Institute of Aeronautics and Astronautics, Reston, VA, 2001.
- [36] John H. Blakelock, *Automatic Control of Aircraft and Missiles, Second Ed.*, Wiley Interscience, New York, 1991.

- [37] Arthur E. Bryson and Yu-Chi Ho, *Applied Optimal Control, Optimization, Estimation, and Control*, Hemisphere Publishing Corporation, New York, NY, 1975, (revised printing).
- [38] Robert D. Broadston, “A Method of Increasing the Kinematic Boundary of Air-to-Air Missiles Using an Optimal Control Approach,” Engineer’s Thesis, Naval Postgraduate School, September 2000.
- [39] Joseph Z. Ben-Asher, Isaac Yaesh, *Advances in Missile Guidance Theory*, American Institute of Aeronautics and Astronautics, Reston, VA, 1998.
- [40] F. B. Tuteur, J. S. Tyler, “Optimal-Control Theory Applied to a Probabilistic Intercept Problem,” *IEEE Transactions on Automatic Control*, Vol 9, Iss. 4, pp. 498 – 507, October 1964.

INITIAL DISTRIBUTION LIST

1. Defense Technical Information Center
Ft. Belvoir, Virginia
2. Dudley Knox Library
Naval Postgraduate School
Monterey, CA
3. Dr. Dan C. Boger
Department of Information Sciences
Monterey, CA
4. Dr. Phillip E. Pace
Department of Electrical and Computer Engineering
Monterey, CA
5. Dr. Murali Tummala
Department of Electrical and Computer Engineering
Monterey, CA
6. 1st Lt. A. Tarik Aydin
Turkish Air Force
Ankara, Turkey
7. Dr. James B. Michael
Department of Electrical and Computer Engineering
Monterey, CA
8. Capt. I. Gokhan Humali
Turkish Air Force
Ankara, Turkey
9. Capt. Kubilay Uzun
Turkish Air Force
Ankara, Turkey
10. Dr. Dale S. Caffall
Missile Defense Agency
Washington, D.C.
11. Professor Man-tak Shing
Department of Computer Science
Monterey, CA

12. Dr. Doron Drusinsky
Department of Computer Science
Monterey, CA
13. LTC Tom Cook
Department of Computer Science
Monterey, CA
14. Mr. L. Lamoyne Taylor
Raytheon Missile Systems Division
Tucson, AZ